EIC Detector R&D Progress Report

The EIC Tracking and PID Consortium
(eRD6 Consortium)

June 24, 2019

The eRD6 Consortium

Project ID: eRD6

Project Name: Tracking & PID detector R&D towards an EIC detector

Period Reported: from January 2019 to June 2019

Brookhaven National Lab (BNL): Craig Woody

Florida Institute of Technology (Fl. Tech): Marcus Hohlmann

INFN Trieste: Silvia Dalla Torre

Stony Brook University (SBU): Klaus Dehmelt, Thomas Hemmick

Temple University (TU): Matt Posik, Amilkar Quintero, Bernd Surrow

University of Virginia (UVa): Kondo Gnanvo, Nilanga Liyanage

Yale University: Richard Majka, Nikolai Smirnov

Project Members:

BNL: B. Azmoun, A. Kiselev, J. Kuczewski, M. L. Purschke, C. Woody

BNL - Medium Energy Group: E. C. Aschenauer

Fl. Tech: M. Bomberger, J. Collins, M. Hohlmann

INFN Trieste: S. Dalla Torre, S. Levorato, F. Tessarotto

SBU: K. Dehmelt, A. Deshpande. P. Garg, T. K. Hemmick, A. Kulkarni, C. Perez Lara, V. Zakharov

TU: M. Posik, A. Quintero, B. Surrow

UVa: K. Gnanvo, N. Liyanage

Yale University: R. Majka, N. Smirnov

Contact Person: Kondo Gnanvo; kgnanvo@virginia.edu

Contents

1 Brief overview of project histories and the document structure **6**

1.1 Brookhaven National Lab (BNL) . . . 6

1.2 Florida Institute of Technology (Florida Tech) . . . 7

1.3 INFN Trieste (INFN) . . . 7

1.4 Stony Brook University (SBU) . . . 8

1.5 University of Virginia (UVa) . . . 8

1.6 Temple University (TU) . . . 8

2 Tracking **9**

2.1 Central Tracker . . . 9

2.1.1 What was planned for this period? . . . 9

2.1.1.1 TPC studies at Brookhaven National Lab . . . 9

2.1.1.2 TPC studies at Stony Brook . . . 10

2.1.1.3 Cylindrical μRWELL studies at Florida Tech . . . 10

2.1.1.4 Cylindrical μRWELL studies at TU . . . 10

2.1.1.5 Cylindrical μRWELL studies at UVa . . . 10

2.1.2 What was achieved? . . . 10

2.1.2.1 TPC studies at Brookhaven National Lab . . . 10

2.1.2.2 TPC studies at Stony Brook . . . 14

2.1.2.3 Cylindrical μRWELL studies at Florida Tech . . . 15

2.1.2.4 Cylindrical μRWELL studies at TU . . . 19

2.1.2.5 Cylindrical μRWELL studies at UVa . . . 20

2.1.3 What was not achieved, why not and what will be done to correct? . . . 27

2.1.3.1 TPC studies at Brookhaven National Lab . . . 27

2.1.3.2 TPC studies at Stony Brook . . . 27

2.1.3.3 Cylindrical μRWELL studies at Florida Tech . . . 27

2.1.3.4 Cylindrical μRWELL studies at TU . . . 28

2.1.3.5 Cylindrical μRWELL studies at UVa . . . 28

2.1.4 What is planned for the next funding cycle and beyond? . . . 28

2.1.4.1 TPC studies at Brookhaven National Lab . . . 28

2.1.4.2 TPC studies at Stony Brook . . . 29

2.1.4.3 Cylindrical μRWELL studies at Florida Tech . . . 29

2.1.4.4 Cylindrical μRWELL studies at TU . . . 29
2.1.4.5 Cylindrical μRWELL studies at UVa . . . 29
2.2 Forward Tracker . . . 30
2.2.1 What was planned for this period? . . . 30
2.2.1.1 Florida Tech Large Carbon Fiber GEM Prototype with zigzag readout . . . 30
2.2.1.2 TU Commercial GEM Prototype . . . 30
2.2.1.3 UVa Large GEM Prototype with 2D U-V readout . . . 31
2.2.2 What was achieved? . . . 31
2.2.2.1 Florida Tech Large Carbon Fiber GEM Prototype with zigzag readout . . . 31
2.2.2.2 TU Commercial GEM Prototype . . . 35
2.2.2.3 UVa Large GEM Prototype with 2D U-V readout . . . 37
2.2.3 What was not achieved, why not and what will be done to correct? . . . 38
2.2.3.1 Florida Tech Large Carbon Fiber GEM Prototype with zigzag readout . . . 38
2.2.3.2 TU Commercial GEM Prototype . . . 39
2.2.3.3 UVa Large GEM Prototype with 2D U-V readout . . . 39
2.2.4 What is planned for the next funding cycle and beyond? . . . 40
2.2.4.1 Florida Tech Large Carbon Fiber GEM Prototype with zigzag readout . . . 40
2.2.4.2 TU Commercial GEM Prototype . . . 40
2.2.4.3 UVa Large GEM Prototype with 2D U-V readout . . . 41

3 RICH Particle ID 42

3.1 Hybrid MPGD for RICH - INFN Trieste . . . 42
3.1.1 What was planned for this period? . . . 42
3.1.1.1 MPGD sensors of single photons at INFN Trieste . . . 42
3.1.1.2 New Photocathode Materials development at INFN Trieste . . . 42
3.1.2 What was achieved? . . . 42
3.1.2.1 MPGD sensors of single photons at INFN Trieste . . . 42
3.1.2.2 New Photocathode Materials development at INFN Trieste . . . 49
3.1.3 What was not achieved, why not and what will be done to correct? . . . 51
3.1.3.1 MPGD sensors of single photons at INFN Trieste . . . 51
3.1.3.2 New Photocathode Materials development at INFN Trieste . . . 51
3.1.4 What is planned for the next funding cycle and beyond? . . . 51
3.1.4.1 MPGD sensors of single photons at INFN Trieste . . . 51
3.1.4.2 New Photocathode Materials development at INFN Trieste . . . 52

3.2 Optical Elements - SBU . . . 52
3.2.1 What was planned for this period? . . . 52
3.2.1.1 Large mirrors development at Stony Brook . . . 52
3.2.1.2 New Radiator Studies at Stony Brook . . . 52
3.2.2 What was achieved? . . . 52
3.2.2.1 Large mirrors development at Stony Brook . . . 52
3.2.2.2 New Radiator Studies at Stony Brook . . . 52
3.2.3 What was not achieved, why not and what will be done to correct? . . . 53
3.2.3.1 Large mirrors development at Stony Brook . . . 53
3.2.3.2 New Radiator Studies at Stony Brook . . . 53
3.2.4 What is planned for the next funding cycle and beyond? . . . 54
3.2.4.1 Large mirrors development at SBU . . . 54
3.2.4.2 New Radiator Studies at Stony Brook . . . 54

4 Critical Issues **54**
4.1 Brookhaven National Lab . . . 54
4.2 Florida Tech . . . 54
4.3 INFN Trieste . . . 54
4.4 Stony Brook University . . . 54
4.5 Temple University . . . 55
4.6 University of Virginia . . . 55

5 Additional information **55**
5.1 Temple University . . . 55

6 Manpower **56**
6.1 Brookhaven National Lab . . . 56
6.1.1 Total manpower effort for MPGD R&D . . . 56
6.1.2 Manpower effort for eRD6 R&D . . . 56
6.2 Florida Tech . . . 56
6.3 INFN Trieste . . . 57
6.4 Stony Brook University . . . 57
6.5 Temple University . . . 57
6.6 University of Virginia . . . 58

7 External Funding **58**

7.1 Brookhaven National Lab . . . 58
7.2 Florida Tech . . . 58
7.3 INFN Trieste . . . 58
7.4 Stony Brook University . . . 58
7.5 Temple University . . . 58
7.6 University of Virginia . . . 58

8 eRD6 New R&D Proposal for FY20 **59**
8.1 Development of Outgas Test System at Temple University . . . 59

9 eRD6 Budget Request for FY20 **60**
9.1 Overall Budget Request and Money Matrix . . . 60
9.2 Budget Request by Institute . . . 60
9.2.1 BNL Budget Request for FY20 . . . 60
9.2.2 Florida Tech Budget Request for FY20 . . . 60
9.2.3 INFN Budget Request for FY20 . . . 61
9.2.4 SBU Budget Request for FY20 . . . 62
9.2.5 TU Budget Request for FY20 . . . 62
9.2.6 UVa Budget Request for FY20 . . . 63

A List of all EIC publications from the eRD6 Consortium **65**

1 Brief overview of project histories and the document structure

The overall main focus of the R&D conducted by the eRD6 consortium has been the development of micro-pattern gas detectors (MPGD's) for tracking and particle identification at a future EIC. Some particular emphasis has been given to applying GEM technology in this context. While each institution has been focusing on certain technical aspects, much synergy has been produced with several collaborative efforts created over the years. For central tracking, BNL, Stony Brook, and Yale have been mounting a long-term investigation of GEM-based TPCs, while more recently Florida Tech, Temple U., and U. Virginia have teamed up to study the potential for a fast central tracker based on μRWELLs with support also from BNL. The latter three groups have previously also closely collaborated on the design, production, and testing of large GEM detector for the forward tracker. They jointly designed GEM foils for forward tracker prototypes that could be used by each group and they have conducted beam tests together at Fermilab. The PID effort was spearheaded and is continued by Stony Brook with a focus on optical elements, which more recently is being complemented by the INFN Trieste efforts on MPGD-based photon detection. The entire group meets bi-weekly to discuss progress and problems and to coordinate efforts. In addition, a smaller subgroup meets regularly on simulation efforts.

Following the recommendation from the review committee in its Jan 2019 report, we have reorganized the structure of this research report to better reflect this internal collaboration within our consortium. Instead of each group reporting all their findings, concerns, and plans separately, we now organize the report by technical topic with each institution reporting its contribution to each topic in the corresponding section. We hope that this will present a more cohesive picture of the overall joint R&D activities of our consortium.

1.1 Brookhaven National Lab (BNL)

The group at BNL is mainly engaged in optimizing micro-pattern gaseous detectors (MPGD's) for reading out a time projection chamber (TPC) for use at the EIC.

Over the last few years we have built and tested numerous planar GEM detectors with long (˜16mm) and short (˜3mm) drift regions and have equipped them with both zigzag pad and strip readout geometries in an effort to study the spatial and angular resolution of a host of detector configurations. The results of these efforts were published in a peer reviewed journal in 2014[1].

In addition, in collaboration with Stony Brook U. and Yale U., we have built a prototype combination TPC-Cherenkov (TPCC) detector to study the feasibility of performing tracking and pID measurements in a common detector volume. The results from these tests were positive and are detailed in a recently completed manuscript that was submitted to the peer review journal, IEEE TNS for publication[2].

More recently we have focused on optimizing the design of the readout plane for a GEM detector made of zigzag shaped charge collecting anodes. We performed both simulations and test beam measurements to study which geometrical parameters of the zigzag drive the performance of the readout. The results of these investigations were recently published in a peer review journal [3], with collaborators from Florida Tech and Stony Brook U.

Our focus is now primarily on investigating various avalanche technologies for a TPC readout including GEM's, Micromegas, a combinations of the two, and μRWELL. This includes finding optimal zigzag parameter sets for the readout of each avalanche scheme, which can be very different than what was studied in the past. It must be noted, however, that the effort to optimize the readout is not covered under the purview of this R&D program, but rather under a separate BNL funded LDRD grant. Nonetheless, we will briefly report on the zigzag R&D since the readout is a fundamental aspect of the detector.

1.2 Florida Institute of Technology (Florida Tech)

The Florida Tech group initially focused on the development of large low-mass GEM detectors with low channel count for the forward tracker (FT) of the EIC detector. In the last funding cycle the group begun shifting focus towards R&D on cylindrical μRWELL detectors for a fast central tracker at an EIC detector.

We designed and implemented radial zigzag strips on large readout PCBs to achieve low-channel count while maintaining good spatial resolution. We constructed a first one-meter-long prototype with such a readout at Florida Tech using a purely mechanical construction technique without any gluing and tested it in beams at Fermilab in 2013. This study showed a non-linearity in the position measurement of hits[4]. We subsequently tested small PCBs and a flex-foil with the improved zigzag strip design with highly collimated X-rays at BNL. A substantial reduction in the non-linearity and an improvement in spatial resolution were observed[5].

Next, we designed a second large Triple-GEM detector that implements the drift electrode and a readout electrode with radial zigzag strips on polyimide foils rather than on PCBs to reduce the material in the active detector area[6]. To provide rigidity to this new detector while maintaining low mass, we produced the main support frames from carbon fiber material. We designed the GEM foils for this second detector so that they could also be used for the second UVa FT prototype ("common GEM foil design"). Initial assembly of this second prototype showed that 3D-printed pull-out and frame components made from ABS did not have sufficient material strength to sustain the mechanical forces needed for stretching. They were consequently replaced by stronger PEEK components and the detector was reassembled from scratch. Over the last year, we added a simulation component to the forward tracker work. For the cylindrical μRWELL, we began preliminary studies with a small planar detector last year. This year, we produced a first conceptual hardware design for a full-size cylindrical μRWELL tracker based on a purely mechanical detector assembly.

1.3 INFN Trieste (INFN)

The task of the INFN participants to the eRD6 Consortium is "Further development of hybrid MPGDs for single photon detection synergistic to TPC read-out sensors".

Particle identification of electrons and hadrons over a wide momentum range is a key ingredient for the physics programme at EIC. One of the most challenging aspects is hadron identification at high momenta, namely above 6-8 GeV/c, where the only possibility is the use of Cherenkov imaging techniques with gaseous radiator. The overall constrains of the experimental set-ups at a collider impose a limited RICH detector length and to operate in magnetic fringing field. The use, for this RICH, of gaseous photon detectors is one of the most likely choice. The goal of our project is an R&D to further develop MPGD-based single photon detectors in order to establish one of the key components of the RICH for high momentum hadrons. This R&D has also some aspects synergistic to the development of TPC sensors: the miniaturization of the read-out elements and the reduction of the Ions Back-Flow (IBF).

The starting point are the hybrid MPGD detectors of single photons [7], developed for the upgrade of the gaseous RICH counter [8, 9, 10, 11] of the COMPASS experiment [12, 13] at CERN SPS. They consists in three multiplication stages: two THick GEMs (THGEM) layers, the first one coated with a CsI film and acting as photocathode, followed by a resistive MicroMegas (MM) multiplication stage. The anode plane is segmented in pads with size 8×8 mm^2. The resistive MM has an original implementation: it is by descrete elements, namely a resistor in series with each pad. The COMPASS photon detectors can operate at gains of at least 3×10^4 and exhibit an IBF rate lower at the 3% level.

The present R&D project develops over several years and it includes further improvements of the hybrid MPGD-based photon detectors in order to match the requirements of high momenta hadron identification at EIC and initial tests relative to the application in gaseous detectors of a novel photocathode concept, based on NanoDiamond (ND) particles [14].

1.4 Stony Brook University (SBU)

SBU is concentrating on the study of Ion Backflow (IBF) for a TPC, a possible candidate for the central tracker in at least one of the detectors for an EIC. Furthermore, the TPC for sPHENIX has the same physical size when used in, e.g., the BeAST EIC detector.

It has been shown that IBF will pose a problem in an EIC detector and that the ultimate EIC TPC device must do more than sPHENIX to achieve the same level of position distortion. Our approach is to investigate new structures in and around the multiplication stage that promise significant better performance when considering IBF.

SBU is finalizing the installation of a unit that allows to produce high quality large size mirrors for RICH applications.

SBU has furthermore proposed to investigate the feasibility of meta-materials for use in possible applications in Cherenkov imaging detectors.

1.5 University of Virginia (UVa)

The initial R&D focus of UVa group was on the development of high performance, low mass GEM detector for the forward tracker of an EIC detector. In the last cycle, our focus has shifted towards the development of cylindrical μRWELL technologies for the fast tracker in the central region of an EIC detector.

Two large GEM prototypes with high granularity two-dimensional (2D) U-V strip readout were designed, built and successfully tested at the Fermilab Test Beam Facility (FTBF) in 2013 and 2018. The excellent spatial resolution in both radial and azimuthal direction have been demonstrated for the two prototypes and results of the first prototype were published in [15]. The analysis is ongoing for the second prototype with improved U-V strip readout design for better spatial resolution in both directions.

Though UVa group mainly concentrated on the development of fine structure 2D U-V strip readout, our R&D effort had strong synergies with the ongoing activities with Florida Tech and Temple U. groups. The second UVa large prototype was the fruit of a collaborative effort by the three institutes to develop a "Common EIC GEM foil" to be used in the assembly of three large GEM prototypes (one per institute), each prototype built with a different readout structure and assembly technique. In addition, we are characterizing thin layer chromium GEM (Cr-GEM) foils that, we anticipate, could be used in low mass GEM detectors.

More recently, our R&D effort has shifted towards the characterization of a small planar 2D strip μRWELL prototype as pre-R&D for the fast signal cylindrical μRWELL detector in the central region of EIC detector. We report here, the preliminary results of the extensive and detailed characterization of the prototype.

1.6 Temple University (TU)

Temple University's (TU) initial R&D efforts have been centered around the assembly and characterization of triple-GEM detectors which include commercialized 2D readout, HV, and single-mask GEM foils. The focus of the eRD3 program was a joint R&D effort between TU and the company Tech-Etch, with the ultimate goal of Tech-Etch manufacturing commercially available large area 2D readout, HV, and single-mask GEM foils. This effort also lead to the highly successful large area CCD scanner, which was built to assess the overall geometric properties of the GEM foils as they were produced by Tech-Etch. The GEM CCD scanner has since provided service to the larger MPGD community such as scanning UVa's chromium GEMs, the BoNuS experiment's GEMs, and $\sim$ 1 m long GEMs for the company Mecro. TU is still supporting and maintaining the GEM scanner and its services are available for use. This R&D work was carried over to eRD6 with the eRD3 + eRD6 merger and is now effectively completed.

All commercial triple-GEM detectors, which were built using the STAR FGT [16] design to keep costs down,

have now been assembled. The majority of the GEM foils supplied by Tech-Etch turned out to be rather poor quality and ended up not being able to fully characterize the detector to our satisfaction. We are actively seeking other funding sources to purchase components supplied by CERN or another reliable commercial vendor to finish and publish these studies.

In parallel to the commercial GEM project, we are also investigating the use of Kapton spacer rings as a replacement to the more traditional G10 spacer grids that are used between GEM layers to keep the foils from sagging. In fact several of the commercial triple-GEM detectors have been built using the Kapton spacer rings. We plan to continue investigating this by making use of equipment that was purchased through a funded SBIR proposal in collaboration with Triton systems ("Direct Write Fabrication of Low Cost Flexible Particle Detector Substrates") (Sec. 5.1).

TU is working with FIT and UVa to develop a cylindrical μRWELL central detector which operates in a μTPC mode. TU has thus far been focusing on the simulation of the detector within the EicRoot framework. Our simulation allows one to easily adjust detector properties and responses. Using measurements from INFN's μRWELL μTPC prototype [17]) we have begun to investigate the momentum resolution. However, the detector response still needs to be made more realistic and would greatly benefit from data acquired from a μRWELL detector operating as a μTPC. These measurements could then be fed into the simulation.

2 Tracking

2.1 Central Tracker

In its Jan 2019 report, the review committee stated that *"the collaboration is encouraged to continue developing the TPC readout with different electronics and studying the Micromegas and μRWELL with zigzag readout in a planar detector configuration"* and that *"further studies of a cylindrical μRWELL barrel layer to act as a fast-tracking layer in a non-TPC EIC detector are strongly encouraged."* The committee also recommended that *"(the μRWELL) efforts between the various institutions should be coordinated."*

We have been following these recommendations closely with respect to the technical developments as detailed below. We have also continued to coordinate the μRWELL efforts with Fl. Tech focusing on the conceptual design of a barrel tracker with cylindrical μRWELLs following guidance from simulation work that the Temple group is currently focusing on. Temple in turn has incorporated measurements from the INFN μRWELL μTPC prototype into the simulation. Meanwhile, UVa has been making strides on the hardware and successfully tested a planar 10 cm $\times$ 10 cm μRWELL detector and sharing their experience with the other groups.

2.1.1 What was planned for this period?

2.1.1.1 TPC studies at Brookhaven National Lab

The goals for the last funding cycle are listed below:

1. Tune the performance of the 4-layer, GEM-based tracking telescope to effectively measure cosmic tracks with high resolution for the purpose of studying tracks reconstructed with the prototype TPC.
2. Study track reconstruction in the TPC prototype.
3. Read out the TPC with different front end electronics (i.e., SAMPA and DREAM) and attempt to evaluate the performance of each case.
4. Study Micromegas and μRWELL with zigzag readout in a planar detector configuration (ie, short drift gap).

5. Continue work on optimizing the design and production of zigzag readouts in parallel with the eRD6 R&D program.

2.1.1.2 TPC studies at Stony Brook

Planned efforts at SBU were to continue the investigation of IBF blocking structures to be used in an MPGD-based readout structure for a TPC. In particular, the concept of a passive gating grid is in the focus of our investigations.

2.1.1.3 Cylindrical μRWELL studies at Florida Tech

We planned to commission the $10\times10\,\mathrm{cm}^2$ μRWELL prototype with zigzag-strip readout and to characterize its performance using X-rays. We also planned to begin the design of the first prototype for a cylindrical μRWELL detector.

2.1.1.4 Cylindrical μRWELL studies at TU

Simulation Results

The cylindrical μRWELL simulation study looks at replacing a TPC with a series of cylindrical μRWELL detectors operating in μTPC mode. Additionally, a cylindrical μRWELL could also be used in addition to a TPC to provide a fast tracking element. There were several key goals identified for this funding cycle:

1. Develop machinery to simulate a μTPC detector, where dead material, gas, drift gap size, hit points, and resolution parameters can be easily adjusted.
2. Use data to implement realistic detector responses. Including the number and resolution of dE/dX measurements based on the angle the track enters the detector, and spacial resolutions in the longitudinal and transverse directions.
3. Once the detector is fully simulated this and the forward MPGD simulation work being done by FIT can be integrated into one cohesive tracking simulation.

2.1.1.5 Cylindrical μRWELL studies at UVa

R&D on μRWELL detector technology: Continue the work on the design of a small cylindrical μRWELL detector with FIT and TU. Procure a second 10 cm $\times$ 10 cm prototype with the R&D focus on low mass and high resolution 2D readout strips patterns. We will also continue the study and characterization of our current small prototype and most importantly the performance of this new technology in high particle rate environment.

2.1.2 What was achieved?

2.1.2.1 TPC studies at Brookhaven National Lab

Beam test of MPGD-based gain stages: We performed a beam test last March to study and compare the performance of 4 different MPGD-based avalanche schemes for possible use in a TPC. As part of an initial evaluation, each detector was tested in a simple planar configuration to gauge each avalanche technology coupled to a zigzag readout. As seen in Fig. 1, the test apparatus consisted of a specially designed mounting fixture that simultaneously positioned 8 detectors, back-to-back in the beam. Each detector layer consisted

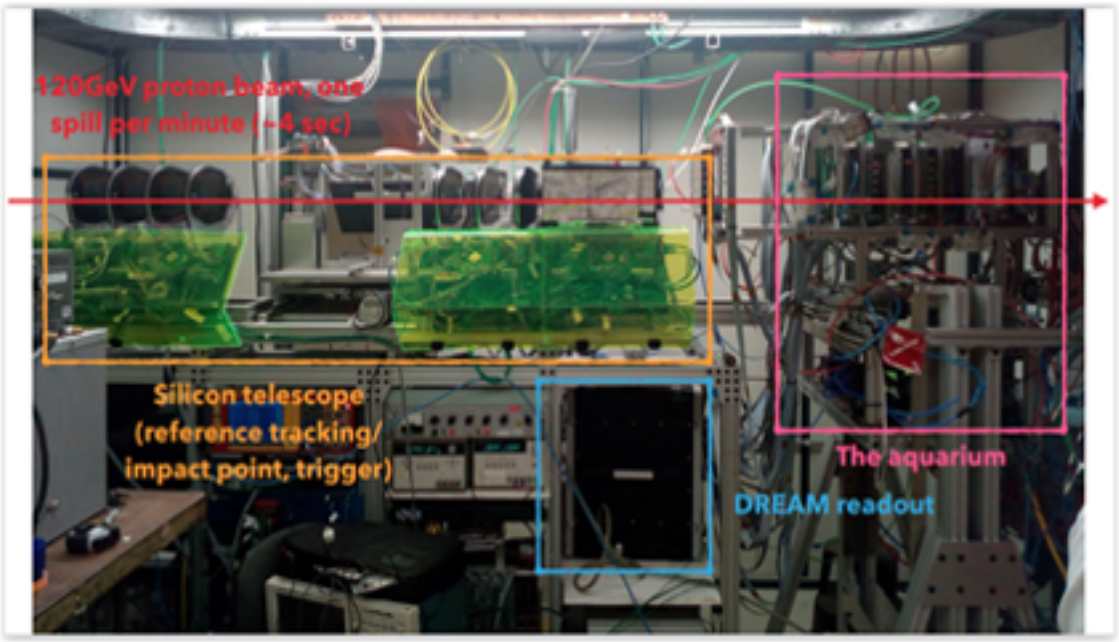

Figure 1: Picture of test beam setup at the Fermilab Test Beam Facility. The mounting fixture apparatus on the right-hand side, referred to as the "aquarium" holds 8 detector layers in the beam and a XY-stage precisely translates the apparatus in the beam.

of either a GEM, Micromegas, μRWELL, or GEM-Micromegas hybrid detector (Fig. 2). The read-out PCB used for each detector is similar to the "multi-zigzag" PCB described in previous reports (Fig. 3), where 100 different zigzag patterns fill a 10 x 10 array of readout cells. In addition, each detector was read out with the DREAM front end electronics, which allowed us to evaluate the suitability of these electronics for a TPC as well.

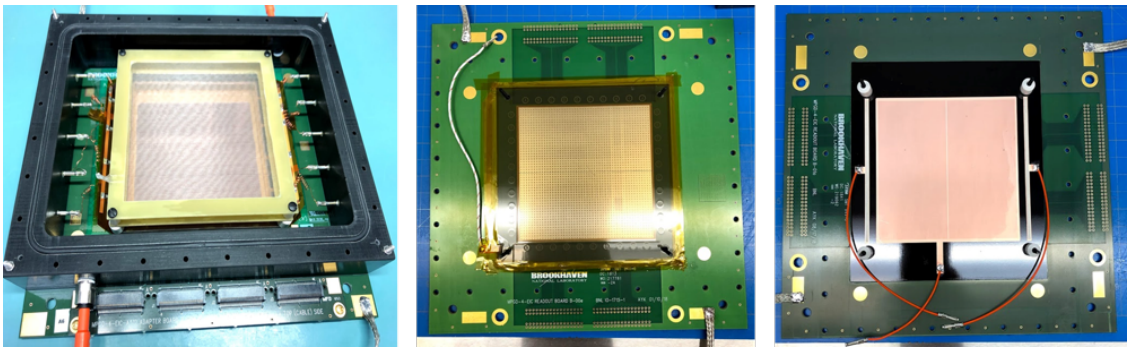

Figure 2: A GEM, Micromegas, and μRWELL detector, respectively.

The mounting fixture was placed in the primary 120GeV proton beam at the FTBF (Fig. 1) for the purpose of measuring the position resolution of each detector across a range of zigzag patterns. The mounting fixture was in turn mounted to a specially designed precision XY-movable stand such that all detector layers were translated in a plane orthogonal to the beam axis. This allowed the beam to scan across all eight detector chambers simultaneously, thereby allowing a multitude of zigzag geometries to be studied with multiple avalanche schemes and detector configurations in a single setup.

Just upstream of this setup a high precision silicon tracking telescope was used to measure reference particle tracks for the purpose of measuring the position resolution. Some preliminary results from the beam test

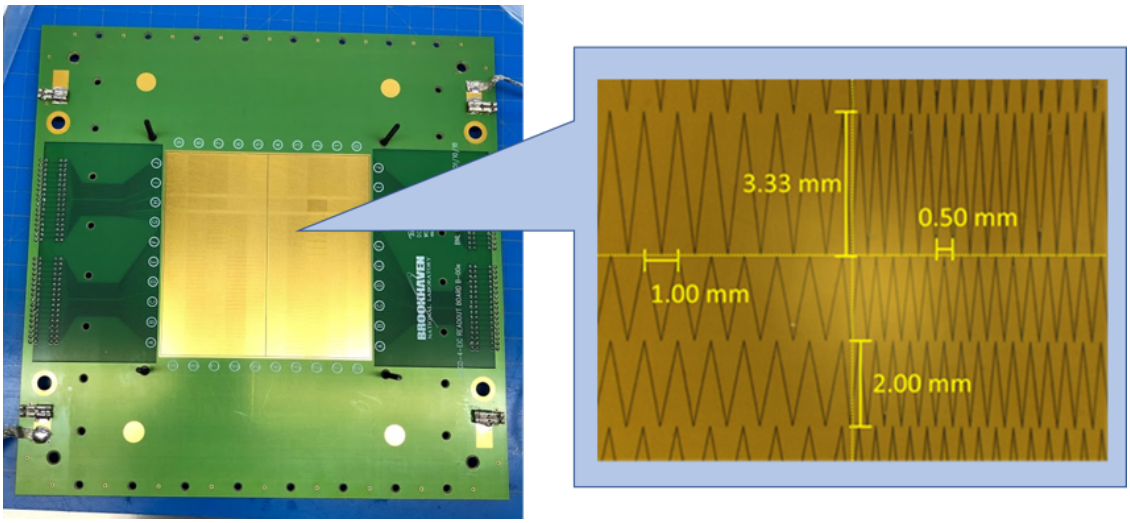

Figure 3: "Multi-zigzag" PCB with different zigzag patterned charge collecting anodes, arranged in an array of 10 x 10 1cm x 1cm cells.

are shown below in Fig. 4 for a particular range of zigzag parameters. A charge weighted mean of the fired strips (or centroid) was used to calculate a position residual with the extrapolated position of the silicon track. A Gaussian fit to the residual distribution was then used to determine the position resolution obtained from each zigzag pattern. Fig. 5 shows an example of a residual distribution fit to a Gaussian and a scatter of the x-residuals versus the x-coordinate. The position resolution versus the degree of zigzag interleaving (or "stretch") is compared for the three different avalanche schemes and shows a relatively similar response, which is an interesting result considering the different ways the charge cloud evolves in each case. The ultimate goal of this study is to find the optimal zigzag parameter set that maps to a minimum in the resolution, however the analysis is not yet fully complete. Upon the completion of this analysis, the results will hopefully be accepted for a presentation at the 2019 IEEE NSS conference.

A total of 4096 DREAM front end electronics channels acquired data from this apparatus, at a data taking rate of almost 10kHz. A 20MHz ADC digitized the analog waveform over 15 samples and a zero suppression threshold was set between 3-5 sigma above the noise level. The input capacitance capability of these electronics makes them suitable for use with the zigzag pads and the relatively large dynamic range of the front end maintains the signal integrity at fairly high gain (˜5000) with a signal to noise at the 1% level. Ultimately, because of these specifications, it was found that this front end electronics option would likely be a viable candidate for a TPC application.

Prototype TPC measurements in the lab: Our mini-TPC prototype was read out on the bench using the SAMPA front end electronics (Fig. 6). The front end card contains 8 32-channel SAMPA chips and was designed in house by engineers in the BNL instrumentation dept. It features a 20MHz ADC, with a analog front end with a 160ns shaping time, around 10μsec memory depth, a fairly large dynamic range and is capable of a streaming readout, making it ideal for a TPC application. We tested a total of 512 channels connected to zigzags with a 2mm pitch, 0.5mm period and a zero stretch parameter in a 4-GEM setup coupled to a field cage with a 10cm drift distance.

Initially the detector was tested with a UV laser beam. UV photons ionize impurities in the gas via a 2-photon process and are capable of generating relatively large amounts of primary charge to approximately mimic the passage of a MIP through the gas. The laser beam enters the field cage via a port at the top (Fig. 7) and exits from a similar port on the opposite side, where a photo-diode measures the light output to provide a fast trigger. After the primary charge drifts to the GEM and is amplified, it is collected onto the pads, as seen in the hit map measurement in the left panel of Fig. 8. In addition, the laser allows for a convenient way to measure the drift velocity of the gas, which was found to be 7.3μsec. (right panel of

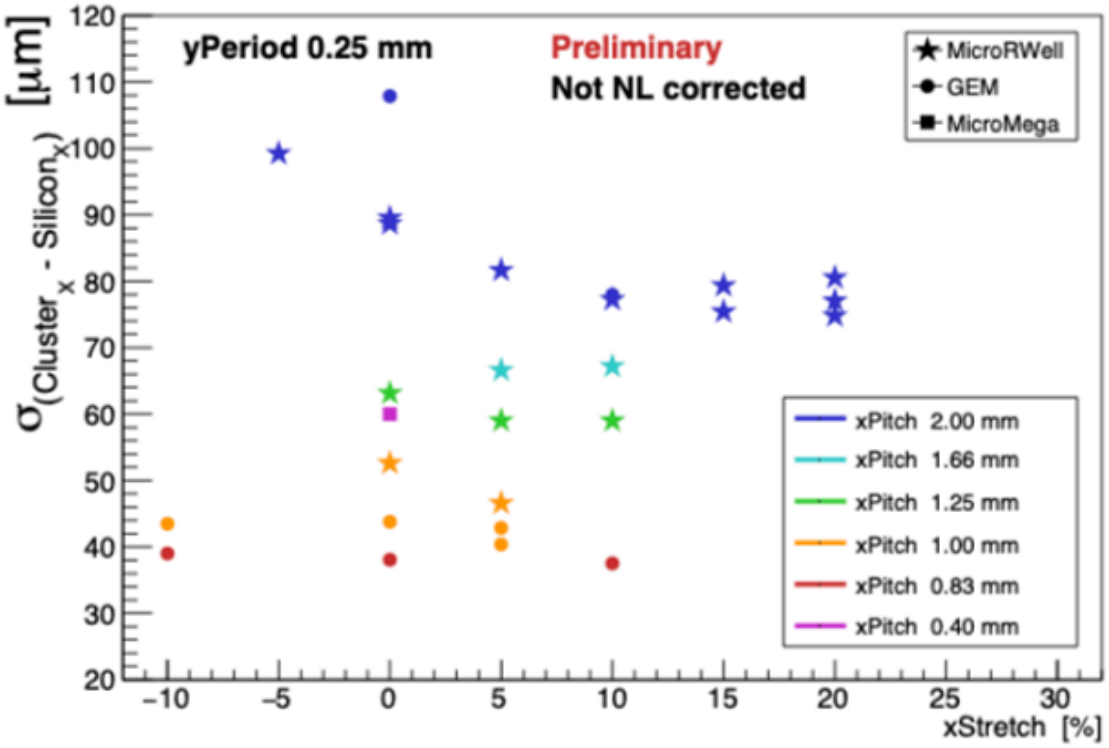

Figure 4: Resolution vs. stretch parameter for a GEM, micromegas, and μRWELL detector.

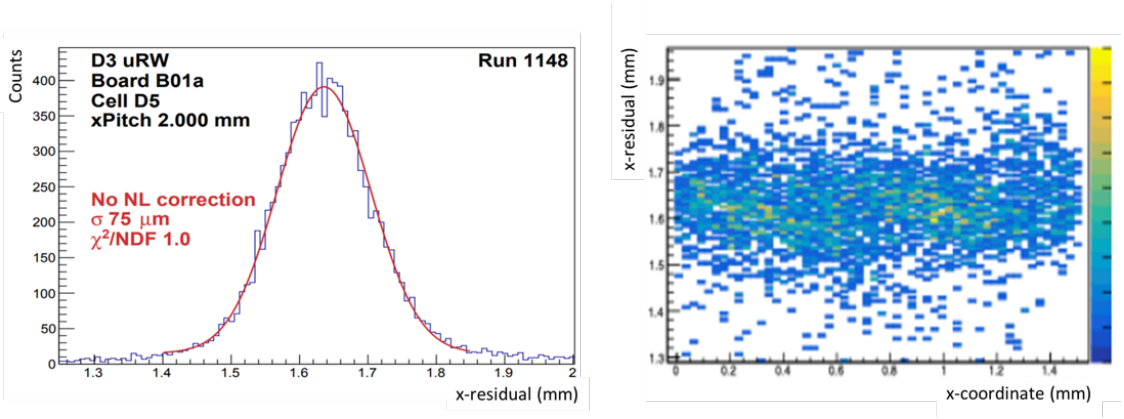

Figure 5: Left: Residual distribution for a zigzag pitch of 2mm, stretch of 15%, and period of 0.5mm; Right: the x-residual scatter for the same cell.

Fig. 8), as expected according to the literature. Finally, a cosmic trigger was formed from the coincidence of three paddle scintillation counters to allow the prototype to capture the signal from cosmic ray tracks. An example of a cosmic ray track measured with the SAMPA is shown in Fig. 9, which is a first step in demonstrating the viability of this incarnation of the SAMPA electronics as a candidate for a TPC.

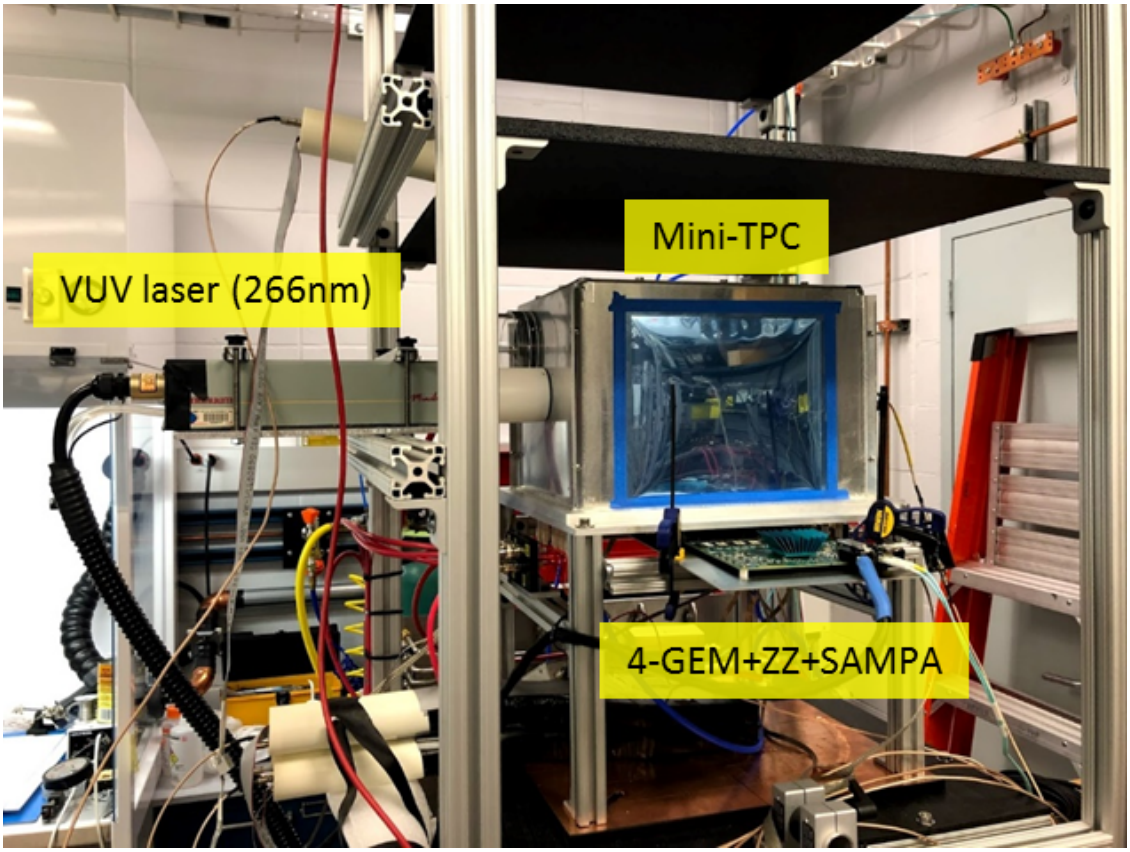

Figure 6: TPC prototype with 4GEM gain stage, zigzag readout, and SAMPA front end electronics. A UV laser beam is used to generate a straight line of ionization in the gas volume.

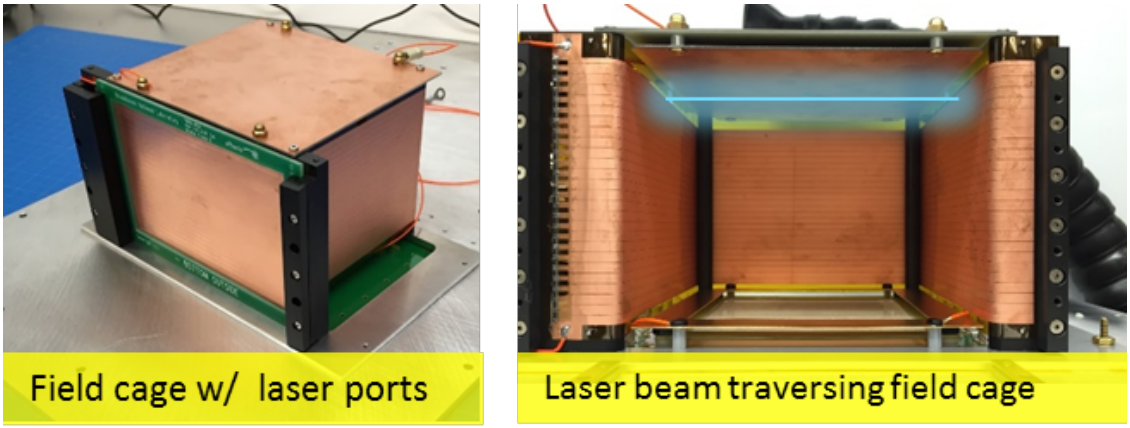

Figure 7: Left: The TPC field cage structure. Right: the laser beam enters the field cage through ports at the top.

2.1.2.2 TPC studies at Stony Brook

In previous TPC applications the problem of charge pile-up due to ion-back-flow (IBF) has been resolved by active gating grids. These grids were actively supplied with a potential over a wire grid that forced ions from the amplification process drifting into the drift volume to be attracted and removed. However, electrons

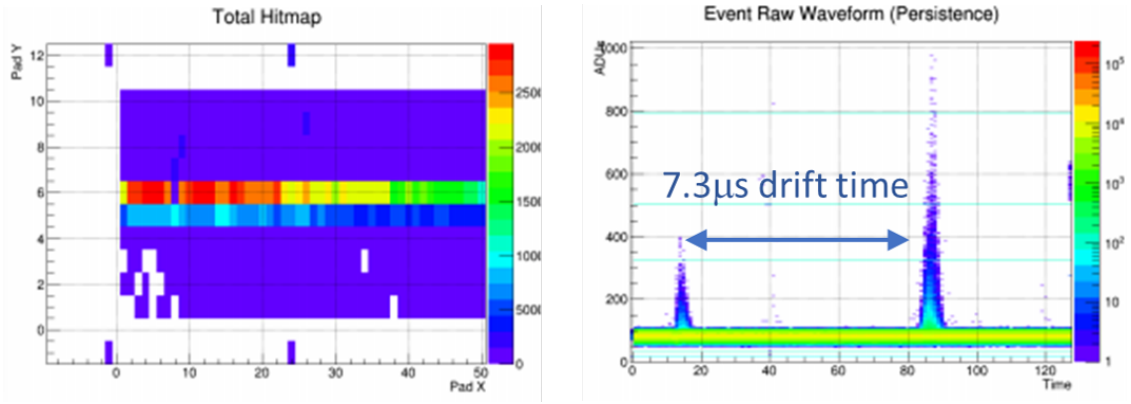

Figure 8: Left: The straight line of ionization from the laser beam is amplified and collected onto a single pad row of zigzags. Right: The drift time measured using digitized waveforms from the SAMPA electronics.

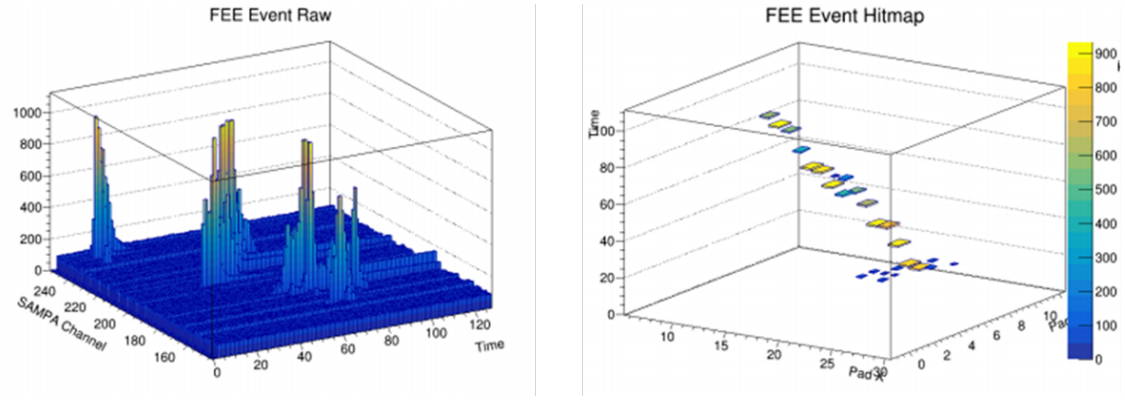

Figure 9: Left: Digitized waveforms of SAMPA electronics from cosmic ray signals. Right: reconsructed cosmic ray in TPC prototype using SAMPA electronics.

suffer the same fate, hence, this procedure can only be applied at certain periods in time which makes the whole a slow readout device. To overcome this limitation a passive grid design has been investigated (Fig. 10). This grid will be permanently powered and should provide a way to attract positively charged ions but leaving the path of electrons unaffected when immersed in a magnetic field,. Another option is to arrange for a grid of wires separated from each other and apply a constant bias voltage between them (bi-polar grid). The effect of the gating can be seen in Fig. 11.
A set of designs have been created and investigated and a promising result can be seen in Figs. 12. In parallel, IBF measurements have been performed with a CF_4 based gas mixtures. The data are being analyzed.

2.1.2.3 Cylindrical μRWELL studies at Florida Tech

Planar 10 cm $\times$ 10 cm μRWELL prototype: The small μRWELL prototype was assembled from the kit previously received from CERN. There are some issues with gas tightness, but despite much effort we have been unable to pinpoint the location of the leak(s) so far. The detector was tested successfully under HV in pure CO_2 without any issues observed.

Conceptual Design Studies for a Full-size Cylindrical μRWELL Tracker: Several design iterations for a cylindrical μRWELL detector were produced with AutoDesk Inventor. Here we discuss only the most recent iteration. The main design principle applied is to place all structural support elements at the end and

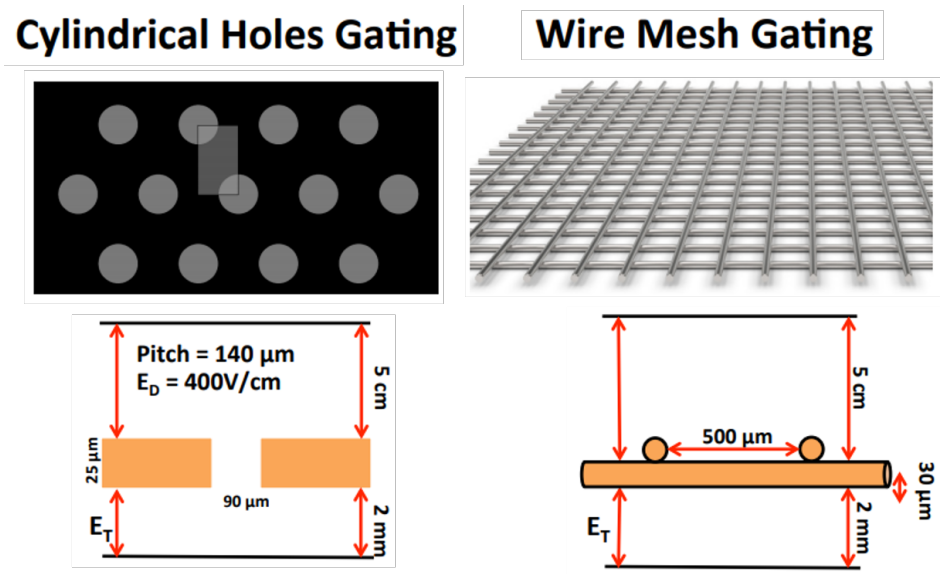

Figure 10: Two different types of passive meshing gates. The upper row depicts the general setup and the lower row the setup with parameters used for simulations. Left: polymer foil with thin copper layer and cylindrical hole pattern, similar to a GEM. Right: interwoven wire mesh, similar to a MicroMeGas.

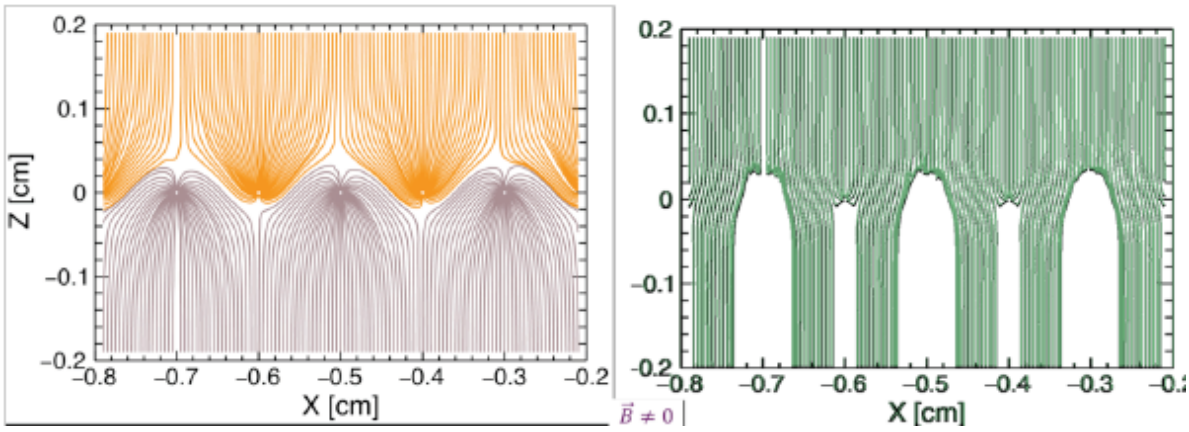

Figure 11: Drift lines for ions and electrons in a bipolar gating grid. Left: yellow lines represent the electrons drift lines, brown lines the ion drift lines, without the magnetic field. Right: electron drift lines with magnetic field turned on.

the outside of the detector while the active detection volume is formed only from thin foils to ensure low multiple scattering in the detector material. The radial dimensions in all designs are based on the preliminary size parameters used in the Temple U. simulations (see below). The designs comprise six complete concentric cylindrical μRWELL detectors; the foil radii are 225 mm for the inner cylinder, then 375 mm, 475 mm, 575 mm, 675 mm, and finally 775 mm for the outermost cylinder. A two centimeter drift gap is formed outside each of these radii with the addition of cylindrical drift foils. For design purposes, each μRWELL foil is modeled to be 50 microns, with another 50 microns for the diamond-like carbon (DLC) layer, and an additional 50 micron for a readout foil, which results in a 150 micron composite foil. The design takes physical constraints on foil sizes into account, specifically the requirement that the maximum width of the base material for all foils is 55 cm.

The primary structural component of the design is what we call the cylindrical stretching frame (Fig. 13

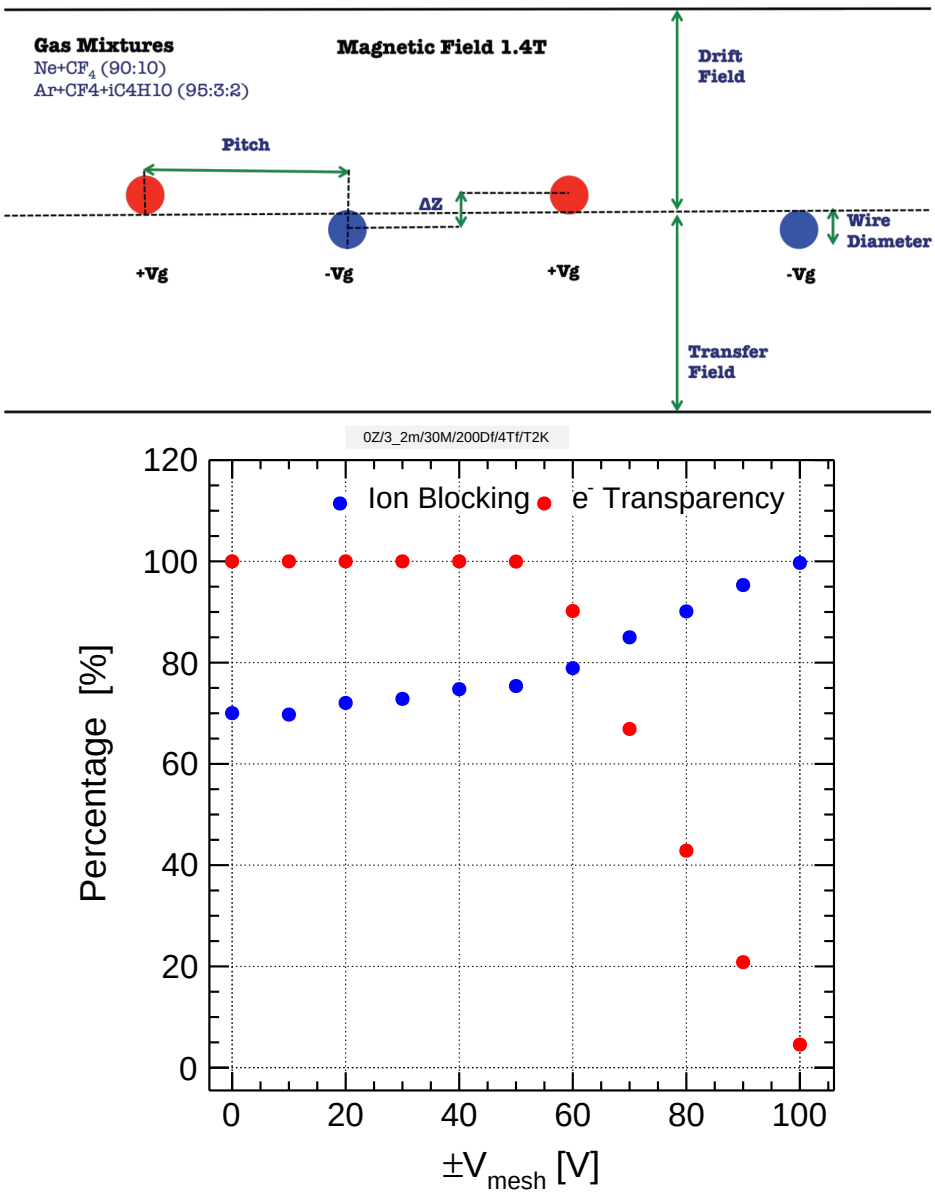

Figure 12: Simulation of ion blocking and electron performance of a static bipolar gating grid with T2K gas (Ar-CF_4-Isobutane 95-3-2). Top: principle of gating structure. Bottom: example of the performance of the bipolar gating grid. At ±60 V between the grid wires an ion blocking of ∼80% is achieved with an electron transmission of ∼90%.

left). This component comprises two carbon fiber rings of different sizes that sandwich a drift spacer made of a strong material such as metal or PEEK. Each carbon fiber ring and the drift spacer in turn sandwich the μRWELL foil and the drift foil, respectively. The readout foil in the μRWELL/DLC/readout composite is longer than the μRWELL and DLC foil and protrudes through the stretching frame to the outside. One of the two carbon fiber rings is longer than the other so that it can mechanically support the readout foil, the readout connectors, and the frontend readout electronics (Fig. 13 right). This assembly will be put at each end of the foils and will be screwed tightly together with radial screws to press the foils and frames together to form a gas volume. The faces of the drift spacers also contain axial holes for attaching axial stretching screws or rods on the outside such that the foils can be stretched simultaneously against fixed plates at each end of the cylinder (Fig. 14 (right)).

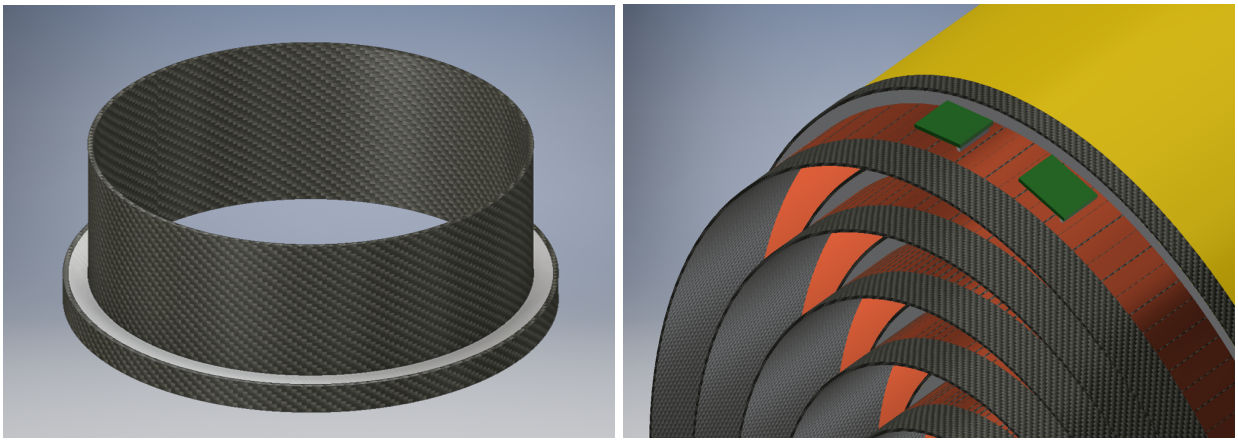

Figure 13: Left: Cylindrical stretching frame assembly of wide ring for readout foil and front-end electronics support (gray), thin ring for clamping drift foil (gray), and drift spacer frame (white). Right: Drift foil (yellow) and μRWELL/readout foils (copper color) sandwiched between frames. Green rectangles indicate potential positioning of front-end readout electronics.

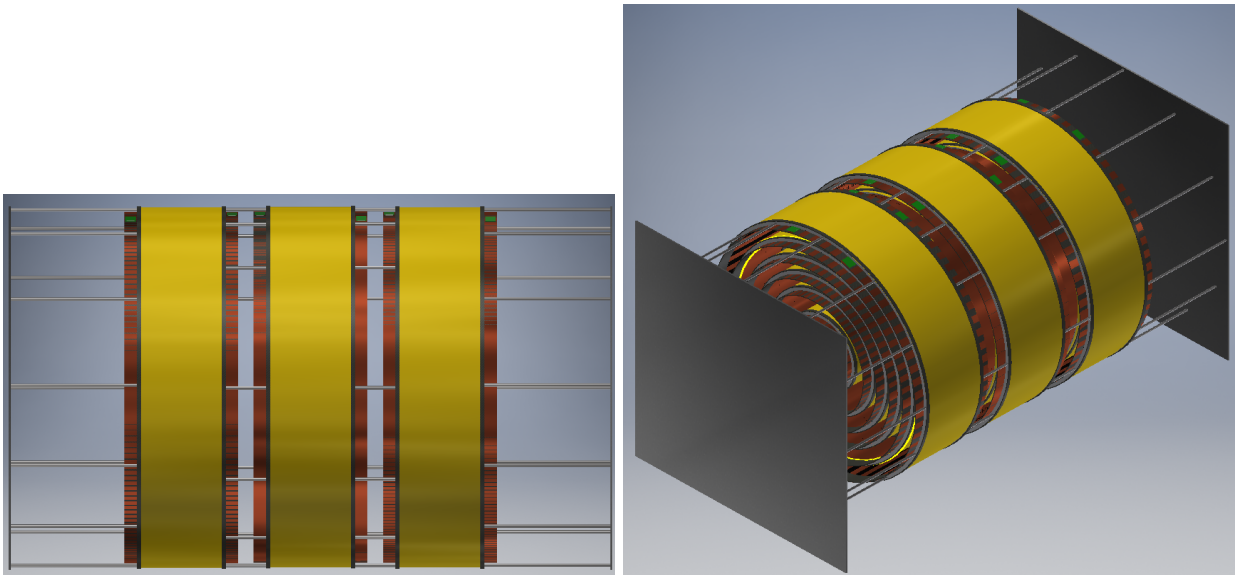

Figure 14: Left: Side view of tracker barrel design composed of three cylindrical μRWELL modules interconnected with thin rods that attach to the drift spacers. Right: Projected view of tracker barrel and endplates that the tracker cylinders would be stretched against. The outer diameter of the tracker barrel is approximately 1.6 m and the total length of the three segments is about 1.8 m.

The limiting factor for this design is the width of the foils. To overcome this, we increase the total length of the detector barrel by combining multiple full-sized sets of detectors together. Thin rods would be attached between two barrel segments to connect them. The current design features three sets of detectors connected together to form the full barrel tracker. The critical issue will be to figure out how to properly stretch all foils in this configuration, in particular for the central detector segment. For a configuration of three 55 cm long detector segments with 7.5 cm axial spacings between them, the detector coverage in pseudorapidity η is visualized in Fig. 15 (left); the number of detector layers traversed by tracks from the IP vs. η is plotted in Fig. 15 (right). Due to the $\approx$18 cm gap in z between the active detector elements in two adjacent barrel segments, the number of layers crossed by a track from the IP shows a severe drop near $|\eta| = 0.45$. In the next iteration of the design, we will attempt to minimize the gap and close this hole in the acceptance, e.g.

by radially staggering the detector layers in the different barrel segments.

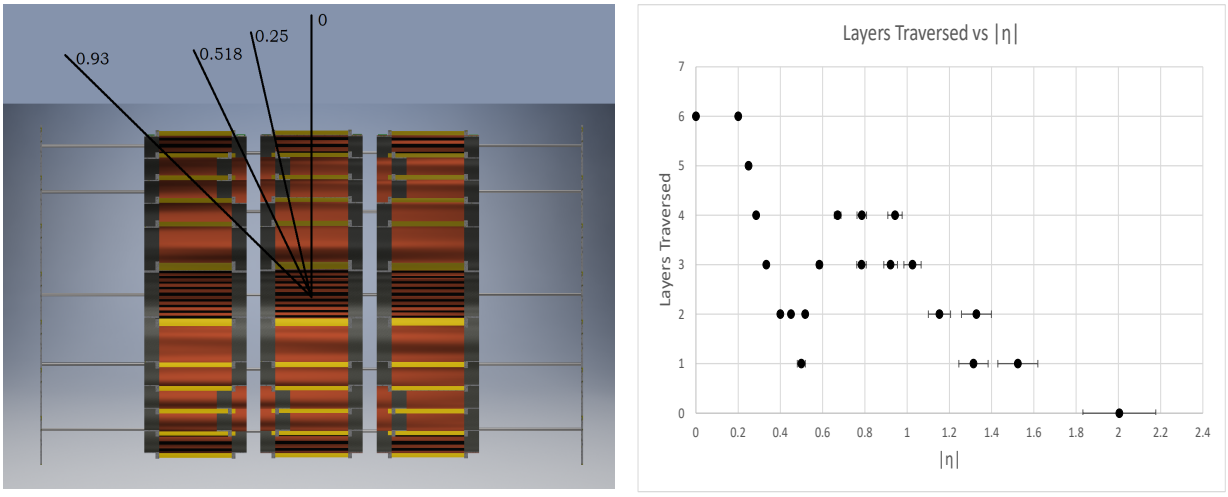

Figure 15: Left: Cross-sectional side view of μRWELL barrel tracker design showing the six detector layers. Black lines indicate pseudorapidity coverage by the detector. Right: Number of μRWELL layers traversed by tracks from the IP vs. η. The drop around $|\eta| = 0.45$ is due to the gap in z between barrel segments in the current design.

2.1.2.4 Cylindrical μRWELL studies at TU

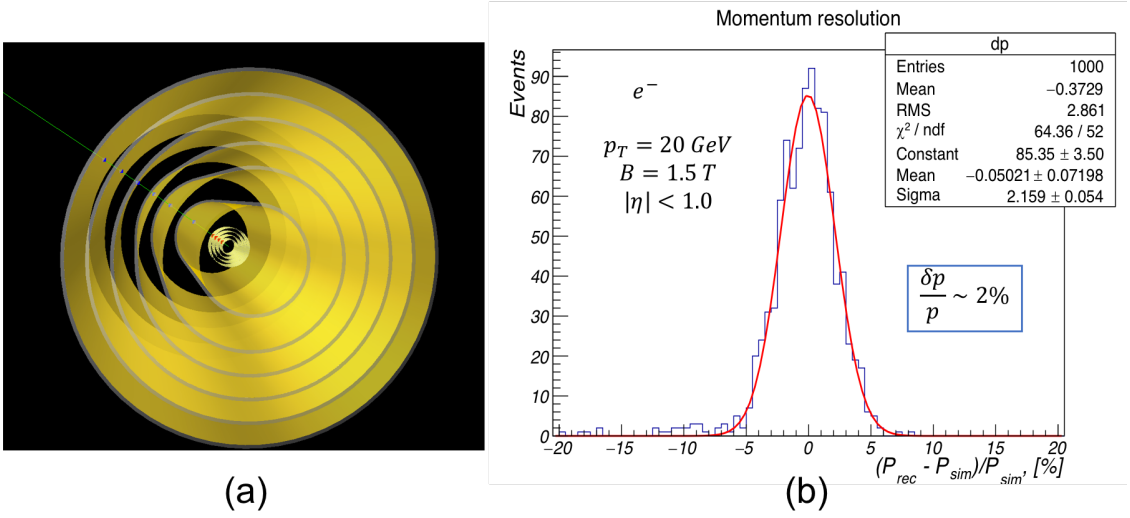

Figure 16: a: Cylindrical μRWELL simulation electron event display. The inner cylindrical layer (4) are the silicon vertex detector, while the outer 6 cylindrical layers represent the μRWELL detectors. The hit points used in the track fitting can be seen in each detector layer. b: The momentum resolution distribution for a 20 GeV electron in a 1.5 T magnetic field passing through the 4 silicon vertex and 6 cylindrical μRWELL detectors as described in the text.

The μRWELL simulation study has met some of the goals laid out for this funding cycle. We have successfully built a simulation framework where the amount of material making up the μRWELL detector, the size of the gas drift gap, the type of gas being used and the number of cylindrical μRWELL detectors can be easily varied.

The next goal of the cylindrical μRWELL simulation involves implementing realistic detector responses. When operating in the μTPC mode, we need to determine how many dE/dX measurements can be made in a given drift gap, what their respective resolutions are, and how they vary with the angle the track enters the detector. The current simulation has digitization in the longitudinal (beam-direction) and transverse directions. Both of these digitizations need realistic resolutions implemented based on the size and type of the gas drift gap used in the simulation. We have used the results from a prototype μRWELL μTPC that was built and tested by INFN [17], where they found an overall spatial resolution of around 100 μm over a range of track angles relative to the readout plane, as a way to assess an initial momentum resolution.

This initial simulation study used 6 low mass cylindrical μRWELL detectors where each detector had a radiation length of 0.17% + 15 mm ArCO2 (70:30) (0.01%) gas gap. The detectors ranged in radii from 225 - 775 mm. Each detector considered only one hit in the gas volume and used a resolution of 100 μm in the longitudinal direction and 100 μm in the transverse direction. Included with the 6 cylindrical μRWELL detectors, was 4 layers of a silicon vertex detector with a pixel resolution of 20 $\mu m\times$ 20 μm. The momentum resolution was then determined using 20 GeV electrons scattering over the range $|\eta| < 1$ in a 1.5 T magnetic field. The event display for one of the electron events can be seen in Fig. 16a, while Fig. 16b shows the $\sim$2% momentum resolution that is obtained.

2.1.2.5 Cylindrical μRWELL studies at UVa

The small planar μRWELL prototype on cosmic setup: We performed an extensive study of our

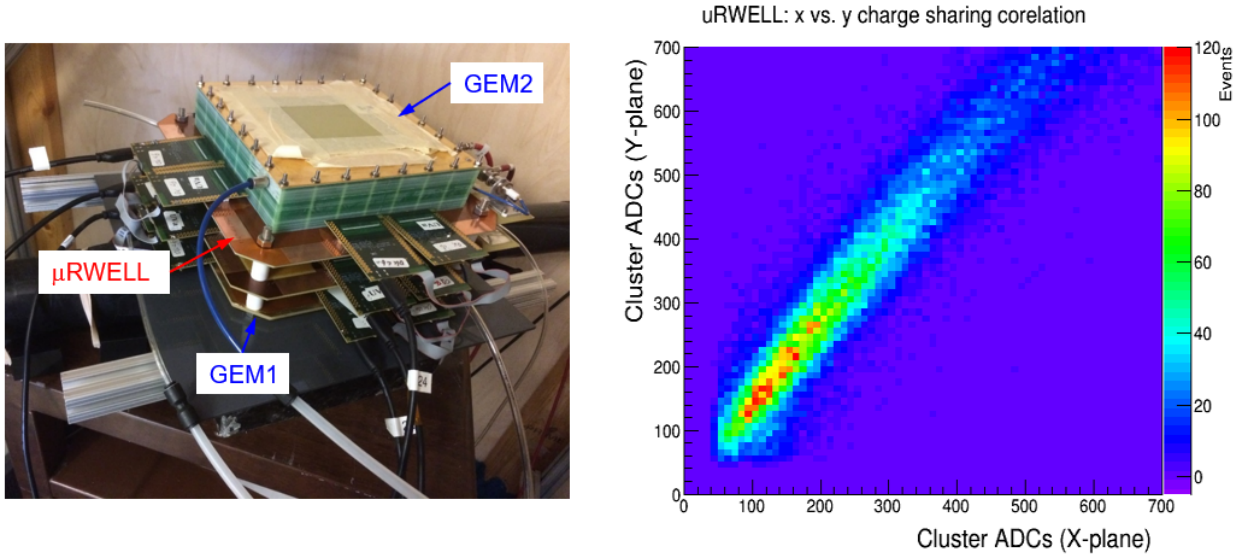

Figure 17: *Left:* Cosmic setup for the study of the small μRWELL prototype with 2D-strip readout. *Right:* Charge sharing correlation plot of the 2D-strip readout.

small (10 cm $\times$ 10 cm) planar μRWELL prototype with 2D strip readout in a month-long cosmic stand setup in the MPGD detector lab at UVa. The setup, as shown on the left picture of Fig. 17, consists of the μRWELL prototype sandwiched between two CERN standard Triple GEM detectors that we used for basic tracking information and for precise efficiency mapping of the μRWELL detector. All three detectors operated with an Ar/CO2 (70/30) gas mixture and were read out with our standard APV25-SRS readout electronics, triggered by an external scintillator / PMT installed underneath the detector stack. With the large amount of collected cosmic data, we were able to study the performances of the prototype as a function of the electric field in the drift region as well as in the μRWELL layer (which is the amplification device) of a μRWELL detector.

Performance of the new 2D-strip readout structure: The top strip layer of the "COMPASS 2D-strip readout", typically used in standard triple-GEM detectors and fabricated from the same base kapton material as for GEM foils, consists of a set of 5 μm thick Cu electrode strips sitting on top of an array of 80 μm wide and 50 μm thick kapton ridges with a pitch of 400 μm, chemically etched from the kapton layer in a perpendicular direction to a second set of 400 μm pitch 340 μ wide array of Cu electrode strips of the bottom strip layer. This 2D readout structure for GEMs is incompatible with the μRWELL detector structure because of the way charges are collected by the strips in μRWELL detector and also, the array 50μm thick kapton ridges would create a periodic valley and peak structure for the μRWELL that is unwanted for DLC layer glued on top of the readout.

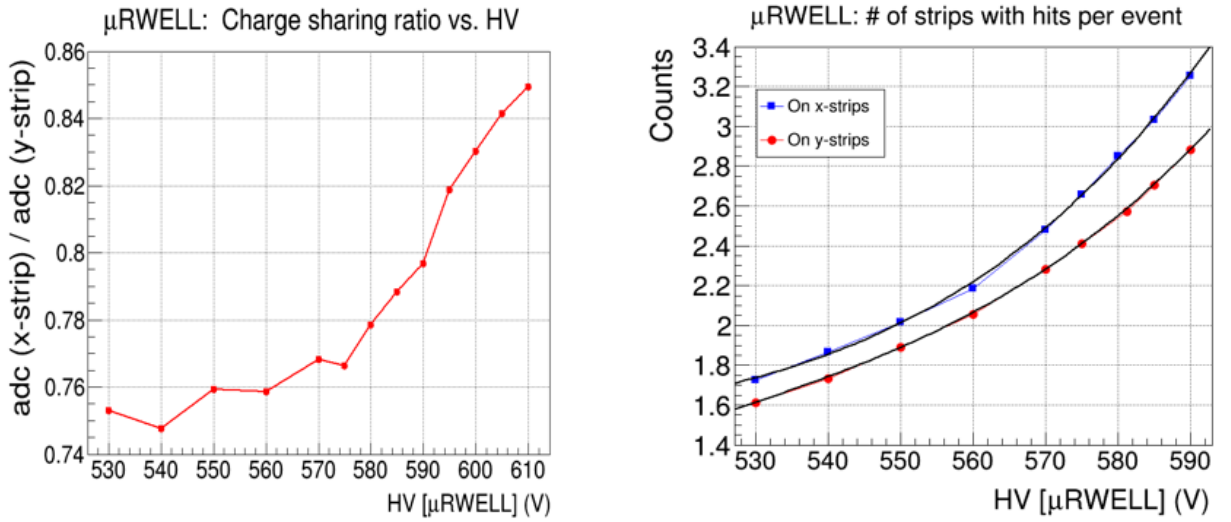

Figure 18: *Left:* x-strips / y-strips charge sharing ratio as a function of the μRWELL amplification HV scan. *Right:* cluster size (average number of hits per cluster) on x-strips (red dots) and y-strips (blue square) as a function of the μRWELL amplification HV scan.

In order to obtain a 2D readout capability with μRWELL detector similar to GEM detectors, we are testing a μRWELL prototype with a new type of 2D-strip readout structure in which both top and bottom Cu electrode strip arrays are printed on either side of a 50 μm thick glass epoxy layer which allows the charge between top and bottom strips electrode to be shared through capacitance coupling. The charge sharing is then defined by the dielectric properties of the glass epoxy layer. The plot on the right of Fig. 17 shows an the charge sharing correlation between the top (y-strips) and bottom (x-strips) strips with the cosmic data. The actual charge sharing ratio between x-strips and y-strips is equal 0.83, but the narrow width of the correlation indicates a good spatial uniformity of the ratio. The left plot of Fig. 18 shows that the charge sharing ratio increases exponentially with the voltage applied to the μRWELL amplification layer (i.e. the detector gain). Cluster size (defined as the average number of strip with hits produced by a cosmic particle in the chamber) on both x and y strips is shown on the right plot, with also a steady exponential increase with the amplification gain. The cluster size on y-strips is slightly smaller than the cluster size on x-strips for which the charges are collected through capacitance coupling.

HV scan of μRWELL amplification structure: Efficiency curves of the prototype was obtained from a HV scan of the μRWELL device, as shown on the left plot of Fig. 19. For this analysis, the electric field in the drift region was maintained at 1 kV / cm (which is equivalent to 300V applied between the drift cathode and the μRWELL) as we scan the voltage on the μRWELL. The efficiency reached in the plateau region is about 94% for y-strips and about 90% for the x-strips. The efficiency of μRWELL prototype was computed based on the tracks formed from the recorded hits in the two GEM trackers. For this preliminary analysis, we did not performed any specific alignment of the three chambers relative to each other and we suspect that detector misalignment would contribute to a couple of percentage drop of the overall efficiency

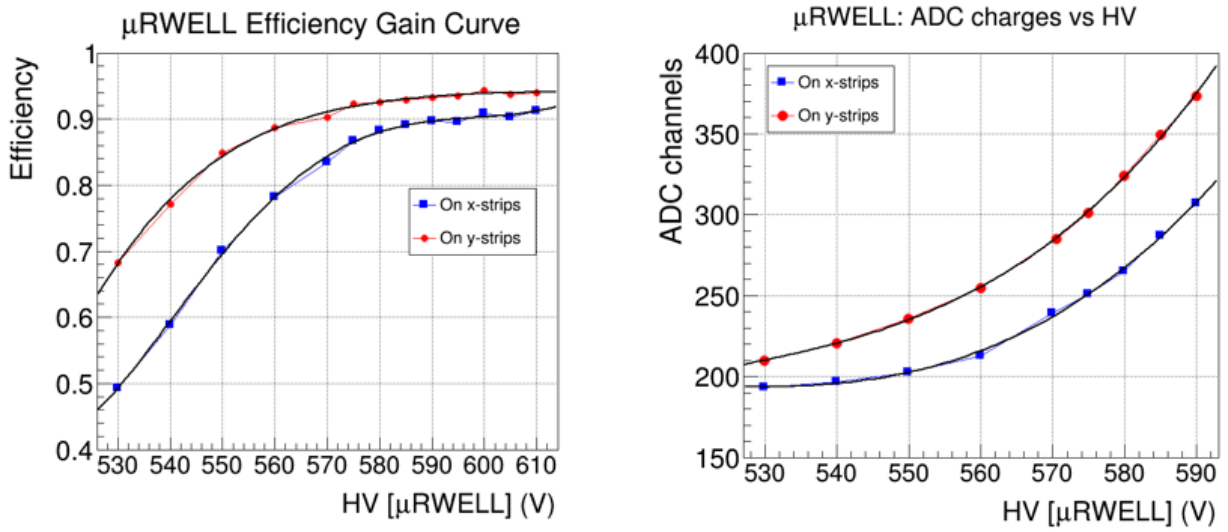

Figure 19: Efficiency (*left*) and Gain (*right*) on x-strips (red circle) and y-strips (blue square) as a function of the μRWELL device HV scan.

μRWELL. However, the relatively large difference between the efficiency on y-strips and x-strips can be explained mainly by the unequal charge sharing between the two strip layers (see Fig. 18). The gain curves (in ADC units) on both x and y strips, plotted as a function of voltage scan of the amplification layer, are shown on the right plot of Fig. 19. The smaller charge collection in the x-strips result in an overall lower signal to noise ratio of the x-strips compared to the y-strips and therefore to the lower efficiency which is even more pronounced at lower gain.

Study of the gain uniformity: The plots on Fig. 20 show the spatial distribution of the average charges

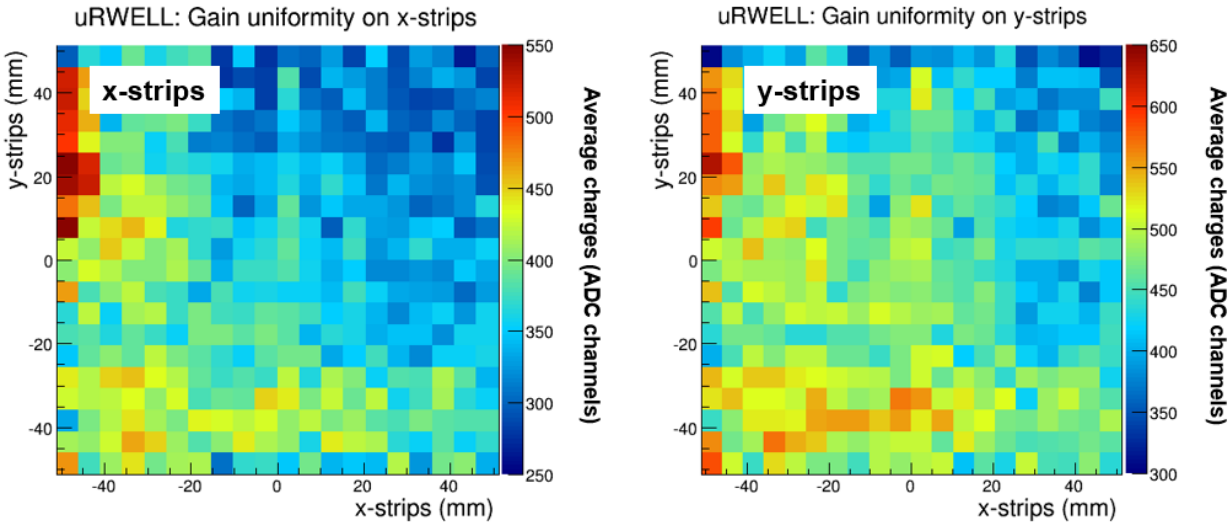

Figure 20: *Left:* 2D spatial distribution of the average charges (in ADC units) collected by the x-strips of μRWELL prototype. *Right:* similar data for the y-strips. The average ADCs plots is a measurement of the gain uniformity of the detector.

(in ADC unit) collected on x-strips (left) and y-strips (right) from a large cosmic data statistic sample for a drift field of 1 kV / cm and a 600 V on the μRWELL device. The spatial distribution of average ADCs is a direct measurement of the gain uniformity in the chamber. We observe a drop up to 50% of the average ADCs in the top right quarter of active area of the detector compared to the bottom left quarter for both x and y strips, though the issue is more pronounced for x-strips than for y-strips. This discrepancy can be partly explained by the non equal pre-amplifier gain of the APV25-SRS electronics used to read out the data. For the cosmic data test, the detectors were readout by two APV25 cards (2 $\times$ 128 e- channels) in each x and y direction in the master and slave configuration of the SRS electronics system. We suspect that the pre-amplifier gain of the master cards is higher than for the slave cards and if this hypothesis is confirmed, the contrast in the perceived detector gain non uniformity (average ADCs) will be the highest between the top right and bottom left quarters as shown on the plots on Fig. 20. There is a very simple test to test this situation and remove the ambiguity of the readout electronic. We will just have to swap the APV25 cards on the detector so that the active area previously covered by an APV25 master card will now be read out by the slave card and vice and versa. With cosmic data taken under the same conditions in these two configurations, we could easily confirm and correct for the contribution of the electronics to the gain non uniformity measured on the detector Other cause of the non uniform gain can originate from non uniformity on non homogeneity of the μRWELL layer used for the detector gain amplification or the diamond like carbon (DLC) material used as resistive layer. μRWELL amplification device is basically a GEM foil with Cu electrode only the top side, a non uniform spatial distribution holes size and geometry in the μRWELL foil will results in correlated non uniform spatial gain distribution. Similarly a non uniform DLC thickness will lead to non uniform distribution of the gain. We plan to pursuing the characterisation of the prototype with cosmic and investigate further the issue.

HV scan in the drift region: We performed a voltage scan in the drift region to study the impact of the electric field on the detector's performances. The measurements were performed at a constant gain by setting the voltage of the μRWELL device to 600 V. The left plot of Fig. 21 shows no dependence on the drift field of the detector efficiency over in a wide scanning range from 400 V/cm to 1400 V/cm. Other detector

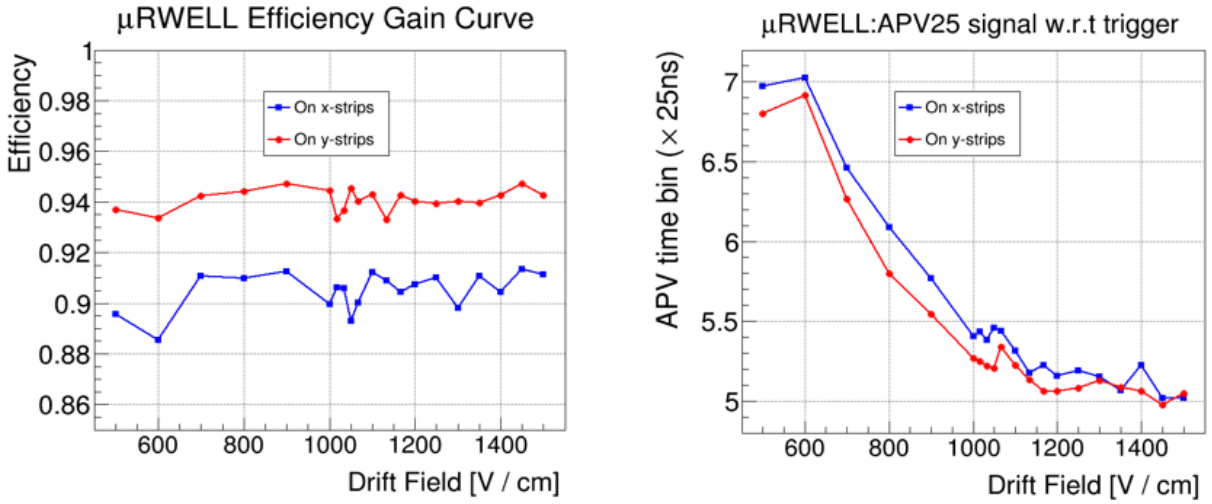

Figure 21: Efficiency (*left*) and signal drift time (*right*) on x-strips (red circle) and y-strips (blue square) as a function of the drift field.

characteristics such as average cluster size or average ADC charges on the readout strips also are shown to be independent of the drift field. The right plot of Fig. 21 shows the expected exponential dependence of peak time of the APV25 signal (in 25 ns time bin) to the drift field. The peak time information on the plots is measured relative to the trigger signal (in arbitrary trigger reference time). The peak time difference (2 APV25 time bin or 50 ns) is the meaningful information here.

Time performances of the μRWELL prototype: In this study, we are comparing the time performances of the signal from the μRWELL prototype to that of a standard Triple GEM detector. Unlike in triple GEM where the signal on the readout strips are induced by the drift of the charges in the induction region between the bottom of the third layer and the anode readout layer, the signal induced on the readout strips of a μRWELL propagate through a resistive layer, the diamond like carbon (DLC). The timing performance of such detector depends on the dielectric properties of the DLC layer.

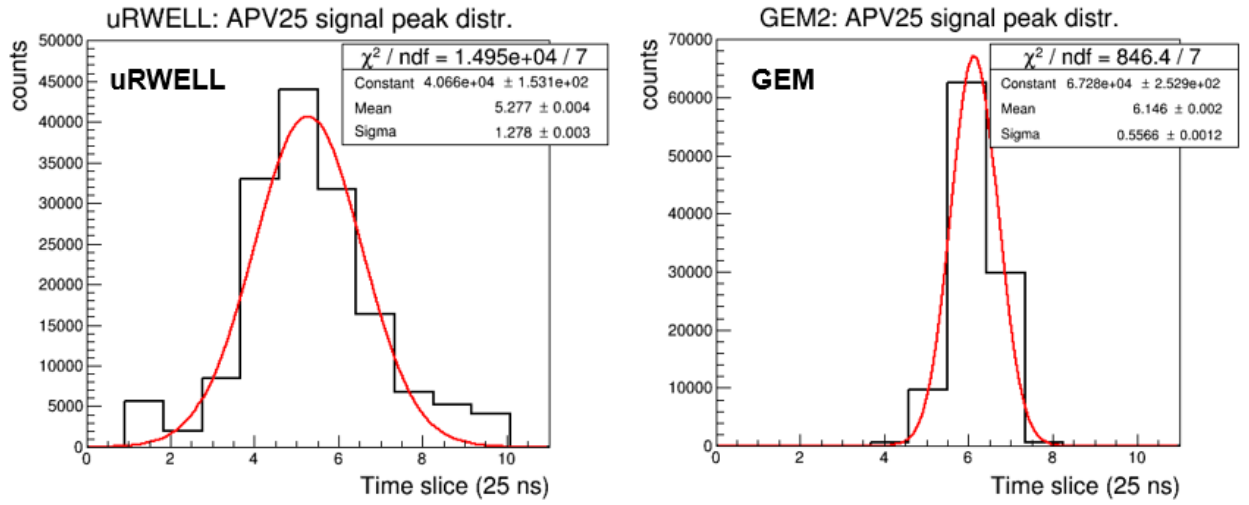

Figure 22: Distribution of the APV25 signal peak (in 25 ns time bins) on the x-strips for μRWELL (*left*) and for GEM2 (*right*).

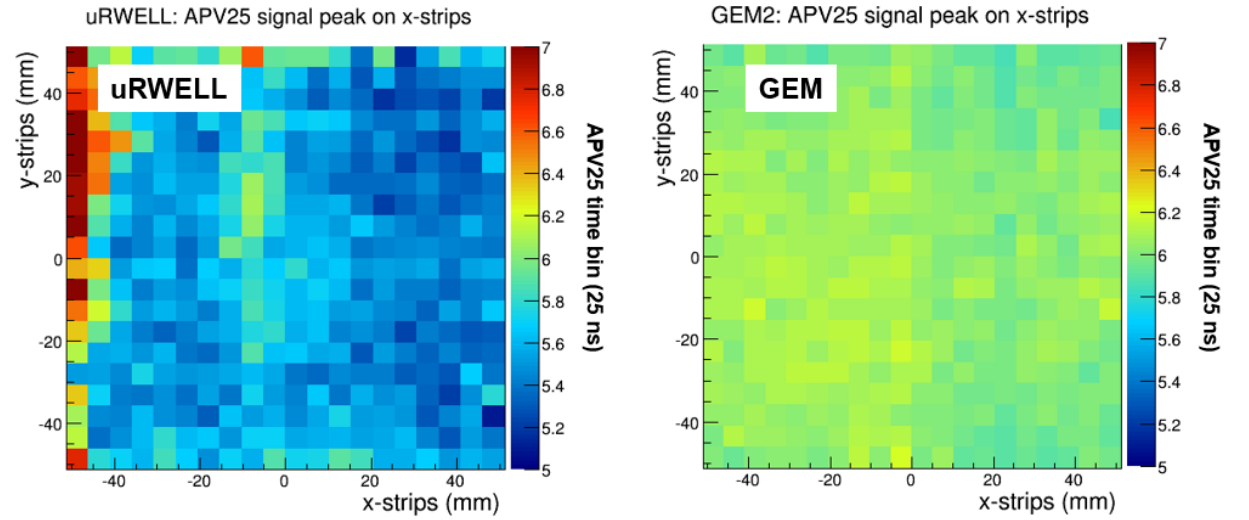

Figure 23: Spatial distribution of the APV25 signal peaking time relative to the trigger on the x-strips for μRWELL (*left*) and for GEM2 (*right*). The color scale represents APV25 time bins (in 25 ns units).

We looked at the peaking time of the APV25 signal relative to the trigger signal. The reference trigger signal is arbitrary here but the trigger latency (delay relative to the trigger) was adjusted so that the peak of the APV signal from the GEM detector occurs in the time sample no 6 of the defined readout time window as one can see on the right plot Fig. 22. From the plot, we also observe that roughly 30% of the hits have their peak time in the neighboring time samples 5 and 7. This is a well documented issue, explained by the fact that the external trigger signal is not synchronized with the APV25 clock which results in about 12.5 ns jitters in

the signal. For the μRWELL detector, the distribution of the APV25 signal peak has its maximum in time sample no 5. This is also expected, since the overall drift time in a single amplification stage detector such as the μRWELL is significantly shorter than for a triple amplification stage GEM detector with additional 4 mm drift length from the transfer gap between the GEM foils and the 2 mm induction gap between the last GEM foil and readout layer. However the width of distribution is twice larger that for the GEM. The wider distribution is related to the resistive layer contribution to the signal timing The 2D spatial distribution of the APV25 signal peaking time signal in the x-strips for both detectors is displayed on Fig. 23. The left plot associated to GEM again shows a very good uniformity distribution of the signal peaking time centered around the time sample no 6 as expected. For the μRWELL prototype, once again, we see a very strong spatial non uniformity. The non uniformity does not seems to follow a clear pattern that we can easily correlate for example to the propagation time of the signal from the hit impact position in he detector to the edge of the strips where the charges are collected by the APV25 readout channels. We observed in fact a randomly distributed non uniformity that we suspect might reveal some intrinsic strong non homogeneity of the DLC layer. The non uniformity of spatial distribution of the APV25 signal peaking time in x-strips

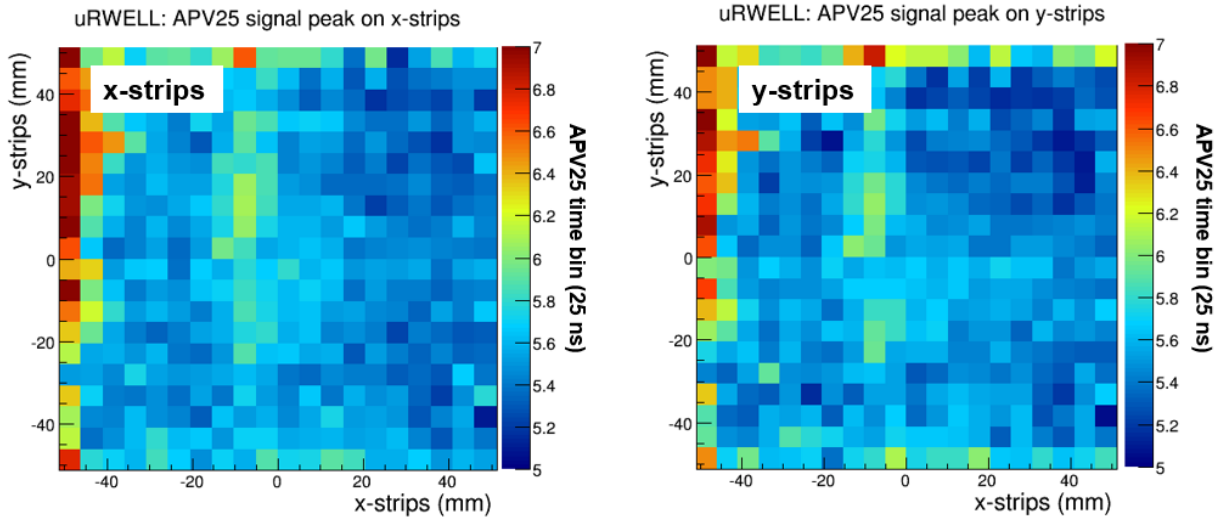

Figure 24: Spatial distribution of the APV25 signal peaking time relative to the trigger on the x-strips(*left*) and y-strips (*right*) for μRWELL. The color scale represents APV25 time bins (in 25 ns units).

and y-strips for the μRWELL prototype are well correlated as shown on the plots of Fig. 24. This is a good indication that the non uniformity is likely caused by the DLC structure itself and probably not by the glass epoxy 2D-strip readout structure. We plan to pursue the study of the non uniformity of the signal peaking time and communicate with μRWELL experts at CERN and in Frascati to understand better the issues that we are observing in these preliminary analysis.

Tracking residuals analysis of the μRWELL in FNAL test beam: A position scan run was performed with the FTBF 120 GeV proton beam during the FNAL test beam campaign in summer 2018 to study the position resolution on different locations on μRWELL prototype active area.

The test beam setup for this study is shown on the left plot of Fig. 25 with the 2D reconstructed beam position at the scanned position on the detector shown the right plot. As we previously presented in Jan 2019 report, the residual distribution in x and y for an initial large statistic run with proton beam impinging at the center of the detector active area are shown on Fig. 26. The width σ_x and σ_y of the residual distribution are respectively equal to 50 μm and 43 μm. σ_y is slightly smaller than σ_x which is also consistent with the slightly unequal charge sharing between x and y strips (see Fig. 18). These results obtained before even correcting for the tracking error contribution to the residual are very encouraging. On can reasonably expect

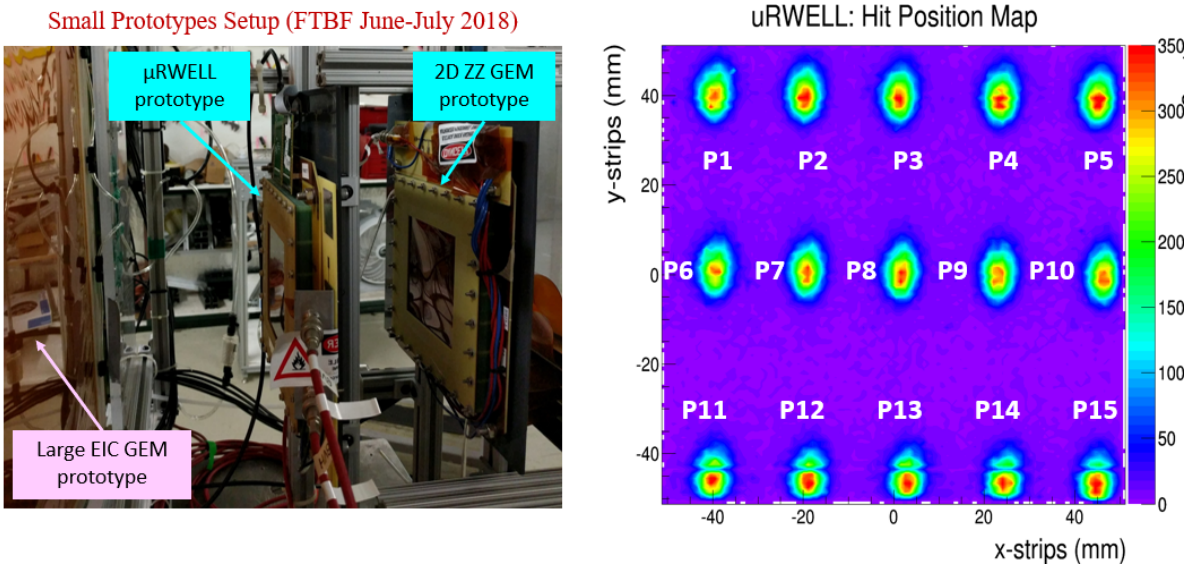

Figure 25: *Left:* 2D-strip readout μRWELL prototypes setup at Fermilab beam test. *Right:* 2D reconstruction of the proton beam spots from position scan run.

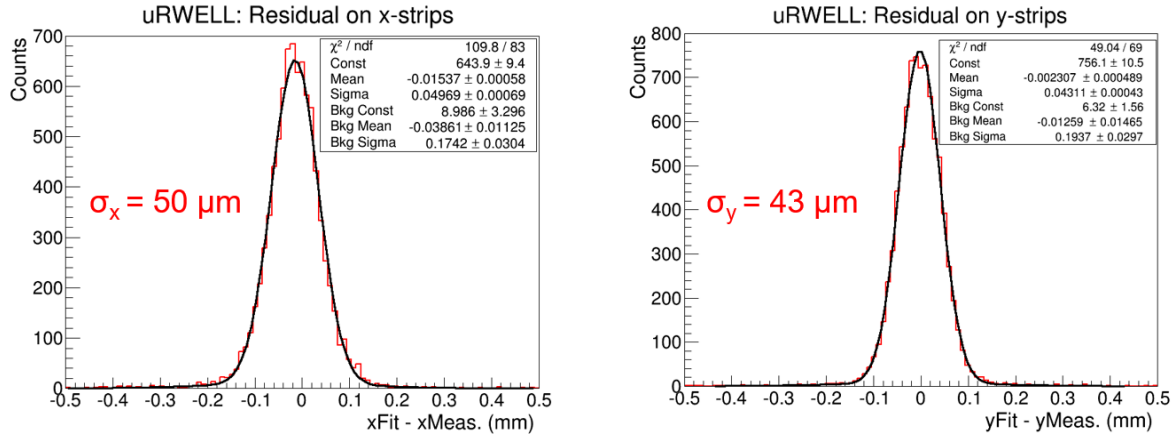

Figure 26: Distribution of the residuals in x (*left*) and y (*right*) strips of the μRWELL prototype from tracking with FNAL 120 GeV proton beam.

a spatial resolution after tracking error corrections better than 40 μm in both x and y directions even with all the non uniformity issues reported in the paragraph above. This would be even a better performance than our expectation for a Triple GEM detector with similar type of readout strip structure. Table 1 shows the width of the tracking residual of the hit position distribution on x and y strips for the different beam spot locations on the μRWELL prototype. In this analysis, the width of the residuals does not be directly represent the spatial resolution of the detector as we do not yet correct for the tracking error contributions. Moreover, the data are slightly worse with the width about 10 μm higher on average on both x and y strips than the performances reported Fig. 26. However can easily explain this discrepancy by the fact that the results from Table 1 where produced when the μRWELL prototype installed on the MT6.2b XY moving table during position scan run. A more precise tracking residual analysis would have to take into account the corrections of offset and rotation misalignment created by movement the detector under test with the XY moving table. the residual plots from Fig. 26 were produced from data taken when the μRWELL prototype was installed on a fixed position outside the XY moving table in a different configuration during the FNAL test beam and the alignment of the detector was under better control. After we implement all the tracking

Table 1: Width of the tracking residual in x and y from beam position scan on the μRWELL prototype

beam spot positions	P1	P2	P3	P4	P5	P6	P7	P8	P9	P10	P11	P12	P13	P14	P5
residuals on x-strips in (μm)	63	62	63	66	66	60	66	69	61	60	60	62	67	66	63
residuals on y-strips in (μm)	52	53	53	50	53	53	53	49	51	59	58	53	52	53	53

fit errors and misalignment corrections into the residual analysis, we will be able to extract the precise position resolution of the prototype in both x and y directions and we can reasonably expect a uniform spatial distribution of the resolution and in the range of or better than 45 μm which once again, is expected to beat the typical position resolution performance of a standard triple GEM with "COMPASS" 2D-strip readout.

2.1.3 What was not achieved, why not and what will be done to correct?

2.1.3.1 TPC studies at Brookhaven National Lab

Although we planned to use the 4-layer cosmic ray telescope to reconstruct cosmic tracks in the lab to study the prototype TPC for this funding cycle, we were not able to do so. The reason for this is that the telescope has been in almost continuous use at the Fermilab test beam facility by collaborating groups for the purpose of measuring reference tracks for various detectors under test.

In the meantime we have conceived of an alternate means of testing the prototype TPC in the lab using a UV laser beam. As described above, UV laser beams have sufficient energy to liberate electrons from molecular impurities via a 2-photon process and thus could provide a means of producing straight lines of charge, analogous to a point-like cluster of charge using an x-ray generator. We have developed a conceptual design of an optical system that can deliver such laser beams into the TPC volume at precise, controlled angles, making it possible to study the tracking resolution of a TPC prototype over a very wide range of incident angles over a very short amount of time compared to accumulating statistics from cosmic rays. In addition, the ionization density is scalable since it is quadratically dependent on the light intensity and allows for the possibility to confine the charge to a small lateral area of the laser beam. Finally, the setup is compact and provides for a convenient trigger by using a photo-diode to catch a portion of the output light. At this point it is becoming evident that the true merits of the 4-layer telescope are for providing reasonably high resolution reference tracks at a beam test facility. For this reason we will pursue finalizing the design of such a laser based calibration tool for possible implementation in the future.

2.1.3.2 TPC studies at Stony Brook

The technical implementation of a passive gating grid has yet to be performed. The work on this project is ongoing.

2.1.3.3 Cylindrical μRWELL studies at Florida Tech

Due to the leak hunting in the planar 10 cm $\times$ 10 cm μRWELL prototype, we have not yet been able to establish signal in this detector and to commission it.

2.1.3.4 Cylindrical μRWELL studies at TU

Although we were able to start investigating the momentum resolution from a series of cylindrical μRWELL detectors, the detector responses within the simulation still need to be made more realistic. The best way to do this is to use data from a μRWELL operating in a μTPC mode with a 15 mm drift gap. From the prototype detector one can measure the dependence of the number of dE/dX measurements, their respective resolutions, the X-Y spacial resolutions, and the dependency these measurements have as a function of the angle the track enters the detector with. These measurements can then be fed into the simulation to produce a realistic detector response.

Following a realistic μRWELL simulation, the central tracking detectors (cylindrical μRWELL and vertex detectors) can be combined with the forward tracking detectors (GEMs) being simulated by FIT. This will allow us to assess the overall tracking performance of these particular EIC sub detectors.

2.1.3.5 Cylindrical μRWELL studies at UVa

R&D on μRWELL detector technology: We have not yet acquire a second μRWELL prototype with low mass readout strips as we originally planned. We have mostly concentrated our effort on the characterization of the current prototype as a first step to have a better understanding of this new technology.

2.1.4 What is planned for the next funding cycle and beyond?

2.1.4.1 TPC studies at Brookhaven National Lab

Our proposed R&D activity for the next funding cycle is as follows:

- July-September: Re-install cosmic ray telescope layers and continue to optimize and tune the system and associated software.
- September-December: Continue to study track reconstruction in the TPC prototype using the SAMPA and/or DREAM electronics.
- September - December: Work on developing a new design for the collimator of our high intensity, narrow beam x-ray source for studying and characterizing the TPC readout.
- September - December: Work on the design and production of new, single-pattern zigzag readout PCB's for the TPC prototype. Time permitting, we will send at least one PCB to CERN for the installation of a μRWELL and one to Saclay for the bulking of a micromegas onto the PCB.

Long-term goals:

- Further tests with the TPC prototype will include testing zigzag readout patterns optimized for a TPC; testing different avalanche schemes in the TPC (eg. Micromegas, and μRWELL); testing promising gas mixtures; and measuring the charge spread, attachment, and IBF.
- Simulation studies of the response of various zigzag readout patterns in combination with different detector gases and avalanche technologies for a TPC.
- Study the production of "laser tracks" in the drift region of the TPC prtotype. By shooting a UV laser through the UV compatible ports of the TPC enclosure, the TPC gas is ionized along the length of the laser beam via a 2-photon process, which mimics tracks left by minimally ionizing particles. These straight-line pseudo particle tracks may be used as a highly effective calibration tool in a full-sized TPC operated in a real experiment, like at the EIC and in smaller bench-top experiments.

2.1.4.2 TPC studies at Stony Brook

The implementation of a passive gating grid and its investigation is highest priority for the study of TPC optimization at SBU.

2.1.4.3 Cylindrical μRWELL studies at Florida Tech

We plan to build a mechanical mock-up of the smallest cylinder in the tracker barrel. The main motivation is to check if foils can indeed be properly stretched according to our design to produce a stable and uniform cylindrical structure from foils. One concern is that two ends of a commercial foil coming off a roll have to be spliced together to form a cylinder. We will investigate how best to implement this splicing to get a uniform foil cylinder. Before endeavoring on doing this with expensive μRWELL foils, we would like to do these tests with a basic kapton foil of a thickness that is comparable to a μRWELL foil. Similarly, we plan to use 3D-printed parts for the rings and frames used in our design for rapid prototyping of the mechanics before going to more expensive PEEK and carbon fiber parts.

If we can successfully build one such cylindrical segment, we would add two more segments in the same way to create a mock-up of one cylinder of the three-segment structure envisioned in our design. The purpose is to study if the foil stretching still works if the three segments are connected together and stretched from the ends.

2.1.4.4 Cylindrical μRWELL studies at TU

For the next funding cycle our main goal is to simulate a realistic cylindrical μRWELL μTPC detector. To do this we need information about the number of dE/dX measurements, their resolutions, spatial resolutions, and how they depend on the angle that the track enters the detector. We are proposing to build a planar 10 cm x 10 cm μRWELL detector with a 15 mm drift gap that we will operate in a μTCP mode. We will use CERN's μRWELL kit, where they will modify the frames so that the drift gap is 15 mm. The detector will be readout making use of the APV based SRS system TU obtained from our new SBIR (Sec. 5.1). We will be able to use cosmics and ^{55}Fe to study the number of hits, dE/dX, spacial, and timing resolutions. The X-Y spacial resolutions can then be compared to the standard (2 mm drift gap) μRWELL detector that UVa tested last summer. We can also use this μRWELL μTPC to investigate the issues that UVa saw during their beam test last summer.

In addition to simulating a more realistic μRWELL detector, we also plan to study how the momentum resolution changes as a function of detector material. Currently the simulation implements an optimistic low mass version of the detector, while the material budget of the standard μRWELL detector is closer to 1.5%. It would be beneficial to see how sensitive the momentum resolution is to the amount of detector material. We plan to have an undergraduate student who is working with our physics group this summer carry out this study.

2.1.4.5 Cylindrical μRWELL studies at UVa

For the coming cycle of FY20 and beyond, we plan to:

1. **Our μRWELL prototype:** continue the characterisation of the prototype, specially we will investigate further the time properties and the non uniformity pattern observed with this detector. As a potential solution for the fast tracking detector in EIC central region, it is important that the time performance of μRWELL detector technology is well understood. We also plan to study the performance of the prototype in high particle rate environment in a setup both using our X-ray test bench and cosmic tracker setup.
2. **New μRWELL-μTPC prototype:** In addition, we are interested in acquiring a second prototype with with 21 mm drift region with built-in field cage system to accurately control the drift electric field. We

plan to operate this prototype in the mini drift and / or micro TPC mode using the newly acquire VMM readout electronics to explore the tracking ability charged particle of single detector as we are proposing for EIC central tracker.

3. **VMM readout electronics:** Complete the procurement the minimal VMM-SRS readout electronics and familiarize ourselves with this new system and its associated DAQ and decoding software. We plan to test the electronic with the μRWELL prototypes and specially testing performances of the system when operating the μRWELL-μTPC prototype in mini drift mode.

2.2 Forward Tracker

In its Jan 2019 report, the review committee recommended that *"the full simulation studies, including the track reconstruction and determination of the impact point on the RICH entrance window of low-mass GEM trackers with chromium foils be completed and its physics impact be determined to close on the issue of the value of chromium foils."*

Unfortunately, we are still struggling with extracting information on track positions from EICroot to calculate residuals as function of detector material, but we continue to pursue the issue. We would also like to take the opportunity to clarify the position of the eRD6 consortium regarding the interest in Chromium GEM foils R&D. The consortium is not advocating the use of Cr-GEMs for the large GEM trackers in the forward region. In this region, we don't expect any significant benefit of minimizing the GEM material mainly because of the material will be dominated by the TPC readout,services and structure and will be main source of multiple scattering for the forward trackers. The consortium is interested in of Chromium GEM as a candidate in the far forward region as one additional tracking detector layer to the forward MAPS layers in order to provide the fast signal information together with the additional space point. In this far forward region where the material budget is to be kept at its minimum, a Chromium GEM detector, with radiation length of the same order of magnitude than one MAPS layer and providing the needed fast signal information will be hugely beneficial for the EIC physics.

2.2.1 What was planned for this period?

2.2.1.1 Florida Tech Large Carbon Fiber GEM Prototype with zigzag readout

Refurbishment of low-mass EIC Forward Tracker GEM detector prototype: The goal for the last funding period was to assemble and operate the refurbished low-mass prototype and to characterize its performance, e.g. gain curves, with X-rays at FIT.

EIC Simulations for Forward Tracker: We planned to measure the hit residuals for tracks through the forward tracker chambers by studying the track impact on a dummy plane about 15 cm past the third GEM ring. The objective is to study how a reduction of material in the GEM chambers affects the spread of fitted track positions due to multiple scattering.

2.2.1.2 TU Commercial GEM Prototype

At the start of TU's eRD3 program, we had been working with Tech-Etch to develop commercially available GEM foils and use these along with Tech-Etch produced HV and 2D readout foils to produce a large low-mass commercial triple-GEM detector. The STAR FGT [16] triple-GEM detector design was selected to be used to build the commercial triple-GEM detector to keep costs down, since all designs, specialized tooling, and DAQ software were already in TU's possession. To assess the manufacturing quality of these larger GEM foils a large area GEM CCD scanner was built. As mentioned in Sec. 1.6 this was a tremendously successful project that went beyond the scope of the eRD3 project and served the broader MPGD community.

Unfortunately, just as Tech-Etch had begun producing quality FGT type GEM foils and were beginning the process of developing 50 cm long foils, they stopped their GEM program. They felt from a business stand point that the GEM program would no longer be beneficial for the company. However, TU was able to obtain 16 single-mask FGT style GEM foils (30 cm x 30 cm) that Tech-Etch had made before shutting down their GEM production. It was TU's intention to build four triple-GEM detectors using these 12 Tech-Etch foils and continue with characterizing the detectors.

In parallel to the commercial GEM project, we are also investigating the use of Kapton spacer rings as a replacement to the more traditional G10 spacer grids that are used between GEM layers to keep the foils from sagging.

The main goals for the current cycle related to the commercial triple-GEM detectors were

1. Identify electrical issues that plagued the first two detectors that were built.
2. Use the remaining 6 Tech-Etch GEM foils to build the last two commercial triple-GEM detectors based on the STAR FGT design.
3. Using the STAR DAQ software characterize the two commercial triple-GEM detectors performance via cosmics and ^{55}Fe.
4. Quantify the effect of using Kapton spacer rings rather than G10 spacer grids.

2.2.1.3 UVa Large GEM Prototype with 2D U-V readout

For the current cycle, we planned to:

1. **Large EIC-FT-GEM prototype:** Continue the analysis of the FTBF data. Present the results of the performances of the prototype at MPGD2019 conference in Spring 2019 and start preparing the draft of the manuscript for publication in peer-reviewed journal.
2. **VMM readout electronics:** Procure a small size VMM-based Scalable Readout System (SRS) if a stable version of the FE cards are available and start testing this new electronics with the our detectors to compare the performances of VMM-SRS readout system with the APV25 electronics.
3. **Draft paper on Chromium GEM (Cr-GEM) studies:** Continue working on the draft paper for the publication of the results in NIMA or TNS journal.

2.2.2 What was achieved?

2.2.2.1 Florida Tech Large Carbon Fiber GEM Prototype with zigzag readout

Refurbishment of low-mass EIC Forward Tracker GEM detector prototype: We appear to have mostly overcome the previously reported problem with shorts between adjacent GEM foils in the Triple-GEM stack of this large prototype detector. Taking advantage of the purely mechanical assembly of this detector, we completely disassembled the detector and replaced the ABS pull-outs with PEEK pull-outs as detailed in the last report. We also replaced the 1 mm inner frame ABS parts with 2 mm PEEK parts. This produces a more sturdy inner frame stack and 2 mm gap sizes for the first transfer gap and for the induction gap instead of 1 mm gaps. It gives us larger safety margin with respect to foils potentially touching and producing shorts. The detector was re-assembled from scratch (Fig. 27 left) and now has a 3/2/2/2 mm Triple-GEM configuration as opposed to the original 3/1/2/1 mm configuration.

A very important aspect of mechanically constructing a large-area gas electron multiplier (GEM) is the sufficient stretching of the GEM foils in the stack. In the re-assembly we were able to pre-stretch each foil during the GEM stack assembly even though the foils were already cut to final size with small margins

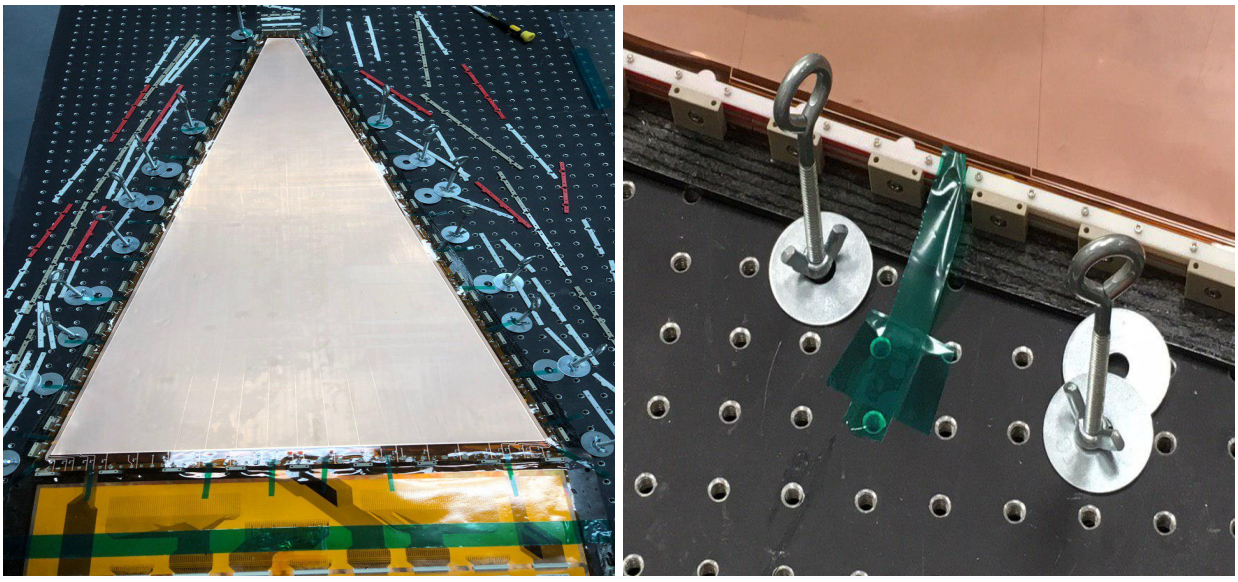

Figure 27: Left: Re-assembly from scratch of large low-mass EIC Forward Tracker GEM detector prototype with carbon fiber frames. Here the GEM3 is being pre-stretched with thin strips of green tapes. Right: Close-up view of GEM foil pre-stretching on the long foil side where a portion of green tape is attached to the small margins of a GEM foil between pull-outs and pulled taut by hand.

around the active area. This was done with thinly cut strips of green tape attached uniformly around the perimeter of each foil and tensioned by hand (Fig. 27). Fig. 28 compares the GEM stack with and without pre-stretching applied. Using a capacitance meter, the capacitances of the foils and between foils were measured to verify the viability of the re-stretched foils and the spacing between foils (Tab. 2). Using a simple parallel-plate-capacitor model, we calculate the gap sizes as $d = \frac{\kappa\epsilon_0 A}{C}$. The results for the measured spacings are also tabulated in Tab. 2. The average GEM stack spacings appear to be close to the nominal 3/2/2/2 mm configuration.

Before closing the chamber, the Al-Kapton window on the top carbon fiber (CF) frame and the HV foil that connects the GEM foils via spring-loaded pins to the HV divider were replaced. The alignment of HV supply pins was verified through capacitance measurements before and after the top CF frame was put in place. Capacitance measurements were performed before and after attaching the top CF frame. The values were on the same order of magnitude, which showed that the top CF frame was properly attached to the rest of the detector. Unfortunately, when the detector was released from the optical table, a short was again observed in the first transfer gap. This is because the detector structure slightly deforms when it moves from being externally supported to fully self-supported. We conclude that the existing carbon fiber skeleton is still not quite strong enough to produce a fully self-supported low-mass detector.

Table 2: Capacitance measurements for GEM foils and transfer gaps and inferred measurement of spacing between electrodes before closing the large low-mass detector.

Gap	Capacitance [nF]	Error [nF]	Avg. Spacing [mm]	Error [mm]
Drift gap	0.427	0.005	3.298	0.064
GEM 1	41.002	0.410		
Transfer gap 1	0.688	0.009	2.047	0.041
GEM 2	41.370	0.414		
Transfer gap 2	0.549	0.007	2.565	0.051
GEM 3	41.452	0.415		
Induction gap	0.760	0.010	1.853	0.037

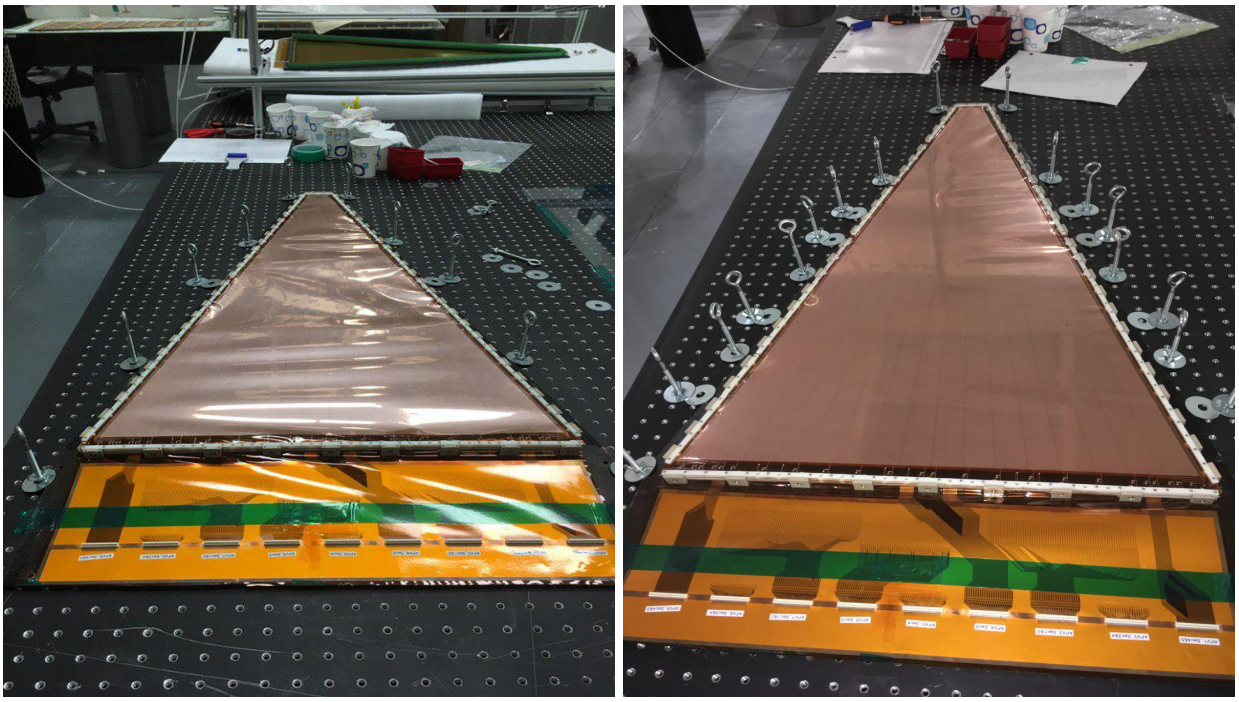

Figure 28: GEM stack without (left) and with (right) pre-stretched GEM foils during stack assembly illustrating the effectiveness of this method.

By trial and error we determined what minimal number of external fixations produced enough mechanical support to avoid all shorts in the gaps. We observed that the detector mainly required fixations at the wide end and the short end of the trapezoid to be free of shorts. The chamber must be mounted on a vertical stand for quality control measurements and would be operated in a vertical position in an EIC detector. To replicate this, a mounting frame was constructed with 80/20 parts that follows the trapezoidal detector shape (Fig. 29 right). The detector was attached to this mounting frame with C-clamps at the short and wide ends as was done in the horizontal fixation to the optical table (Fig. 29). Capacitance measurements confirmed that no shorts were present in the detector in vertical position and that the detector is now ready for high voltage testing.

EIC Simulations for Forward Tracker: The impact of adding a second large-area GEM detector to the far forward region of the BeAST detector, i.e. behind the RICH detector, is studied by simulating the detector in the EicRoot framework. Specifically, the momentum resolution and the number of hits available for track fitting are studied as a function of particle scattering angle and particle momentum. The results suggest that the addition of a large area GEM can significantly improve the momentum resolution of the BeAST detector.

The simulated detector components for the standard BEAST detector geometry include the beam pipe, the silicon and vertex trackers, the forward GEM detectors ("inner forward GEM" detectors), the time projection chamber, and the ring imaging Cherenkov (RICH) detector gas volume. The new test geometry adds outer forward GEM detectors behind the RICH to this standard geometry as shown in Fig. 30. The impact of the outer GEM detector on the overall performance of the BeAST detector is studied by simulating the performance of the BeAST detector in the standard and test configurations while varying the particle parameters (scattering angle and momentum). For the purposes of this simulation, it is assumed that the detector would operate with a 1.5 T B-field.

The scattering angle θ is varied from 5° to 75°. The impact of the outer GEMs is confined to scattering angles within the angular acceptance of the outer forward GEM of $\theta < 35°$ (corresponding to a pseudorapidity of

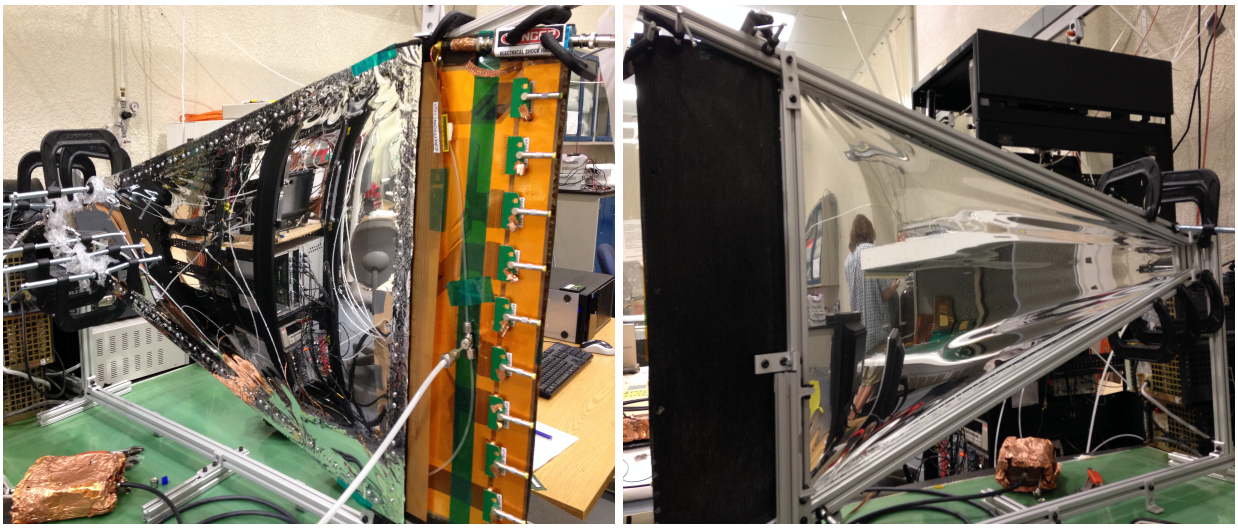

Figure 29: Large low-mass GEM detector mounted in vertical position (front and back).

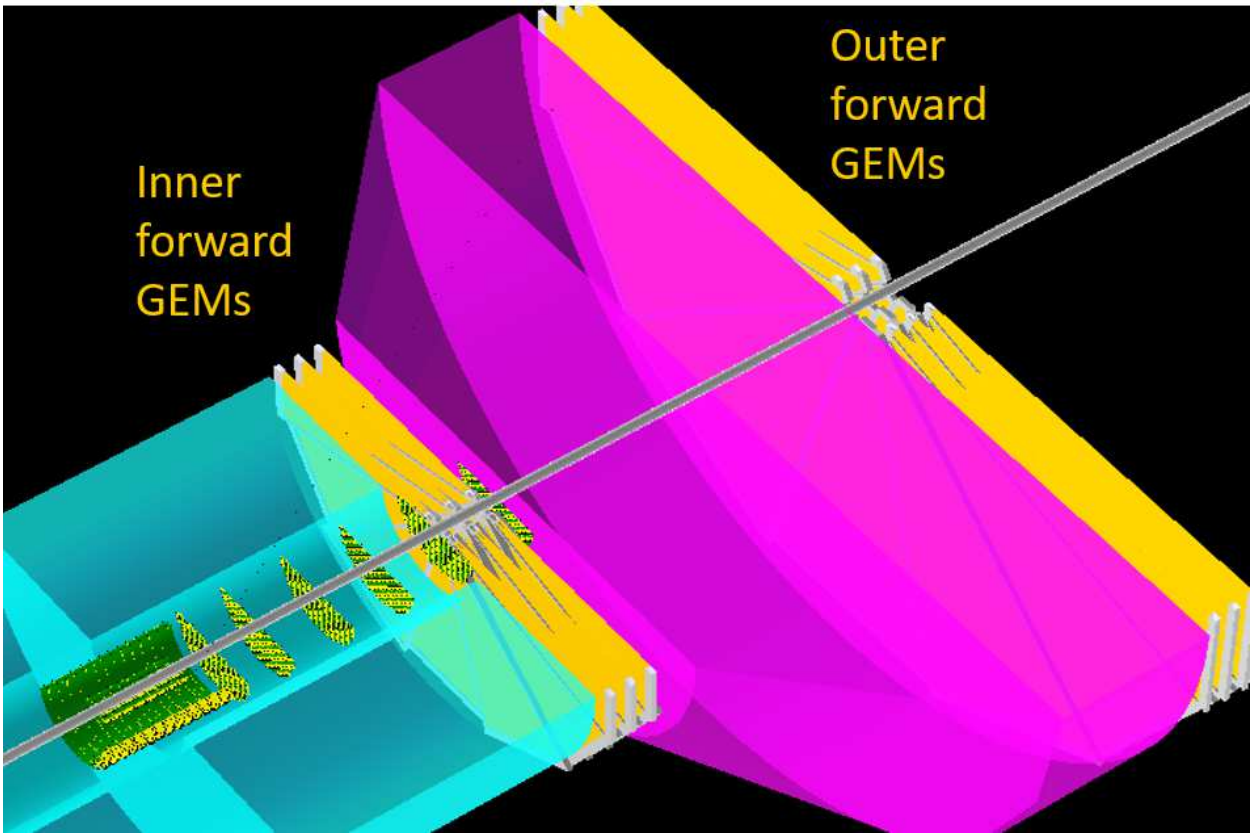

Figure 30: Simulated BeAST test geometry with additional outer forward GEM detectors.

$\eta > 1.154$). It should be noted that the dimensions of the outer GEMs in these simulations is chosen to approximately match the angular size of the inner GEMs. Thus the limiting value of 35° may be subject to change if the dimensions of the outer GEMs are altered.

From the results shown in Fig. 31 (top), it is clear that the outer GEMs significantly improve the momentum

resolution, particularly for small scattering angles where the improvement reaches a factor of two. The particular structure of the graph is believed to be due to the varying number of hits on the individual detectors. In order to verify this, we plot the average number of hits in each tracking subdetector as a function of θ in Fig. 31 (bottom). Over the full $\theta < 35^\circ$ acceptance region of the outer forward GEM, both inner and outer GEM subdetectors provide a constant number of hits while the number of TPC hits drops rapidly below $\theta = 15^\circ$ and the number of vertex hits is down to one hit below $\theta = 18^\circ$. In this angular range, the number of forward Si hits is comparable to the number of hits in each GEM subdetector. The design of the two GEM subdetector is very similar, so adding the outer forward GEM doubles the total number of GEM hits in this region. The forward Si detector, inner GEMs, and outer GEMs each contribute roughly a third to the total number of track hits in this region. Fig. 32 shows the fraction of all hits that are in the outer GEMs. This explains the significant impact of the outer forward GEM in the angular range below $\theta = 15^\circ$ ($\eta > 2$).

Fig. 33 shows the momentum resolution as a function of momentum while keeping the scattering angle fixed at $\theta = 15.41^\circ$ ($\eta = 2.00$). It demonstrates that the significant improvement from outer GEMs holds over a large momentum range from 1 GeV/c to 60 GeV/c.

2.2.2.2 TU Commercial GEM Prototype

We have now used all 12 single-mask GEM foils, 4 readout foils, and 4 HV foils provided by Tech-Etch to produce a total of four triple-GEM detectors following the STAR FGT design. This design encompasses a complex and sensitive assembly procedure which is difficult to master. Unfortunately, with Tech-Etch ending its GEM production program we only had 12 GEM foils of rather poor quality at our disposal. With each build iteration improvement was made. The building process also provided hands on detector building experience for new graduate students who recently joined our physics group.

As was discussed in our previous eRD6 report, we were able to identify the cause of the electrical shorts which led to our first two triple-GEM detectors being inoperable due to excessive sparking (Fig. 34). While powering these detectors we noticed that there was about twice as much current being drawn from the detector as compared to two STAR FGT triple-GEM detectors (taken from the STAR experiment) that we used as a baseline comparison. The shorts were caused by unused HV contacts that were located near occupied HV contacts. There are three HV pads per GEM HV segment, but for each GEM layer a HV connection is only made to one pad. This shorting was fixed for the third and fourth triple-GEM detectors by removing all unused connection pads (Fig. 35).

Performing leakage current measurements after completing the assembly of the third commercial triple-GEM detector we notice that one GEM layer displayed a high leakage current. However, with the other two GEM layers showing satisfactory performance, we were able to power the detector and take cosmic data with it operating effectively as a double-GEM detector. When powering up the third commercial triple-GEM detector, we saw the current that was being drawn from the detector matched the two reference STAR FGT detectors. This suggests that the excess current drawn from the first two prototype commercial detectors was also caused by this shorting issue. Figure 36 shows the X and Y hit locations from a cosmic run for the third commercial triple-GEM detector in panel (a) and compared to one of the STAR FGT triple-GEM detectors in panel (b). Two things are revealed from this comparison. First, the large acceptance "holes" seen in panel (a) have been identified as two dead APV chips. Secondly, looking at the hit density (the z-axis: blue = a few hits and red = a lot of hits) one can see that there are many more hits in the STAR FGT detector as compared to the commercial GEM detector. We think this is related to the efficiency of running with a double-GEM compared to a triple-GEM detector.

After the initial assessment of the third commercial triple-GEM detector, we finished the assembly of the fourth and final commercial triple-GEM detector using the last of our Tech-Etch produced foils. Unfortunately there were a couple issues during the assembly. One of the GEM foils was overstretched and glued to a frame. This resulted in the frame that the GEM was glued onto to bend. When assembling the GEM stack, this layer did not sit flush with the layers above and below it. In spite of this we were able to achieve a good seal by applying a resin sealant around the outside of the detector. Another issue during the assembly

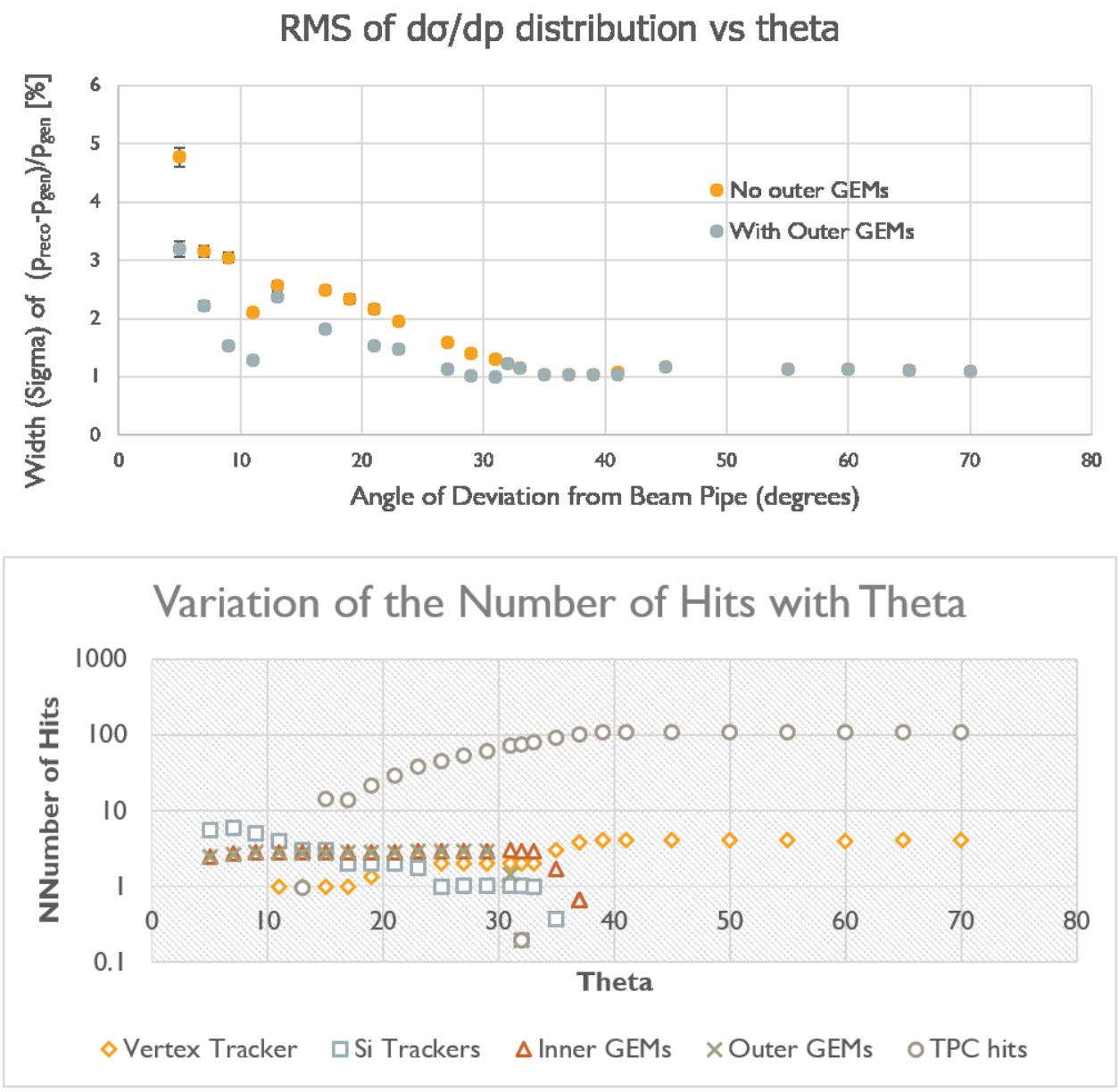

Figure 31: Top: Momentum resolution vs. scattering angle θ for 10 GeV/c pion tracks from simulation of the standard BeAST detector with (gray) and without (orange) outer forward GEMs added. Bottom: Average number of hits in each tracking subdetector vs. scattering angle Theta.

process was that one foil was accidentally punctured. It was a small hole that pierced one of the GEM HV sectors. Since these were the only foils we had remaining we continued assembling the detector. Upon completing the assembly and insuring the detector had a good air tight seal we flushed with N2 gas over a weekend. Leakage current measurements were then performed, revealing high currents (at the order of μA) on most of the HV sectors.

The issues related to the last two commercial triple-GEM detectors are still being investigated. However, with one detector missing a GEM layer and the other showing high leakage currents over the majority of its HV segments, complete characterization of these detectors is not likely.

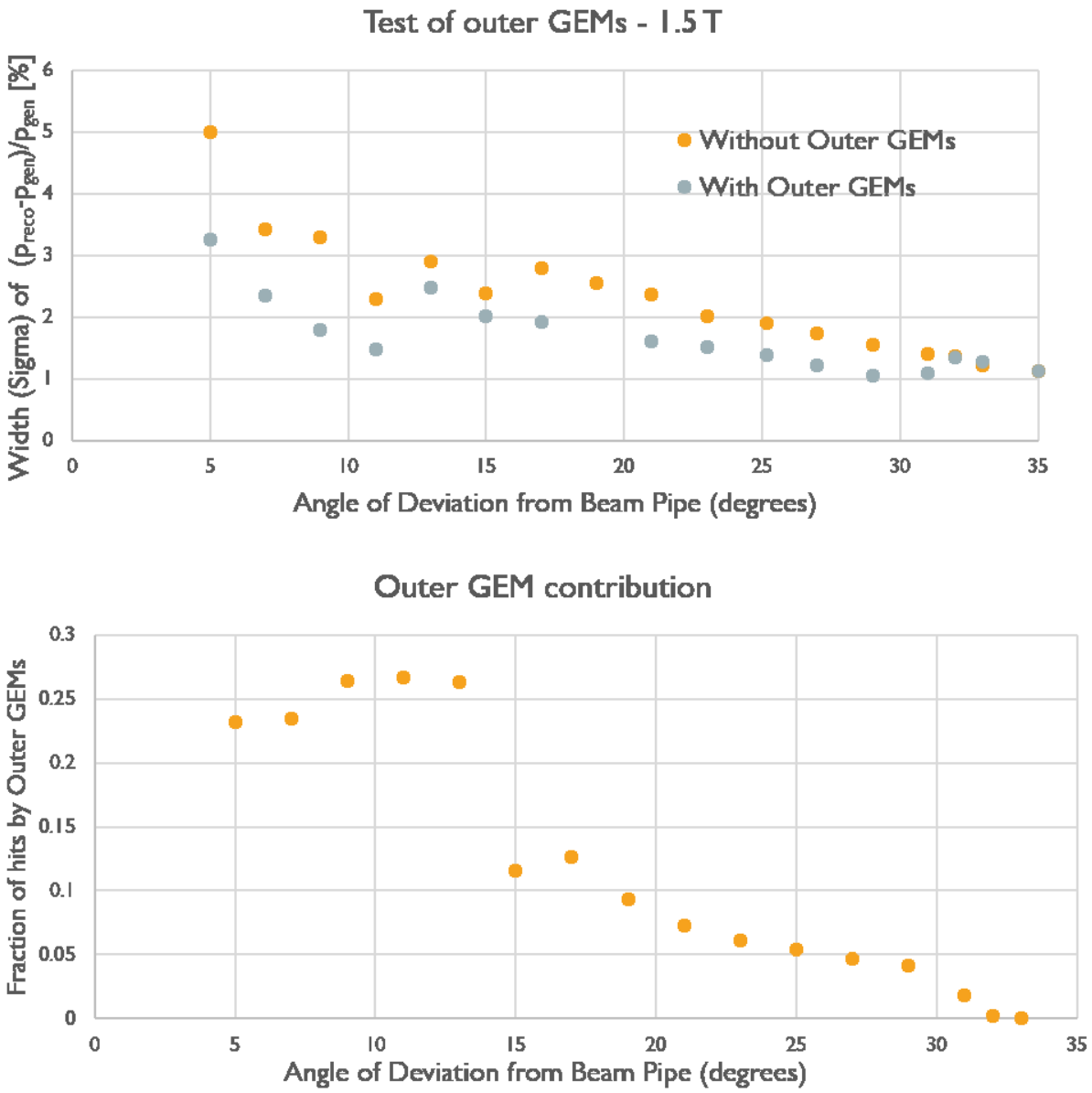

Figure 32: Top: Momentum Resolution vs. scattering angle θ within angular acceptance of outer GEMs. Bottom: Fraction of all hits that are in outer GEMs vs. θ.

2.2.2.3 UVa Large GEM Prototype with 2D U-V readout

1. **Large EIC-FT-GEM prototype:** We are still investigating the signal distortion with double zebra contact scheme of the U-V strips observed from the test beam in July 2018 leading to a measured spatial resolution twice larger than the expected performances. Several productive discussions with experts at CERN, suggest that the signal dis torsion issue may be caused by poor electrical contact quality of the type of zebra strip that we used to connect the U-V strips to the APV25 readout. In this coming cycle, we plan to acquire different types of zebra strips and perform a comparative study of their performances with the large GEM prototype.

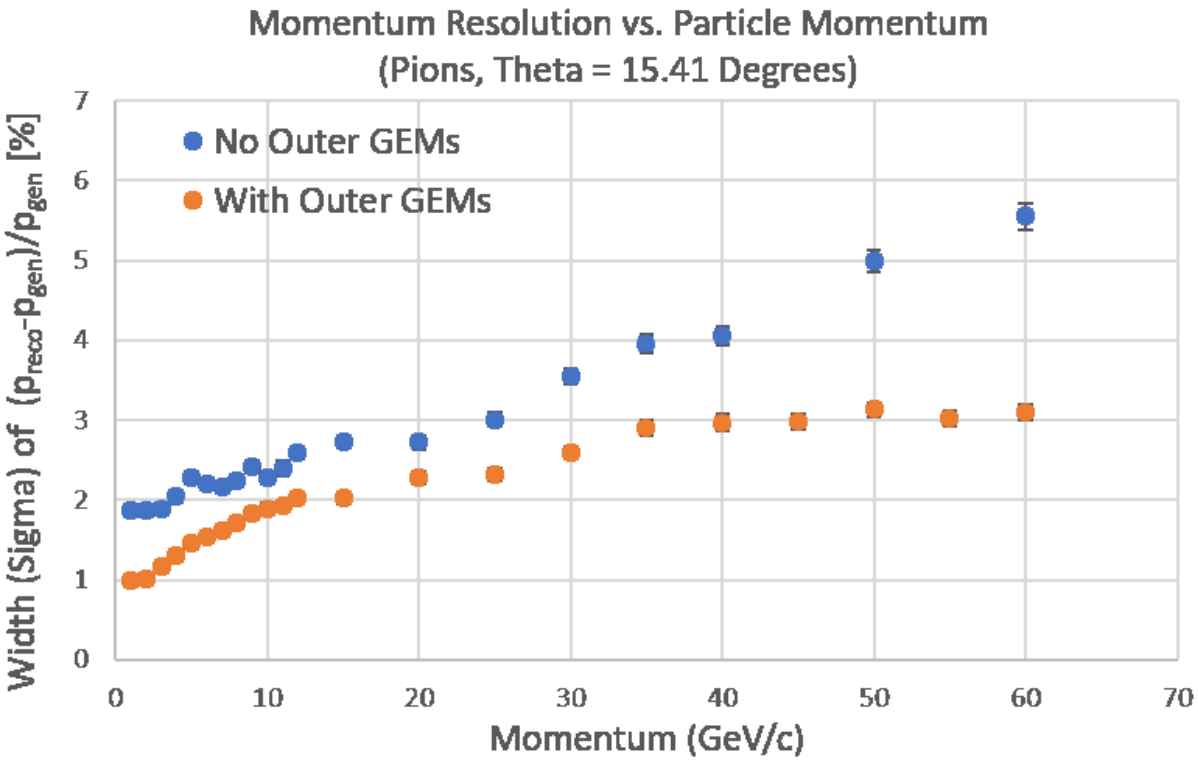

Figure 33: Momentum resolution vs. momentum for pions at fixed scattering angle $\theta = 15.41°$ ($\eta = 2.0$) with (orange) and without (blue) outer forward GEMs added.

2. **Procurement of VMM Readout Electronics:** We have placed the order for the small scale (512 channels) VMM-SRS readout electronics developed and supported by the CERN based RD51 community for MPGD tracking detectors. VMM chip was developed at BNL for the LHC ATLAS Muon Chamber upgrade at CERN. We expect to receive some parts of the readout system by the end of the summer 2019 and we will dedicate a significant portion of the next cycle activities to educate ourselves with the new system and to study its performance with our existing GEM and μRWELL prototypes.

3. **Draft Paper on Chromium GEM studies:** The draft of the manuscript for the Chromium GEM foil (Cr-GEM) studies is ongoing.

2.2.3 What was not achieved, why not and what will be done to correct?

2.2.3.1 Florida Tech Large Carbon Fiber GEM Prototype with zigzag readout

On the hardware side, the complete rebuild of the detector took quite some time so that we have not yet been able to commission the detector. We have just started the quality control procedure with HV testing in pure CO_2. On the simulation side, we are still struggling with extracting information on track positions from EICroot to calculate residuals as function of detector material. This is due to the complexity of the EICroot track fitting code, inexperience of our undergraduates, lack of in-house post-doctoral support from the project, and limited availability of EICroot experts.

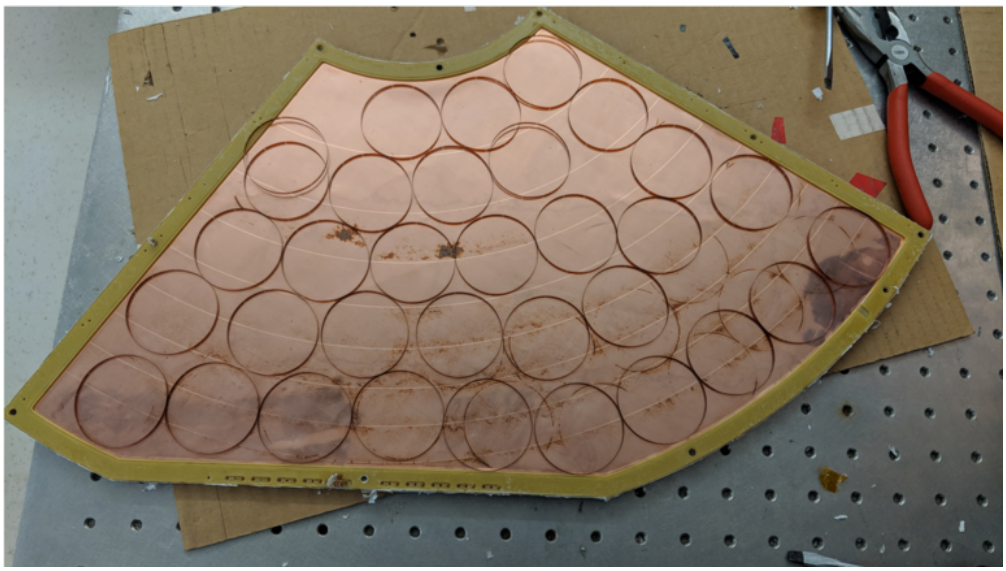

Figure 34: The condition of a commercial GEM foil from the first detector built after excessive sparking

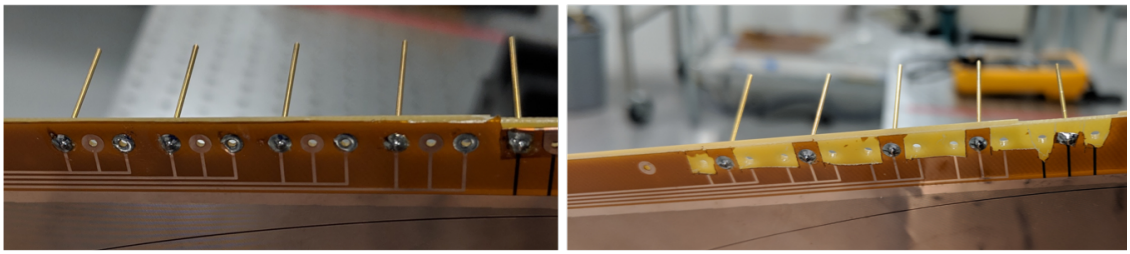

Figure 35: Groups of 3 pads are associated with one of the 9 HV sectors, but only one HV connection is made per sector. Our first two commercial triple-GEM detectors left the unused HV pads in tact (a). While our last two commercial GEM detectors removed the unused HV pads (b).

2.2.3.2 TU Commercial GEM Prototype

The issues related to the last two commercial triple-GEM detectors are still being investigated. However, with one detector missing a GEM layer and the other showing high leakage currents over the majority of its HV segments, complete characterization of these detectors is not likely. We are actively seeking other funding sources to purchase reliable components by CERN or other new reliable commercial vendors to complete and publish these studies.

2.2.3.3 UVa Large GEM Prototype with 2D U-V readout

1. **Large EIC-FT-GEM prototype:** The analysis of the test beam data for the large GEM prototype was put on hold while we are still investigating the U-V strips signal distortion issues, previously reported in the Jan 2019 report. Discussions with experts at CERN suggest that the problem may be due to poor electrical contact between the zebra strip and the detector U-V strip readout contact pads. We plan to test different types of zebra strips and study of their performances on the large GEM prototype.

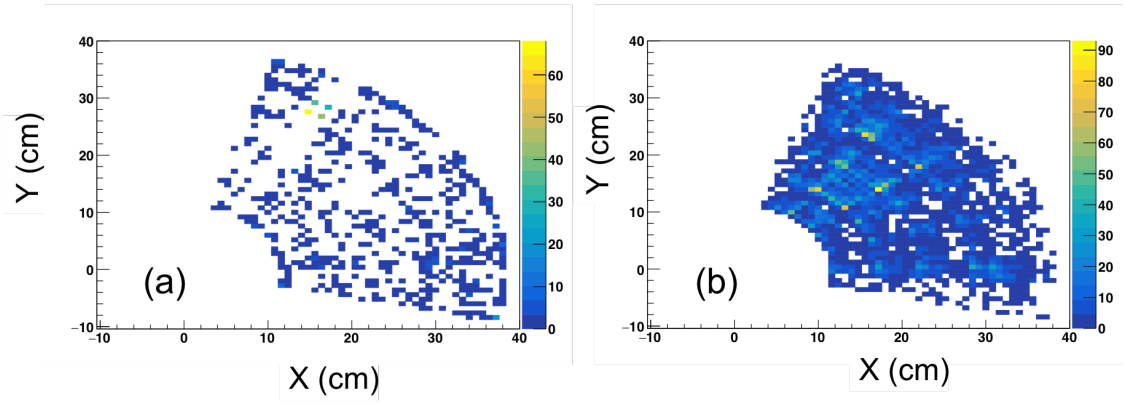

Figure 36: X-Y hit locations reconstructed from cosmic ray data for (a): Commercial triple-GEM detector. (b): STAR FGT triple-GEM detector from the STAR experiment.

2. **VMM readout electronics:** The cost of the VMM-SRS system turned out to be higher than what initially we budgeted for, based on our experience with the APV25-SRS system. As consequence, we were unable to procure all the parts needed with the funds we received for the current cycle. We plan to request additional funding for the acquisition of the full system.

3. **Draft paper on Chromium GEM (Cr-GEM) studies:** The draft of the manuscript is going at a slow pace as we primarily concentrate our current R&D effort on the characterization of μRWELL prototype.

2.2.4 What is planned for the next funding cycle and beyond?

2.2.4.1 Florida Tech Large Carbon Fiber GEM Prototype with zigzag readout

On the hardware side, we plan to perform a full set of quality control tests on the refurbished low-mass prototype and to characterize its performance, e.g. gain curves, with X-rays at FIT. On the simulation side, we will continue to reach out to EICroot tracking experts so we can study track-hit residuals as a function of forward tracker material.

2.2.4.2 TU Commercial GEM Prototype

We are planning to investigate the issues that we experienced with our last two commercial triple-GEM detectors that we built.

Temple University recently received some funding from an SBIR working with Triton Systems, a company based in Massachusetts, who will be investigating an alternative technique to producing 2D readout boards (Sec. 5.1). From this SBIR TU has already purchased a standard CERN GEM kit and SRS system. The GEM kit has already been assembled, and tested for leakage current (<3 nA per foil) and capacitance ($\sim 5.5 - 6$ nF) for each foil. A high voltage distribution board is now being assembled. Most of this work was carried out by an undergraduate student who was hired by the college to work in our group. We have also installed and tested the DAQ software, RCDAQ, on our detector lab computer which will be used with the SRS system. We are expecting our SRS crate to arrive by the end of July.

We do plan on using the CERN GEM kit and SRS system to investigate and quantify the effect of the Kapton spacer rings. The measurements will follow and build on those done already for us by BNL. We had sent BNL several Kapton spacer rings for them to place in between each of the GEM layers in their 10 cm x 10 cm quad-GEM detector. Fig. 37 (a) shows one of the BNL quad-GEM layers with a Kapton spacer ring inserted and panel (b) shows an initial look at the X-Y hit reconstruction of the detector. From this plot

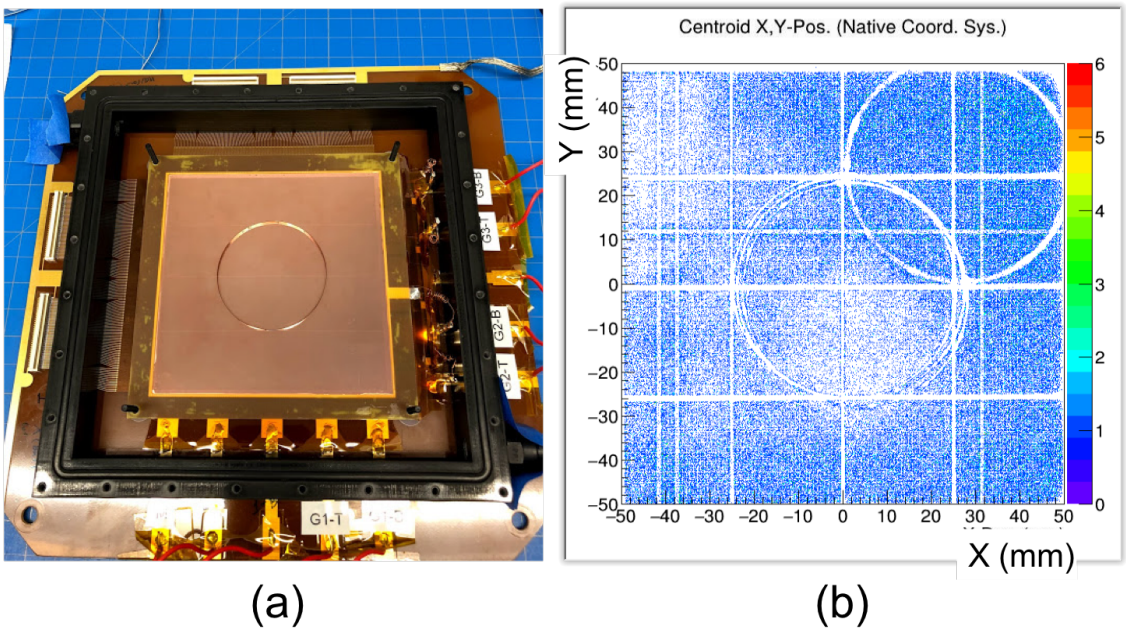

Figure 37: Kapton ring test done by BNL. (a): Shows one of the four GEM layers with a Kapton ring inserted. (b): X-Y hit reconstruction of the 10 cm x 10 cm quad-GEM with spacer rings inserted.

you can see a clear inefficiency due to the Kapton rings (circular gaps), you can also see that the Kapton rings move within each layer. The vertical and horizontal gaps are artifacts that need further investigation. TU plans on reproducing this measurement with more statistics and perform a more in depth analysis to quantify the inefficiency caused by using Kapton rings compared to G10 spacer grid segments.

2.2.4.3 UVa Large GEM Prototype with 2D U-V readout

For the coming cycle of FY20 and beyond, we plan to:

1. **Large EIC GEM prototype:** Test different types of zebra strips with the large EIC GEM prototype. We strongly suspect that the type of zebra that we are currently using for the prototype is the source of poor spatial resolution, which can be explained by distorted signal observed in the FNAL 2018 beam test data. We plan to test this hypothesis make a decision on the best type of zebra strip for this application.
2. **VMM readout electronics:** Complete the procurement the minimal VMM-SRS readout electronics and familiarize ourselves with this new system as well as its associated DAQ and decoder software. We plan to test the new readout electronic with the large EIC GEM prototype and compare its performance with the APV25-SRS readout system.

3 RICH Particle ID

3.1 Hybrid MPGD for RICH - INFN Trieste

3.1.1 What was planned for this period?

3.1.1.1 MPGD sensors of single photons at INFN Trieste

The activity foreseen for the year 2019 includes the completion of the analysis of the data collected at the 2018 test beam exercise where a first version of the prototype was studied. The realization and characterization by laboratory tests of a second version of the prototype is also foreseen.

3.1.1.2 New Photocathode Materials development at INFN Trieste

The activity foreseen for the year 2019 is related to the status of the R&D. The initial studies to understand the compatibility of a photocathode based on NanoDiamond (ND) particles with the operation in gaseous detectors and, in particular, in MPGD-based photon detectors, have been performed in 2018. The characterization of THGEMs with ND coating, both in the case of hydrogenated and non-hydrogenated powder has presented unexpected features, even if very different in the two cases. The foreseen activity consists in further laboratory studies to explore these performance in order to understand the origin of the modified THGEM behavior by producing under controlled parameters a new set of small-size THGEMs, that then will be fully characterized.

3.1.2 What was achieved?

3.1.2.1 MPGD sensors of single photons at INFN Trieste

The activity of the period January-June 2019 is reported. It includes the analysis of the test beam data, further laboratory studies of the same prototype with more measurements suggested by the test beam data and design studies in view of the second version of the prototype.

The prototype architecture is shortly recalled before discussing the test beam results. It consists in two staggered THGEM layers, the first one also acting as photocathode substrate, followed by a resistive MM by discrete elements. The detector active surface is 100×100 mm^2. The THGEM geometrical parameters are: 400 μm hole diameter, 800 μm pitch, 400 μm thickness and hole without a rim. The MM has 128 μm gap; the pad-size is 3×3 mm^2 with 3.5 mm pitch, forming a matrix of 32×32 pads (in total 1024 pads). The pads are grouped in 32×4 modular units; each unit is equipped with a connector interfacing the signal pads to the front-end electronics and a second, identical connector, providing the biasing voltage to the anode pads via protection resistors, one per pad, housed in a dedicated resistor board.

The data have been collected during the test beam studies of the prototype performed at CERN over two weeks between the end of October and the beginning of November 2018. During the test-beam period, we have been main-users for part of the time and otherwise we have worked in parasitic mode. High energy (>100 GeV) muons and pions have been alternatively delivered. A fused silica radiator is mounted onto the prototype; it has cylindrical symmetry and a dedicated design: the majority of the Cherenkov photons generated by minimum ionizing particles with trajectories quasi-parallel to its axis hit the detector surface in a ring-shaped area (Figs. 38, 39). A shutter is situated between the radiator and the photocathode and it is remotely controlled via a piezoelectric actuator. The adequate subset of the beam particles has been selected by an arrangement of scintillator counters. Two sets, each formed by a horizontal and a vertical bar, defining an area of 5×5 mm^2, placed one upstream and the other downstream of the prototype have been used. The quadruple coincidence has provided the trigger. Data have been collected with two different

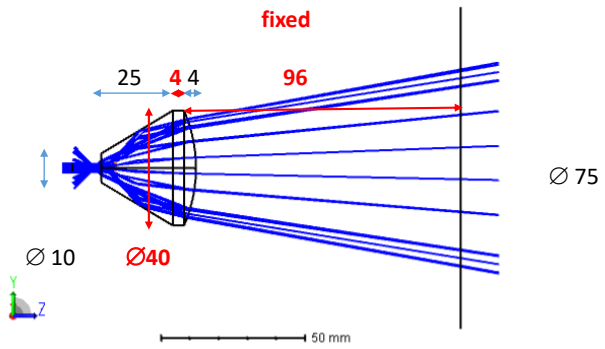

Figure 38: Cross-section of the fused silica radiator with cylindrical symmetry. The blue lines are examples of Cherenkov photon trajectories; a large fraction of them intercepts the photocathode surface (the vertical black line in the drawing) in a ring-shaped region, even if some of the photons hit the photocathode in different areas. The majority of the photons generated in the radiator are trapped inside the radiator itself due to total reflection; there are no examples of these trajectories in the drawing.

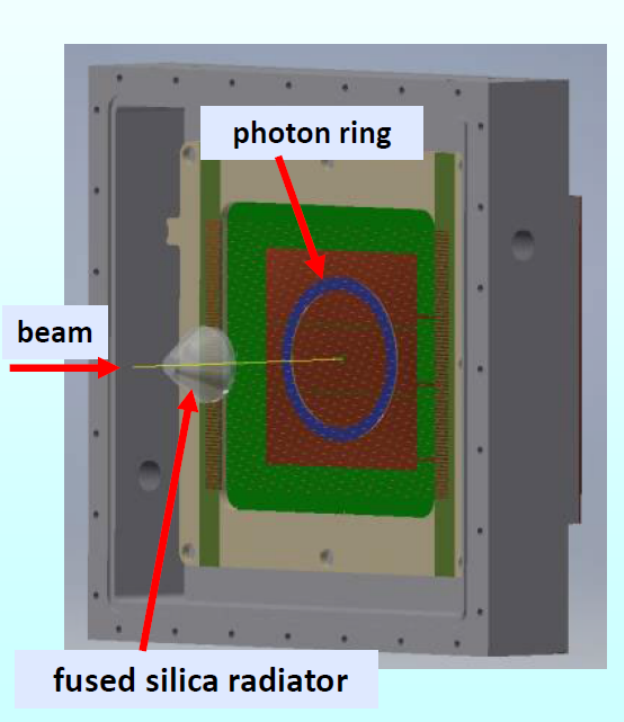

Figure 39: Skematic drawing illustrating the formation of the ring image in the photon detector by Cherenkov photons generated in the fused silica radiator.

gases: (a) Ar:CH_4 = 50:50 and (b) pure methane. The results presented in this report are related to the data collected with gas (a), a part when explicitly mentioned.

The read-out system is based on the SRS/APV25 system [18] developed within the RD51 collaboration. The 1024 pads are read-out by eight APV25 chips, 128 channel each. An adapter card has been designed to interface the SRS FE-card with the SRS/APV25 card to the prototype connector arrangement. The chip control and the DAQ is ensured by the novel DAQ Raven system, entirely LabView based, developed

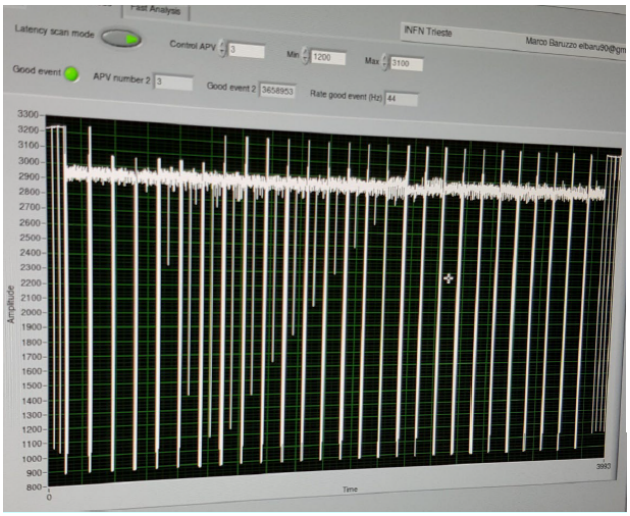

Figure 40: 27 consecutive measurements of the signal amplitude in all the 128 channels of an APV25 chip are shown; the time interval between two consecutive measurements is 25 ns. The development of a physical signal versus time can be seen in one of the APV25 channels.

within our R&D activity in order to ensure large acquisition band width. The Raven system architecture and performance have been reported about in January 2018. Dedicated interface boards have been designed and realized to interface the detector connectors and the SRS/APV25 FE boards. For each APV25 channel, the amplitude is read and digitized every 25 ns and, for each triggered event, 27 consecutive measurements of the signal amplitude are register (Fig. 40). The prototype read-out chain is not optimized in term of noise, as illustrated in Fig 41; the relatively high noise level, typically around 3300 electrons equivalent, is due to several features: the intrinsic noise introduced by the SRS implementation in the configuration used by us, the need of an adapter card and noise related to the boards equipping the prototype. Concerning the last source of noise, the cards with resistors supplying the HV to the individual pads and the read-out adapter cards are parallel with small distance between them. We do not regard the present noise figure as an intrinsic limitation of the detector architecture. In fact, the novel photon detectors installed on the COMPASS RICH detector, which have a hybrid MPGD architecture as well, and are read-out by APV25 FE chips[19], exhibit a typical noise level lower than 900 electrons equivalent [7].

The gain measured from the various pads is non-uniform at the $\pm 20\%$ level, as already reported previously. This non-uniformity was traced back to the design of the anode PCB, where the lines from the pads to the connectors are affected by different capacitance. The PCB design is the same for each group of 128 channels, each read-out by a single APV25 chip. This hypothesis could be cross-checked with the prototype fully equipped with the read-out electronics: the same noise pattern is reproduced for each group of 128 channels (Fig. 42). Therefore, the following algorithm is applied in order to normalize the amplitude measured in the different pads: the amplitude is scaled with the noise parameter normalized to the mean noise figure.

Figure 43 presents the time distribution of the highest amplitude signal in each event. The overall background level in the spectra obtained for different threshold settings is in agreement with expectations. In the following, a cut at 4.5 σ is used. These spectra also suggest a time cut applied by requiring the highest amplitude in the time windows between 6 and 10 APV25 cycles, corresponding to a 100 ns-wide time-range. One more cut is applied to the data, when studying the prototype response to Cherenkov photons: a geographical cut in order to select the area where the photoelectrons are detected; this area is shown in Fig. 44.

When the maximum amplitude is above threshold in two or more adjacent pads, a cluster is formed and the associated amplitude is the sum of the measured amplitudes. Figure 45 shows the cluster-size distribution obtained subtracting the cluster-size histograms for data collected with shutter open and shutter closed, after

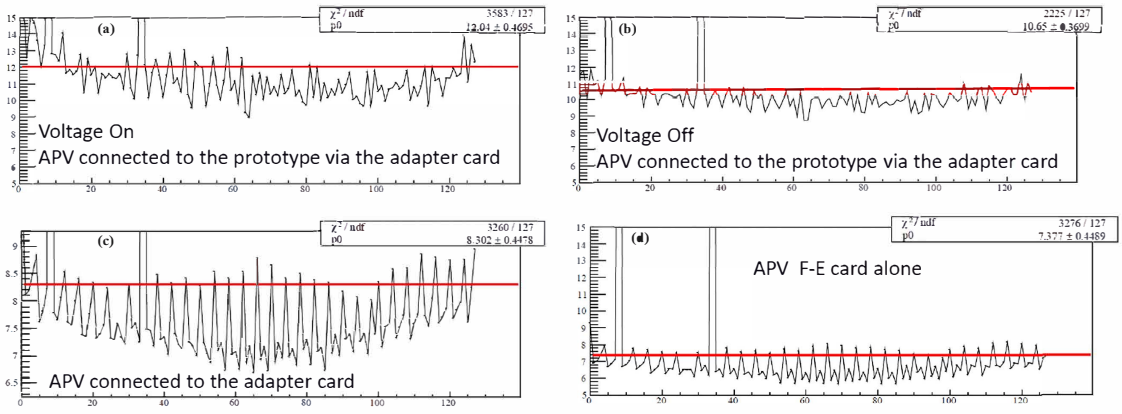

Figure 41: Noise level of the 128 channels of an APV-25 chip, measured in four different arrangements; (a) APV-25 chip connected to the interface card and to the detector, HV on; (b) APV-25 chip connected to the interface card and to the detector, HV off; (c) APV-25 chip connected to the interface card and not connected to the detector; (d) APV-25 chip not connected to the downstream read-out chain.

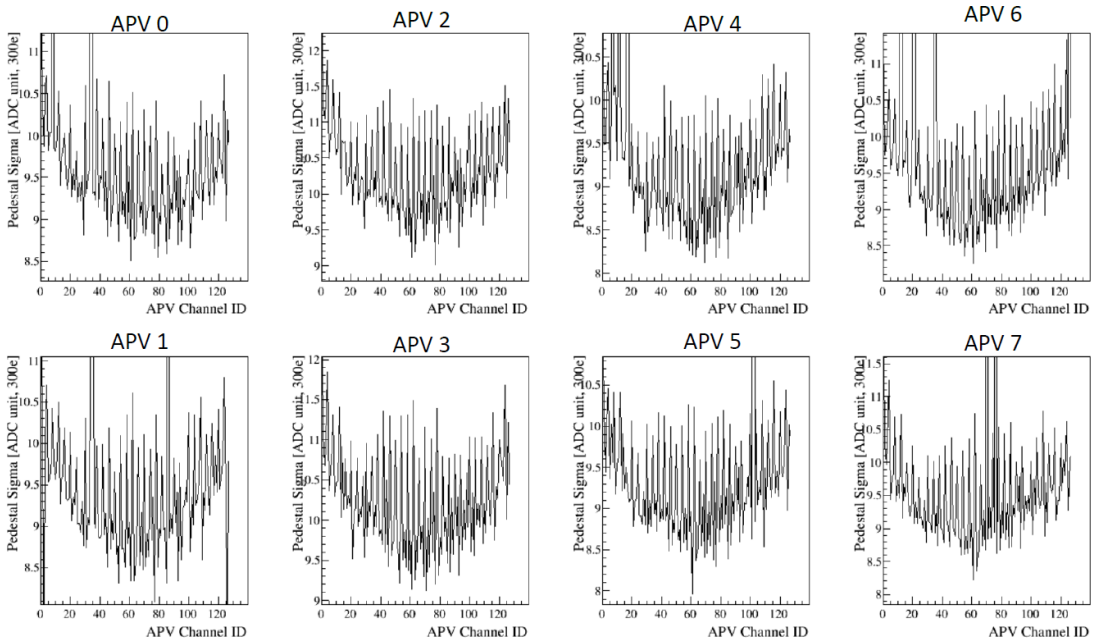

Figure 42: The noise pattern for the 1024 read-out channels of the prototype, grouped according the APV25 FE chips. The same noise pattern of the 128 channels is observed for each FE chip.

proper normalization to the number of triggers; this subtraction procedure is applied in order to remove the contribution from signals due to minimum ionizing particles that cross the prototype and are, therefore, detected.

The gain can be extracted fitting the amplitude spectra, expected to be exponential for single photoelectrons. Again, a procedure of subtraction of spectra collected with shutter open and closed in applied (Fig. 46). The resulting gain value is of about 30k.

The intrinsic detector time resolution is accessed from the raise edge of the shaped signal, sampled at 40 MHz

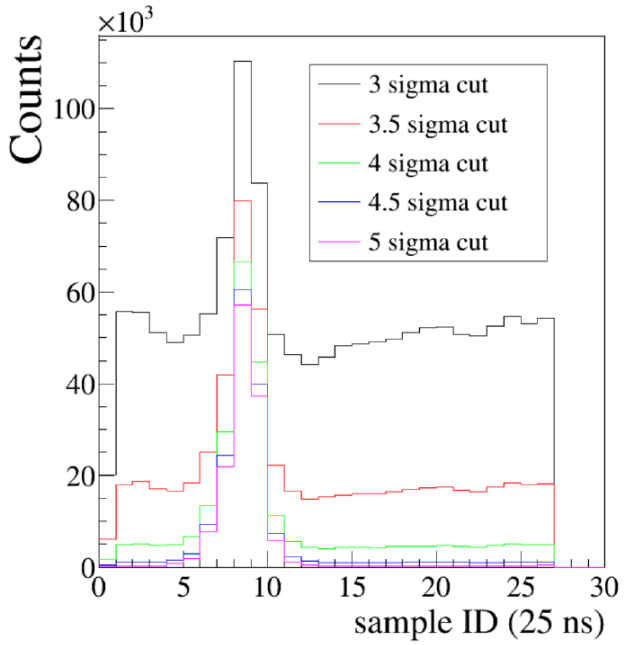

Figure 43: Time distribution of the highest amplitude signal in all the read-out channels applying different threshold levels. The time units are APV-25 cycles, 25 ns wide, and the threshold levels refer to the r.m.s. of the noise distributions of each single channel.

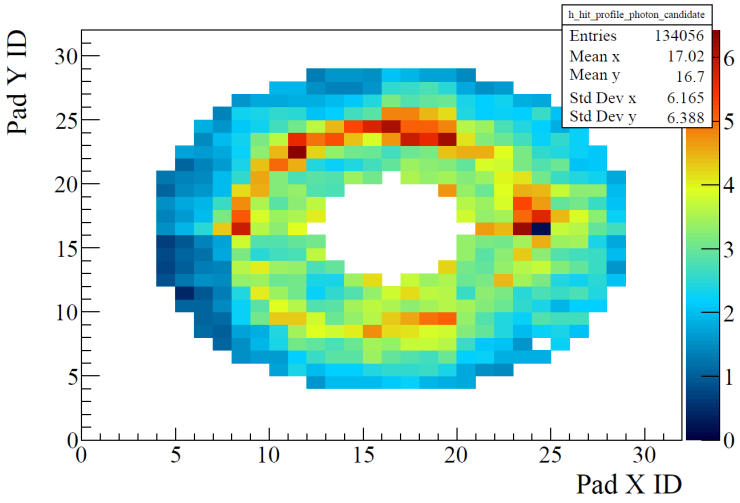

Figure 44: 2-D histogram of the selected ring-area.

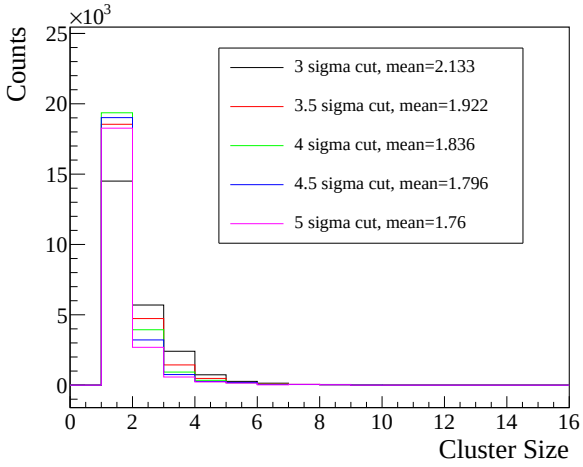

Figure 45: Cluster size distribution obtained subtracting the histograms obtained collecting data with shutter open and shutter closed, normalization to the same number of events. Different threshold cuts have been applied.

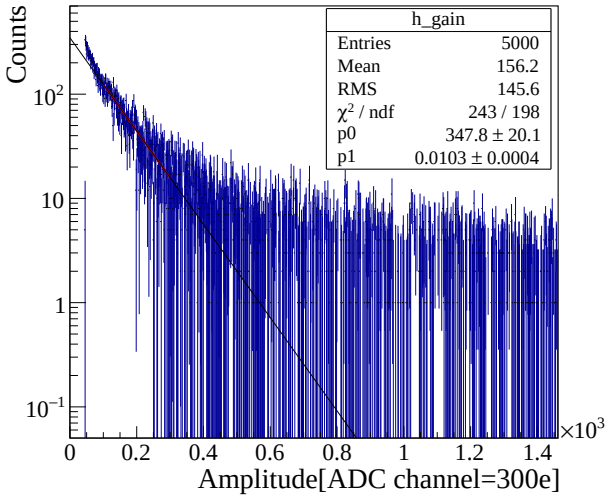

Figure 46: Amplitude spectrum resulting subtracting the spectra collected with shutter open and closed. The amplitude is in ADC channels, where 1 channel corresponds to 300 electrons equivalent.

by the APV25. The algorithm used applies a linear fit to the 4 amplitude measurements before the signal maximum and the signal time is defined as the time when the signal amplitude is 10% of the maximum (Fig. 47). At the test beam, the trigger time has not been measured, therefore it is assumed random within a 25 ns frame and its contribution to the measured time resolution can be subtracted in quadrature. The time resolution is remarkable: about 14 ns in spite of dealing with single photoelectron detection and a three-stage gaseous detector.

The possibility to operate the detector in pure methane is related to the higher voltage required. In particular, higher biasing voltage applied to the first THGEM results in a high electric field at its top surface, a parameter that enhances the effective photoelectron extraction. At the same time, the need of higher voltages implies a potentially more critical operation of the gaseous detector. At the test beam, the prototype has been successfully operated in pure methane; this is tested by the gain evolution versus the high voltage applied to

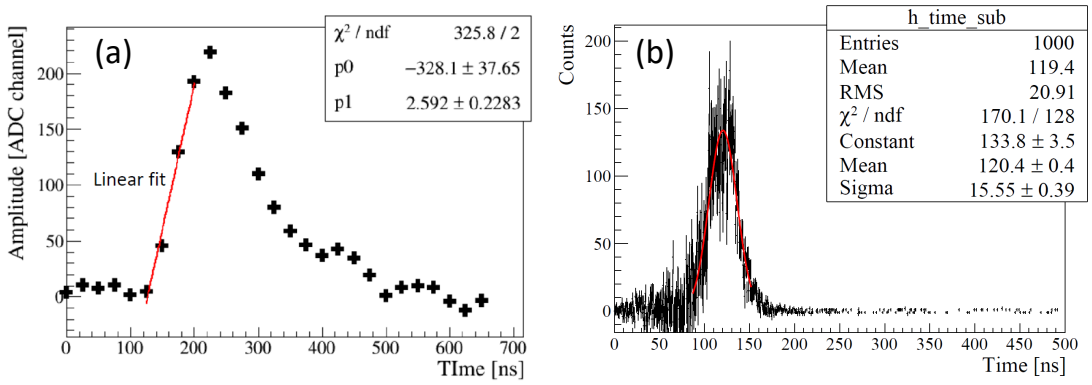

Figure 47: Time resolution; (a) the 27 consecutive measurements of the amplitude of a typical signal are shown, together with the fit used to extract the time information (details in the text); (b) the time spectrum obtained subtracting the the spectra for data collected with shutter open and shutter closed, with normalization to the same number of events. The measured width includes the random contribution of the unmeasured trigger time.

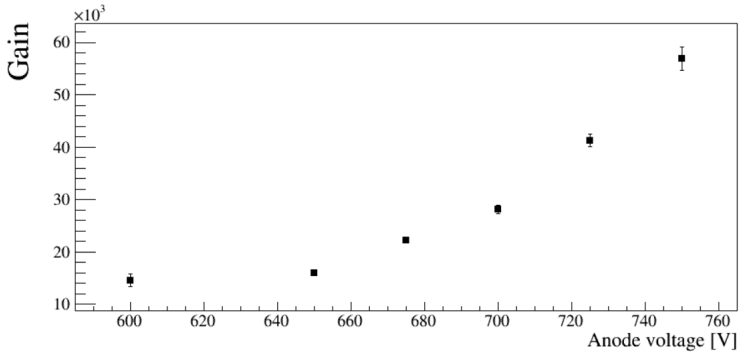

Figure 48: Gain evolution of the prototype operate with pure methane versus the voltage applied to the MICROMEGAS stage.

the MICROMEGAS stage (Fig. 48) and to the first THGEM stage (Fig. 49). The completion of the analysis of the data collected with methane is ongoing.

A new campaign of laboratory studies has been started in parallel. In laboratory, using a pulsed light source, contrary to the test beam data, there is no need of disentangling the photoelectron signals from the ionizing particle signals. Therefore, important performance figures, as the gain one, can be confirmed.

The design of a second version of the high-space resolution prototype was originally planed to overcome the gain non-uniformity only, and was, therefore, a straightforward upgrade of the first version. This approach has been reconsidered. In fact, in decreasing the pad size to 3×3 mm^2, while preserving the concept of extendibility to large size detectors, which imposes to have all the equipment related to a group of pads included in the same area covered by the pads themselves, we have reached a physical limit and we cannot improve further the space resolution. At the same time, the pad miniaturization has also results in practical problems, as the use of dense connectors and the noise issues related to the extremely compact arrangement. Therefore, we would like to adopt a different approach for the design of the second version of the prototype, introducing a DCL resistive layer on top of the anode pads. The resistive layer will result in a charge distribution over more pads, making possible an increased space resolution. This technique is being implemented in interesting R&D projects devoted to tracking by MPGD (for instance: [20]). Its applicability for single

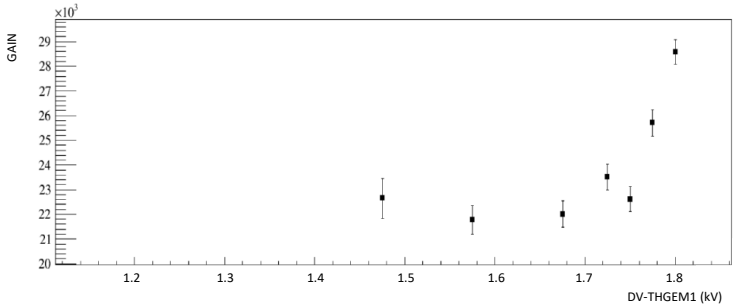

Figure 49: Gain evolution of the prototype operate with pure methane versus the voltage applied to the first THGEM stage.

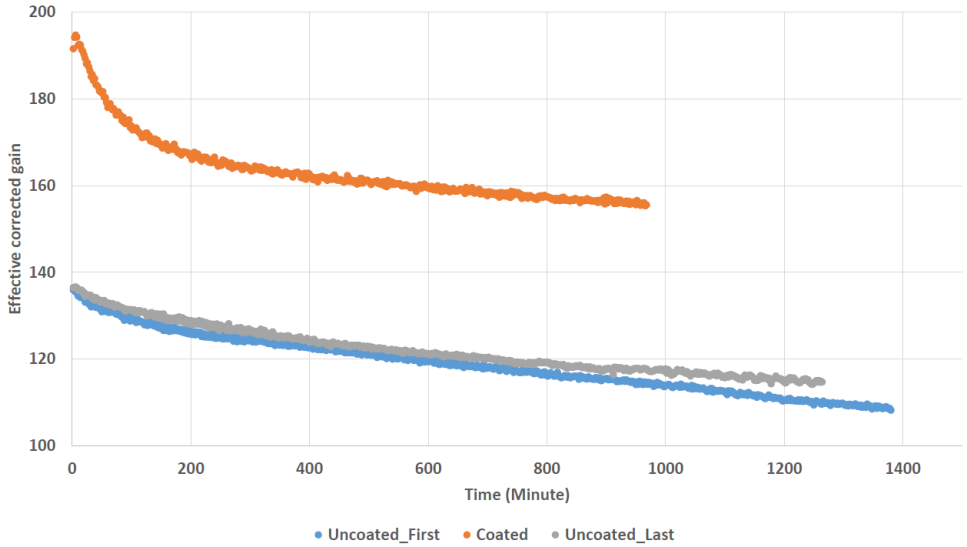

Figure 50: The gain evolution of a THGEM, partially coated with ND powder; the evolution versus time is shown illuminating with an ^{55}Fe source the uncoated region and the coated region; a second measurement illuminating the uncoated region confirms the stability of the results.

photon detection has to be demonstrated, as limitations can arise from the small signal amplitude generated by single photoelectrons. The design of the second version of the prototype according to the new approach is ongoing.

3.1.2.2 New Photocathode Materials development at INFN Trieste

The effort to understand the performance features of THGEMs coated with a ND layer has progressed by laboratory studies. The gain variation versus time over long time periods (up to more than 1 m) has confirmed the higher gain obtained for coated THGEMs respect to uncoated ones, when the applied voltage bias is the same (Fig. 50). Figure 51 illustrates the evolution of the resolution vs time. It is observed that, for uncoated THGEMs, the resolution is preserved over time. For coated ones, the resolution is by far poorer and it severely evolves with time. These features are under discussion to extract a consistent picture of the behaviour of coated THGEMs.

In 2018 it was shown that the breakdown voltage of THGEM coated with Hydrogenated ND (HND) powder

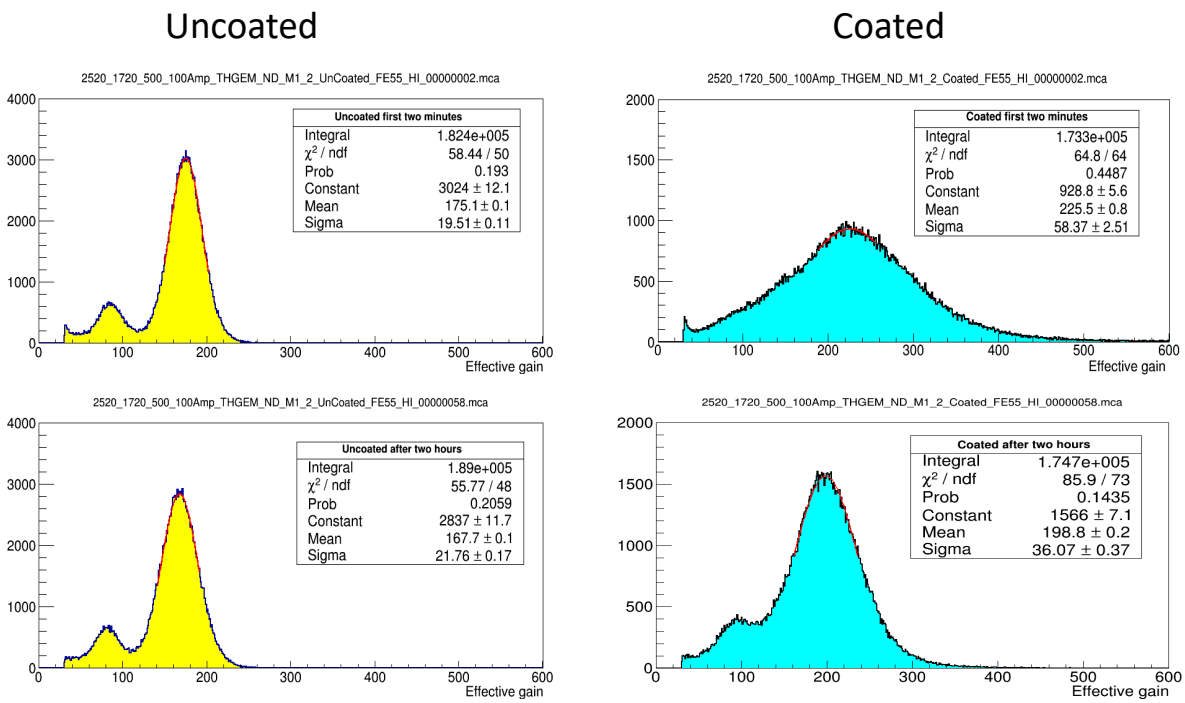

Figure 51: Amplitude spectra collected illuminating the THGEM with an ^{55}Fe source; the left plots are collected illuminating the uncoated THGEM region; the right plots are collected illuminating the THGEM region coated with ND powder; the plots in the top row presents spectra collected within the first minute after starting the illumination; the bottom row spectra collected 2 h after starting the illumination.

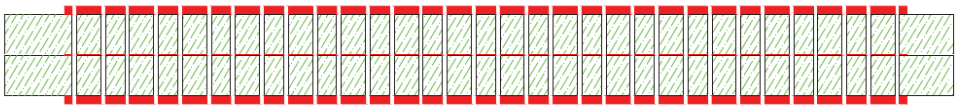

Figure 52: Sketch of the THGEM formed with two layers (not to scale); the metallized coating is indicated in red.

is at voltages too low respect to what required in stable photon detectors. Most likely, during the coating process, a NDH layer is deposited also inside the THGEM wholes and this lowers the electrical rigidity of the device. Nevertheless, HND are of major interest because of the higher Quantum Efficiency (QE) respect to ND powders. An attempt to overcome this difficulty is ongoing. The THGEMs are produced in two layers, each one of thickness one half that of the final THGEM, and where only one of the faces is Cu-coated. One of the two halves is coated on the metalized face, then the final THGEM is obtained by gluing the two halves (Fig. 52). The HND can at most be present on the walls of the coated THGEM, not in the second layer forming the THGEM. The goal is to operate the THGEM coated with HND at the required HV bias. The production of the two layers forming the THGEMs is ongoing.

In parallel, the exploration of the characteristics of the ND powder used as photo-converters continues. The QE obtained using powders with different grain size has been measured. For small grain-size (a few nm) the QE is low. It increases with grain size up to sizes of about 50 nm. It does not increase further for larger grain-sizes (Fig. 53).

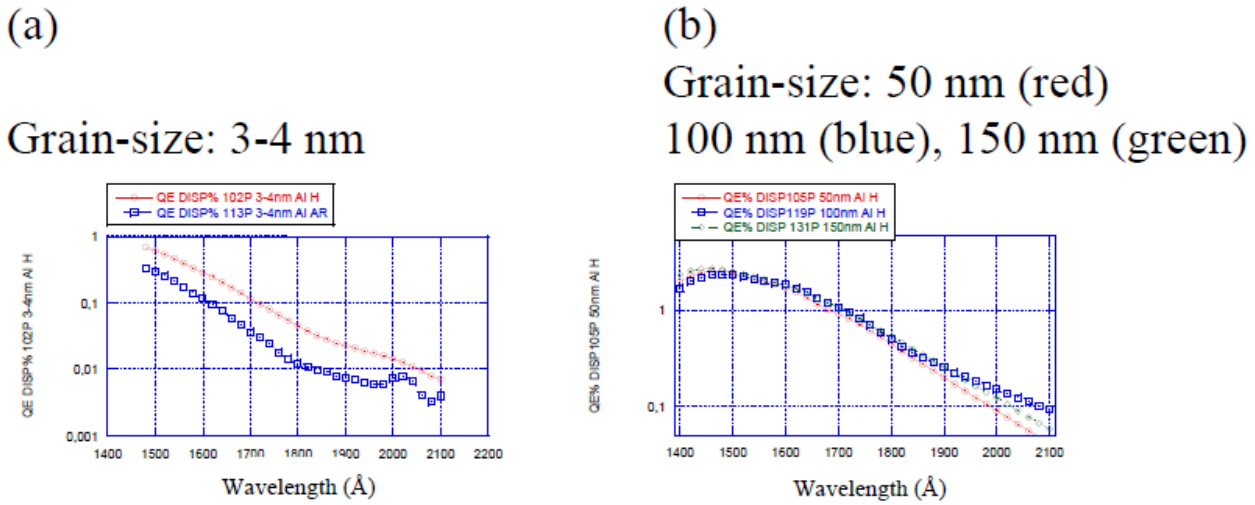

Figure 53: QE obtained using ND powders characterised by different grain-size; (a) small grain-size: 3-4 nm; (b) large grain-size: 50 nm, 100 nm, 150 nm.

3.1.3 What was not achieved, why not and what will be done to correct?

3.1.3.1 MPGD sensors of single photons at INFN Trieste

The analysis of the test beam data is progressing according to schedule. Extra complementary activity, not originally planned, is being performed, namely the further laboratory studies of the prototype.

Concerning the second version of the prototype, its construction has been delayed in view of a substantial modification of the detector principle, as explained in Sec. 3.1.2.1. This choice can result in a higher performance detector, even if it causes some delay respect to the original planning.

3.1.3.2 New Photocathode Materials development at INFN Trieste

The exploratory activity is progressing according to the planning.

3.1.4 What is planned for the next funding cycle and beyond?

3.1.4.1 MPGD sensors of single photons at INFN Trieste

The construction and characterization of the second version of the prototype is now foreseen for the year 2020.

Related milestone
September 2020: The completion of the laboratory characterization of the second version of the photon detector with miniaturized pad-size.

3.1.4.2 New Photocathode Materials development at INFN Trieste

The THGEMs formed with two layers, where only the upper layer is exposed to hydrogenated ND coating process, will be fully characterized. In parallel, further studies dedicating to define the properties of ND powders with different characteristics are planned.

Related milestone
September 2020: Studies and characterization of a THGEM formed with two layers, coated with hydrogenated ND powder.

3.2 Optical Elements - SBU

3.2.1 What was planned for this period?

3.2.1.1 Large mirrors development at Stony Brook

The installation and commissioning of mirror coating equipment was planned in the present funding cycle.

3.2.1.2 New Radiator Studies at Stony Brook

We were planning on continuing the investigation of meta-materials suited for the application of Cherenkov photon detection. Students working on the project were expected to familiarize with the FEM software and to model appropriate materials.

3.2.2 What was achieved?

3.2.2.1 Large mirrors development at Stony Brook

The evaporator unit for the mirror coating project has been moved out of its place into a new location because of possible interference with the ongoing sPHENIX TPC project which will be constructed in the area that was held by the evaporator.
The new place is in a previously refurbished target room at SBU which had to be prepared for the accommodation of the evaporator vessel. The needed service lines (water cooling and power) are being provided.
A postdoctoral fellow was assigned to the installation of the equipment and we also have a master student whose thesis will be the installation and commissioning of the mirror coating equipment.
The equipment of the electron-/ion-beam equipment and the rotary motor system for mirror blank rotation has been installed. However, at the time of this write-up it was found that slight modifications have to be applied due to an incompatibility of the equipment and evaporator. These incompatibilities are concerning the sealing of the evaporator unit when equipped with the electron-/ion-beam feedthroughs. This will only delay the startup of the commissioning process.

3.2.2.2 New Radiator Studies at Stony Brook

SBU students have familiarized themselves with the COMSOL package that has been purchased for calculating the behavior of meta-materials with Finite Element Methods (FEM). They have modeled a possible implementation of the material (Fig. 54, left) that might describe a Cherenkov radiator with promising properties like Cherenkov angles comparable to dense materials but with high momentum reach comparable to less dense materials. Fig. 54, right panel shows the implementation in COMSOL with different views.
The field of optical meta-materials so far has struggled to deliver on all its perceived promise of revolutionizing optics. One difficulty is to engineer meta-materials that are made of building blocks much smaller

than the wavelength under consideration. Those blocks can be designed in countless variations. Up to now the approach of shaping such devices is the trial-and-error approach which didn't lead to the desired results yet. A promising step is the development of software that lets users start by telling the software the optical property they want - how their meta-material needs to interact with light - and their starting materials. The

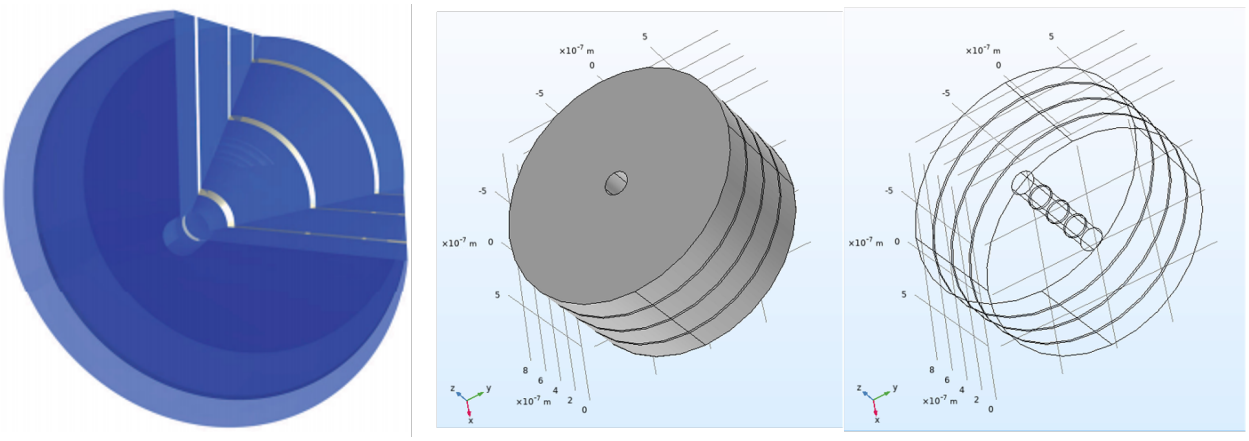

Figure 54: Left: An implementation of a metamaterial: thin silver cylinders embedded in a dielectric with filling factor of 0.076. The thickness of the layers equals 20 and 234 nm for the silver and the dielectric, respectively. Right panel: the implementation modeled in COMSOL.

software, Mirage [21], generates designs that match those criteria from a library of more than 100 templates and takes out the guesswork of the design. Or, users can draw their own designs, and the program will check them for errors. This software was developed by experts from Sandia laboratories. The sponsor of that project is the Defense Advanced Research Projects Agency (DARPA) and many groups have expressed interest in using the software in their research, amongst them is our group. The final decision has not come out yet as of the write-up of this document. In the meantime we are in contact with the developer of that software, Ihab El-Kady, who is an expert in meta-material research. Our attempt to invite another expert in that field, Fran Capasso failed on several occasions due to scheduling problems.

3.2.3 What was not achieved, why not and what will be done to correct?

3.2.3.1 Large mirrors development at Stony Brook

The final installation of the mirror coating equipment has been delayed due to the move of the evaporator into a new a location.
The manpower presently assigned to this project will bring it to an end in a foreseeable time.

3.2.3.2 New Radiator Studies at Stony Brook

The ultimate design of a meta-material fulfilling the requirements for a large aperture Cherenkov radiator and simultaneously large momentum reach has not been found. This was expected because of time consuming guesswork in the design process.
With the advent of design software like Mirage this guesswork is expected to be taken away.

3.2.4 What is planned for the next funding cycle and beyond?

3.2.4.1 Large mirrors development at SBU

The installation has been finalized pending some modifications and the graduate student working on the project for his master thesis will perform the commissioning of the device in the remaining funding cycle.

3.2.4.2 New Radiator Studies at Stony Brook

We are awaiting the release of the Mirage software so that the students assigned to this project will be able to find a solution to the meta-material problem. In the meantime we will continue the standard approach of determining suitable meta-materials with the trial-and-error approach.

4 Critical Issues

4.1 Brookhaven National Lab

Up to this point we have demonstrated that the position resolution of a GEM-based planar (ie, single space point) detector consisting of zigzag shaped charge collecting anodes meets the performance requirements needed at the EIC. As a result, the R&D on zigzag based readouts is no longer supported under this R&D program. Since we are now studying a TPC detector configuration, which generates a significantly different charge profile projected onto the readout plane, the parameters of the zigzag geometry must be re-evaluated to ensure optimal charge sharing. Therefore, while we will certainly draw on our previous experience to optimize the zigzag geometry for a TPC readout, we will require additional funding from eRD6 to fully optimize these designs.

4.2 Florida Tech

The departure of our post-doc Aiwu Zhang back in December 2016 without replacement has slowed down progress. While our students are doing a great job and are very enthusiastic about building and testing prototype detectors and running EICroot simulations, they have limited experience.

4.3 INFN Trieste

No technical critical issue is expected for the completion of the planed 2020 activity.

The request support for year 2020 has been kept at the minimum needed to perform the planed activities. Therefore, a reduction of the resources requested would result in the suppression of one or both the foreseen tasks (according to the reduction level).

4.4 Stony Brook University

No critical issues.

4.5 Temple University

In order to move forward with implementing a more realistic cylindrical μRWELL detector operating in μTPC mode into our simulation we need the guidance of real measurements. This includes measuring parameters such as the number of dE/dX measurements, resolutions (spacial and time), and how the parameters vary with the angle the tracks enter the detector. The most straight forward way to do this would be to build a 10 cm x 10 cm μRWELL with a 15 mm drift gap so that it could be operated in μTPC mode. Such a prototype would compliment the standard (3 mm) μRWELL detector that UVa built last summer, as well as provide an opportunity to further investigate some issues that they saw with their detector.

4.6 University of Virginia

No critical issues.

5 Additional information

5.1 Temple University

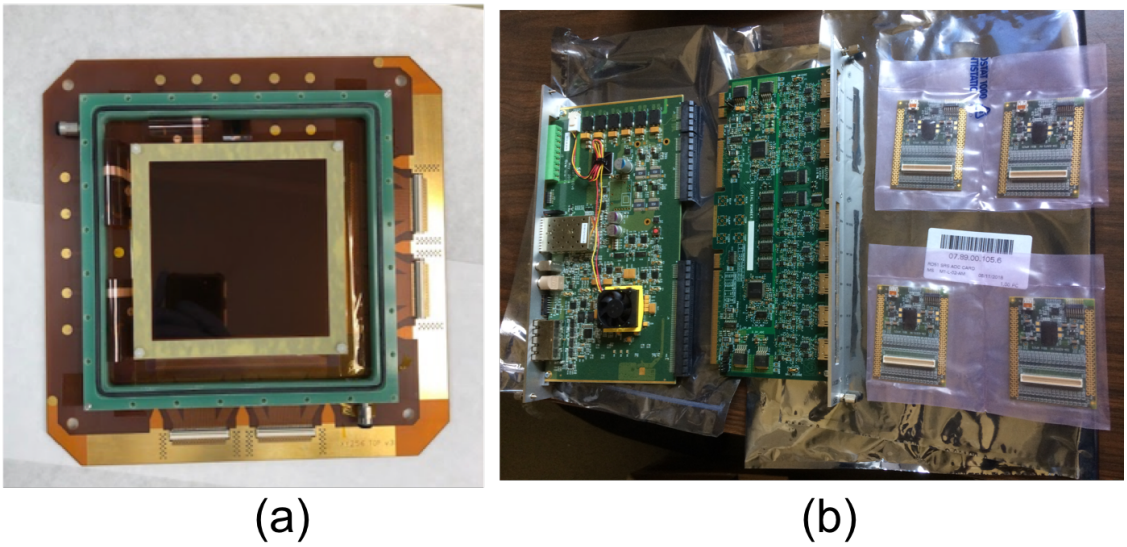

Figure 55: (a) Standard CERN 10 cm x 10 cm triple-GEM kit assembled in the Temple clean room. (b) SRS FEC, ADC, and four APV hybrid cards.

Temple University recently received some funding from an SBIR Phase 1 proposal working with Triton Systems, a company based in Massachusetts, who will be investigating an alternative technique to producing 2D readout boards. The proposal focuses on "Direct Write Fabrication of Low Cost Flexible Particle Detector Substrates". Direct write techniques offer exceptional flexibility for realizing designs without the need for a static, pre-made photomask. The process can be readily performed on non-planar, or structured, substrates. Recent advances in direct writing have also demonstrated that features can be printed directly onto side walls of pre-existing structures on the device being fabricated. Furthermore, 3D structures are also possible using direct writing (e.g. 3D printing is a direct write method), and have been produced using insulating as well as conductive materials. Whereas the aforementioned photolithography/etching methods are batch processes, direct writing is compatible with many continuous (e.g. roll-to-roll) processes, and is inherently compatible with other types of direct write processes, for example, the laser drilling process used to produce

the vias in the polyimide substrate. Temple University is motivated to continue this collaboration beyond Phase 1.

The readout boards produced via this new production technique will be installed in a standard 10 cm x10 cm CERN GEM kit (Fig. 55 a) with a hybrid APV25 SRS system (Fig. 55 b). Cosmic and ^{55}Fe measurements will be made and compared to the same measurements taken with a CERN and Tech-Etch produced readout board, since the three use different production techniques. Each board will be identical in terms of mounting holes, connections, and readout structure (following the standard Compass readout scheme). The boards will only differ in production method.

6 Manpower

6.1 Brookhaven National Lab

Our total manpower effort on MPGDs for EIC, which includes eRD6 as well as other activities, is listed below. All scientific and engineering manpower is being supported by internal BNL funds. Funds are requested from eRD6 for technical support.

6.1.1 Total manpower effort for MPGD R&D

- 2 Senior Scientists: Martin Purschke (0.2 FTE), Craig Woody (0.2 FTE)
- 2 Physics Associates: Bob Azmoun (0.6 FTE), Alexander Kiselev (0.6 FTE)
- 1 Electronics Engineer: John Kuczewski (0.1 FTE)
- 1 Technician: Bill Lenz (0.5 FTE).

6.1.2 Manpower effort for eRD6 R&D

- 2 Senior Scientists: Martin Purschke (0.1 FTE), Craig Woody (0.1 FTE)
- 2 Physics Associates: Bob Azmoun (0.2 FTE), Alexander Kiselev (0.2 FTE)
- 1 Electronics Engineer: John Kuczewski (0.1 FTE)
- 1 Technician: Bill Lenz (0.3 FTE).

6.2 Florida Tech

- Marcus Hohlmann, Professor, 0.25 FTE, not funded under this R&D program.
- Matthew Bomberger, physics graduate student (M.S.), funded with $5.6k stipend in summer 2019 by this R&D program.
- Jerry Collins, physics graduate student (Ph.D.), funded with $10.9k stipend in spring and summer 2019 by this R&D program.
- Akshath Wikramanayake, physics undergraduate student (graduated), not funded.
- Michael Werbiskis, physics undergraduate student, not funded.

6.3 INFN Trieste

From INFN Trieste:

- C. Chatterjee (Trieste University and INFN, PhD student)
- S. Dalla Torre (INFN, Staff)
- S. Dasgupta (INFN, postdoc)
- S. Levorato (INFN, staff)
- F. Tessarotto (INFN, Staff)
- Triloki (ICTP and INFN, fellowship)
- Y. Zhao (INFN, postdoc)

The contribution of technical personnel from INFN-Trieste is also foreseen according to needs.

From INFN BARI:

- Grazia Cicala (NCR staff and INFN)
- Antonio Valentini (Bari University and INFN, professor)

Globally, the dedicated manpower is equivalent to 3 FTE.

6.4 Stony Brook University

- K. Dehmelt, Research Scientist, 0.3 FTE
- T. K. Hemmick, Professor, 0.1 FTE
- P. Garg, Postdoc, 0.1 FTE
- A. Kulkarni, Grad student, 0.75 FTE
- C. Perez Lara, Postdoc, 0.1 FTE
- V. Zakharov, Grad student, 0.5 FTE

All personnel is not funded under this R&D program.

6.5 Temple University

- B. Surrow, Professor, 0.1 FTE
- M. Posik, Assistant Research Professor, 0.2 FTE
- A. Quintero, Post-doc, 0.2 FTE
- J. Nam and N. Lukow, graduate student, 0.1 FTE

6.6 University of Virginia

None of the labor at UVa is funded by EIC R&D. The workforce is listed below:

- N. Liyanage; Professor; 0.1 FTE
- K. Gnanvo; Senior Research Scientist; 0.3 FTE

7 External Funding

7.1 Brookhaven National Lab

All scientific and engineering manpower is being supported by internal BNL funds. However, technical support for our eRD6 activities requires support from eRD6 funds.

Additional work on R&D on Micropattern Detectors for EIC is also being provided by a BNL LDRD in collaboration with Saclay and Stony Brook. This is supporting our continued work on zig-zag readouts with GEMs and Micromegas and we do not request any funding for this effort from EIC R&D funds. However, our proposed work on TPC R&D for EIC would not be covered under LDRD funds.

7.2 Florida Tech

None.

7.3 INFN Trieste

A support of 22 keuro for the year 2019 has been granted by INFN. INFN has also provided the matching resources to extend the postdoc position to one full year.

A support of 25 keuro will be requested for the year 2020, as well as matching resources to extend the postdoc position to one full year.

7.4 Stony Brook University

There is no external funding for this R&D effort.

7.5 Temple University

As of this writing no external funding has been used for eRD6 related projects.

7.6 University of Virginia

UVa has DOE basic research grant from Medium Energy Physics.

8 eRD6 New R&D Proposal for FY20

8.1 Development of Outgas Test System at Temple University

The collaboration plans a new initiative to assemble a material test facility to validate new potential materials (including various printable plastics) verses outgassing worries. The committee agrees that this could be a useful addition to the community facilities but wonders if a somewhat more sophisticated system including gaseous component measurement tools might not be significantly more valuable at detecting possible problem materials than the proposed simple wire avalanche detector. We have taken the committees comments from last summer into account and have modified our outgassing test facility design accordingly.

Motivation for Research

With current trends in MPGD assembly moving towards 3D printed structures (sPHENIX, eRD6), many of the printing materials will need to be tested, in particular for their outgassing properties, before they can be used in a detector. As outgassing can hinder the performance of a MPGD detector, it is vital that only printing materials with a low outgas behavior are selected. An outgassing testing apparatus can also be used to find alternatives to low outgassing chemicals that are currently used in MPGD assembly, such as Nuvovern varnish, which is used to coat frames to prevent them from outgassing. While this varnish set itself is not too expensive, the transportation of it to the US costs around 1000 euro, making it a non viable option for small R&D programs.

Not only will this outgassing setup compliment eRD6's own R&D, but can also be used by the broader MPGD community. Temple University has already successfully established a similar relationship with their CCD GEM scanner, which has serviced the larger MPGD community, with foils being scanned for experiments such as BONUS and CMS, as well as EIC related R&D (large CERN EIC foil, Cr-GEM). We envision a similar situation with an outgas testing setup that will serve our specific eRD6 R&D, the broader EIC R&D, as well as the general MPGD community.

We propose the assembly of an outgas testing setup at Temple University. This setup would follow the ASTM E-595 standard, which is currently used by industry and NASA for quantifying outgassing properties of materials. This test method determines a materials outgassing behavior by measuring two parameters: the total mass loss (TML) and the collected volatile condensable material (CVCM). This test method measures the mass loss of materials being subjected to 125^oC at less than 5×10^{-5} torr for 24 hours. The mass loss is characterized into non condensable and condensable mass loss. The non condensable mass loss is determined by measuring the sample weight before and after the testing procedure. This determines the TML of the material. The condensable mass loss is determined by collecting the vapor leaving the sample onto collector plates located above the samples which are kept at 25^oC. The difference in weight between the material collected on the cooled plates and the initial sample determines the materials CVCM. Materials with TML $< 1\%$ and CVCM $< 0.1\%$ are quantified as low outgassing materials and would be suitable in an MPGD detector.

Funding Request

The test apparatus consists of an 8 in. diameter vacuum chamber which is connected to a turbo pump system ($12k) and held at a pressure of 5×10^{-5} torr. This chamber will allow us to test up to 6 samples simultaneously. The samples are placed in compartments on copper bars, which can be heated and held at 125^oC. Collector plates located above the corresponding sample compartments and held at 25^oC via a water chiller and circulator ($4k). The sample compartments and collecting plates are aligned and isolated from the other samples so that vapor from one compartment does not contaminate another compartments collector plate. The TU machine shop will be able to do the design, order materials, do the machining, install the electric heater (to heat up the samples) and control assembly for about $10k. To weigh the samples we will make use of an already existing balance which has sensitivity to 0.01 mg. Finally the ASTM E-595 procedure calls for conditioning the samples before testing, by maintaining the relative humidity level at 50%. To do this we will need to purchase a desiccator ($2k).

9 eRD6 Budget Request for FY20

9.1 Overall Budget Request and Money Matrix

The institutional budget requests presented below are summarized in the following. The overall money matrix of R&D project vs. Institute for the eRD6 funding requests for FY20 is presented in Table 3

Table 3: Fully loaded cost matrix of institutes and R&D topic for the eRD6 FY20 budgetary request

k$	**MPGD RICH**	**Forward Tracker**	**μRWELL Tracker**	**TPC Readout**	**Meta-Materials**	**Outgassing Test Stand**	**Total**
BNL & Yale U.				75			**75**
Florida Tech		9	38.84				**47.84**
INFN Trieste	44						**44**
Temple U.			15.801			56.216	**72.017**
UVa		13	20.075				**33.075**
Total	**44**	**22**	**74.716**	**75**		**56.216**	**271.932**

9.2 Budget Request by Institute

9.2.1 BNL Budget Request for FY20

The bulk of the budget request for this funding cycle is for manufacturing new, single zigzag patterned PCB's for use in our TPC prototype. The PCB will have the standard form-factor, with a 10cm x 10cm acceptance and can be used in a planar detector mode for preliminary testing, then can be installed into the base-plate of the TPC for longer term testing. At least two of these PCB's will have a micromegas and a μRWELL installed onto them, so that a variety of avalanche schemes may be tested in a TPC setup. Finally, it must be reiterated that this budget request is to be shared with the Yale group since they will collaborate on much of this work.

Table 4: TPC R&D at BNL & Yale (FY20)

	Baseline (k$)	**-20% (k$)**	**-40% (k$)**
Single pattern zigzag readout boards	12	9.6	7.2
Additional GEM detectors	5	4	3
Micromegas for single pattern ZZ readout	5	4	3
μRWELL for single pattern ZZ readout	5	4	3
Technical support	12	9.6	7.2
Gas and other expendables	6	4.8	3.6
Travel	5	4	3
Total	50	40	30
Overhead	25	20	15
Total with overhead	**75**	**60**	**45**

9.2.2 Florida Tech Budget Request for FY20

We request funding to cover stipends for two graduate students, Matt Bomberger and Jerry Collins, and a stipend for two undergradute summer students. Bomberger has been working on the project as an under-

graduate for three years and after graduation in May 19 we recruited him into the M.S. program with the goal of having him produce a thesis on the large, low-mass forward tracking detector. Collins has produced the design of the cylindrical μRWELL system and will work on designing, producing, and testing the mechanical mock-up. We also request funds for travel to BNL to conduct X-ray scans of the small μRWELL prototype or to FNAL if the consortium plans another beam test effort there, for the P.I. to attend one EIC R&D review meeting, and for travel to a conference for presenting results. A small amount is requested for materials for the μRWELL mechanical mock-up and consumables such as gas.

Table 5 breaks down the funding request for the Florida Tech projects, along with the 20% and 40% reduced funding scenarios. In the 20% reduced scenario, we drop support for the undergraduate summer students and reduce travel. In the 40% reduced scenario, graduate student support is also reduced, and travel is further reduced. Florida Tech does not charge benefits or overhead on students for the current grant.

Table 5: **Florida Tech** - FY20 budget request including scenarios with 20% and 40% reduction.

	Request	**-20%**	**-40%**
Graduate Student Stipends (2 stud.)	\$30,000	\$30,000	\$21,000
Undergraduate Summer Stipend	\$6,000	\$0	\$0
Travel	\$5,000	\$2,600	\$2,250
Materials	\$3,000	\$3,000	\$3,000
Indirect Cost Base (travel & material)	\$8,000	\$5,600	\$5,250
Indirect Cost (48% negotiated rate)	\$3,840	\$2,688	\$2,520
Total	**\$47,840**	**\$38,288**	**\$28,770**

9.2.3 INFN Budget Request for FY20

The 2020 activity consists in the continuation of the two tasks already pursued in 2018 and 2019 and detailed in Secs. 3.1.4.1 and 3.1.4.2.

The founding request for this R&D activity, 44 k\$ in total, includes three main chapters:

1. the financial support for a postdoc (7 months) fully dedicated to the project: the contribution of a dedicated personnel unit will offer a crucial boost to the R&D program; this support will be complemented by INFN resources in order to result in one full-year postdoc contract dedicated to the project;

2. traveling resources, mainly to have the possibility of closer interaction with the whole eRD6 Consortium and to follow the evolution of the EIC project: two trips to US require about 6000 \$; a minor support is requested to allow travelling to and from Bari and Trieste for the common work about the ND photocathodes: this needs is estimated to be 2000 \$; another minor support is requested for material procurement, to interact with the producers when non-standard components are needed and for the construction of specific detector elements that must be produced at CERN: this needs is estimated to be 2000 \$;

3. Consumables have to cover prototype components and prototype operation costs; the needs for the next year will be partially covered by the delayed availability of the support granted for this year. Consumables for FY2020 include:

   - Material and fabrication of THGEMs to be used as ND photocathode substrates: 2000 \$;
   - ND powder samples: 2000 \$;
   - the production of a new MM for the miniaturized pad prototype according to the new principle (Sec. 3.1.2.1) will be largely covered by the 2019 support; specific support is needed for the DLC resistive anode: 2000 \$;

- Miscellanea of laboratory small items: 2000 $.

Cost reductions in -20% and -40% scenarios
The requests have been carefully analyzed and kept at a minimal level. Any reduction would severely impact. In the "-20%" hypothesis one of the two foreseen activity has to be stopped. In the "-40%" hypothesis the whole INFN Trieste activity will be stopped.

The requests are summarized in Table 6.

Table 6: Funding request INFN

item	cost (k$)	overhead (k$)	total (=cost+overhead) (k$)
manpower	20	4	24
traveling	10	2	12
consumables	8		8
total	38	6	44

9.2.4 SBU Budget Request for FY20

No additional funding is requested for FY20.

9.2.5 TU Budget Request for FY20

Motivation for Research

Cylindrical μRWELL Request

As part of our 2020 activities we will continue to develop the cylindrical μRWELL μTPC simulation. This would ideally require the assembly of a 10 cm x 10 cm planar μRWELL with a 15 mm drift gap operating in μTPC mode. Table 7 lists the funding request needed to build this prototype. The nominal request and two alternative funding scenarios are presented.

Table 7: TU funding request for μRWELL μTPC.

Item	Request ($)	-20% ($)	-40% ($)
Postdoc (%)	(10%) 5,637	(5%) 2,818	(5%) 2,818
Fringe benefits (26.85%)	1,513	757	757
Total Personnel	7,150	3,575	3,575
Material	800	800	200
Equipment	3,200	3,200	3,200
Modified Total Direct Costs	7,950	4,375	3.775
Overhead (58.5%)	4,651	2,559	2,208
Total Project Costs	**15,801**	**10,134**	**9,183**

Outgassing Test Facility

Building on the success of the GEM CCD scanner, we would like to build an outgassing test facility to assess the outgassing properties of materials. Such a facility would not only directly benefit the eRD6 consortium, but also the larger MPGD community as well. Table 8 shows our nominal funding request for materials,

equipment, and manpower needed to assemble the outgassing test facility, along with the -20% and -40% budget scenarios.

Table 8: TU funding request for outgassing test facility.

Item	Request ($)	-20% ($)	-40% ($)
Postdoc (%)	(20%) 11,274	(10%) 5,637	(5%) 2,818
Fringe benefits (26.85%)	3,026	1,513	757
Total Personnel	14,300	7,150	3,575
Material	10,000	10,000	10,000
Equipment	18,000	18,000	18,000
Modified Total Direct Costs	24,300	17,150	13,575
Overhead (58.5%)	14,216	10,033	7,941
Total Project Costs	**56,216**	**45,183**	**39,516**

9.2.6 UVa Budget Request for FY20

For this cycle, UVa requesting funding to pursue the R&D on low material 2D readout μRWELL-μTPC prototype that will operate in mini-drift (μTPC) mode as expected for the cylindrical μRWELL tracker in the central region . We will also request additional funding to complete the acquisition of the small VMM-SRS readout electronics. UVa had was granted some funding for the VMM-SRS system in the FY19 funding cycle. However, the VMM-SRS system turned out to be significantly more expensive than our in ital budget had estimated. The VMM FE hybrid card is more than a factor twice the cost for the equivalent APV25 version and in addition, several new components are required to operate VMM-SRS. We are also

Table 9: UVa FY20 budget request with 20% and 40% reduction scenario

Item	**Budget Request**	**-20% scenario**	**-40% scenario**
μRWELL-μTPC	$6,000	$4,000	$0.00
Two small GEMs	$10,000	$8,000	$5,000
VMM Electronics	$5,000	$4,000	$5,000
Zebras strips	$1,000	$1000	$1000
Lab supplies & expendables	$3,000	$2,000	$1,500
Travel (fully loaded)	$5,000	$4,000	$3,000
Overhead (61%)	$3,075	$2,460	$1,845
Total	**$33,075**	**$25,460**	**$17,345**

looking to purchase two small triple-GEM detector with 2D strip readout to setup a cosmic stand for the study of the planar μRWELL-μTPC and we will acquire a set of different type of zebra strips to study their performance with our large EIC GEM prototype. The remaining funding request are for travel to conferences, EIC meeting, test beam, detector lab supplies, technical support and overhead.
Table 9 presents the full breakdown for UVa's funding request along with 20% and 40% reduced funding scenarios.A 20% reduced funding scenarios would limit our ability to built a μRWELL-μTPC prototype and fully complete the procurement of the VMM-SRS readout electronics. We will likely opt for a standard μRWELL prototype. With a 40% reduced funding scenario, we will very likely drop the new μRWELL prototype altogether and will concentrate mostly in the procurement of the full VMM-SRS system instead

References

[1] B. Azmoun et al. "A Study of a Mini-Drift GEM Tracking Detector". In: *IEEE Transactions on Nuclear Science* 63.3 (June 2016), pp. 1768–1776. ISSN: 0018-9499. DOI: 10.1109/TNS.2016.2550503.

[2] Craig Woody et al. "A Prototype Combination TPC Cherenkov Detector with GEM Readout for Tracking and Particle Identification and its Potential Use at an Electron Ion Collider". In: 2015. arXiv: 1512.05309 [physics.ins-det]. URL: https://inspirehep.net/record/1409973/files/arXiv:1512.05309.pdf.

[3] B. Azmoun et al. "Design Studies for a TPC Readout Plane Using Zigzag Patterns with Multistage GEM Detectors". In: *IEEE Transactions on Nuclear Science* (July 2018), pp. 1–1. ISSN: 0018-9499. DOI: 10.1109/TNS.2018.2846403.

[4] Aiwu Zhang et al. "Performance of a Large-area GEM Detector Read Out with Wide Radial Zigzag Strips". In: *Nucl. Instrum. Meth.* A811 (2016), pp. 30–41. DOI: 10.1016/j.nima.2015.11.157. arXiv: 1508.07046 [physics.ins-det].

[5] Aiwu Zhang et al. "A GEM readout with radial zigzag strips and linear charge-sharing response". In: *Nucl. Instrum. Meth.* A887 (2018), pp. 184–192. arXiv: 1708.07931 [physics.ins-det].

[6] Marcus Hohlmann et al. "Low-mass GEM detector with radial zigzag readout strips for forward tracking at the EIC". In: *2017 IEEE Nuclear Science Symposium and Medical Imaging Conference (NSS/MIC 2017) Atlanta, Georgia, USA, October 21-28, 2017*. 2017. arXiv: 1711.05333 [physics.ins-det]. URL: http://inspirehep.net/record/1636290/files/arXiv:1711.05333.pdf.

[7] J. Agarwala et al. "The MPGD-based photon detectors for the upgrade of COMPASS RICH-1 and beyond". In: *Nuclear Instruments and Methods in Physics Research Section A: Accelerators, Spectrometers, Detectors and Associated Equipment* (2018). ISSN: 0168-9002. DOI: https://doi.org/10.1016/j.nima.2018.10.092. URL: http://www.sciencedirect.com/science/article/pii/S0168900218314062.

[8] E. Albrecht et al. "Status and characterisation of COMPASS RICH-1". In: *Nuclear Instruments and Methods in Physics Research Section A: Accelerators, Spectrometers, Detectors and Associated Equipment* 553.1 (2005). Proceedings of the fifth International Workshop on Ring Imaging Detectors, pp. 215–219. ISSN: 0168-9002. DOI: https://doi.org/10.1016/j.nima.2005.08.036. URL: http://www.sciencedirect.com/science/article/pii/S0168900205016001.

[9] P. Abbon et al. "Read-out electronics for fast photon detection with COMPASS RICH-1". In: *Nuclear Instruments and Methods in Physics Research Section A: Accelerators, Spectrometers, Detectors and Associated Equipment* 587.2 (2008), pp. 371–387. ISSN: 0168-9002. DOI: https://doi.org/10.1016/j.nima.2007.12.026. URL: http://www.sciencedirect.com/science/article/pii/S0168900207024576.

[10] P. Abbon et al. "Design and construction of the fast photon detection system for COMPASS RICH-1". In: *Nuclear Instruments and Methods in Physics Research Section A: Accelerators, Spectrometers, Detectors and Associated Equipment* 616.1 (2010), pp. 21–37. ISSN: 0168-9002. DOI: https://doi.org/10.1016/j.nima.2010.02.069. URL: http://www.sciencedirect.com/science/article/pii/S0168900210002676.

[11] P. Abbon et al. "Particle identification with COMPASS RICH-1". In: *Nuclear Instruments and Methods in Physics Research Section A: Accelerators, Spectrometers, Detectors and Associated Equipment* 631.1 (2011), pp. 26–39. ISSN: 0168-9002. DOI: https://doi.org/10.1016/j.nima.2010.11.106. URL: http://www.sciencedirect.com/science/article/pii/S0168900210026422.

[12] P. Abbon et al. "The COMPASS experiment at CERN". In: *Nuclear Instruments and Methods in Physics Research Section A: Accelerators, Spectrometers, Detectors and Associated Equipment* 577.3 (2007), pp. 455–518. ISSN: 0168-9002. DOI: https://doi.org/10.1016/j.nima.2007.03.026. URL: http://www.sciencedirect.com/science/article/pii/S0168900207005001.

[13] P. Abbon et al. "The COMPASS setup for physics with hadron beams". In: *Nuclear Instruments and Methods in Physics Research Section A: Accelerators, Spectrometers, Detectors and Associated Equipment* 779.Supplement C (2015), pp. 69–115. ISSN: 0168-9002. DOI: https://doi.org/10.1016/j.nima.2015.01.035. URL: http://www.sciencedirect.com/science/article/pii/S0168900215000662.

[14] Luciano Velardi, Antonio Valentini, and Grazia Cicala. "UV photocathodes based on nanodiamond particles: Effect of carbon hybridization on the efficiency". In: *Diamond and Related Materials* 76.Supplement C (2017), pp. 1–8. ISSN: 0925-9635. DOI: https://doi.org/10.1016/j.diamond.2017.03.017. URL: http://www.sciencedirect.com/science/article/pii/S0925963516306999.

[15] Kondo Gnanvo et al. "Performance in test beam of a large-area and light-weight GEM detector with 2D stereo-angle (UV) strip readout". In: *Nucl. Instrum. Meth.* A808 (2016), pp. 83–92. DOI: 10.1016/j.nima.2015.11.071. arXiv: 1509.03875 [physics.ins-det].

[16] B. Surrow. "The STAR Forward GEM Tracker". In: *Nucl. Instrum. Meth A* 617 (2010), p. 196. DOI: 10.1016/j.nima.2009.09.012.

[17] M. Poli Lener. "The Micro-RWELL". In: *CepC Workshop* (2018).

[18] S Martoiu et al. "Development of the scalable readout system for micro-pattern gas detectors and other applications". In: *Journal of Instrumentation* 8.03 (Mar. 2013), pp. C03015–C03015. DOI: 10.1088/1748-0221/8/03/c03015. URL: https://doi.org/10.1088%2F1748-0221%2F8%2F03%2Fc03015.

[19] P. Abbon et al. "A new analogue sampling readout system for the COMPASS RICH-1 detector". In: *Nuclear Instruments and Methods in Physics Research Section A: Accelerators, Spectrometers, Detectors and Associated Equipment* 589.3 (2008), pp. 362–369. ISSN: 0168-9002. DOI: https://doi.org/10.1016/j.nima.2008.02.077. URL: http://www.sciencedirect.com/science/article/pii/S0168900208003148.

[20] M. Alviggi et al. "Small-pad resistive Micromegas for high rate environment: Performance of different resistive protection concepts". In: *Nuclear Instruments and Methods in Physics Research Section A: Accelerators, Spectrometers, Detectors and Associated Equipment* (2018). ISSN: 0168-9002. DOI: https://doi.org/10.1016/j.nima.2018.10.052. URL: http://www.sciencedirect.com/science/article/pii/S0168900218313676.

[21] Sandia Labs. *Mirage software automates design of optical metamaterials*. 2019. URL: https://www.sandia.gov/news/publications/labnews/articles/2019/04-12/mirage.html (visited on 04/11/2019).

A List of all EIC publications from the eRD6 Consortium

BNL publications:

[1] B. Azmoun et al. "Design Studies for a TPC Readout Plane Using Zigzag Patterns with Multistage GEM Detectors". In: *IEEE Transactions on Nuclear Science* (July 2018), pp. 1–1. ISSN: 0018-9499. DOI: 10.1109/TNS.2018.2846403.

[2] B. Azmoun et al. "A Study of a Mini-Drift GEM Tracking Detector". In: *IEEE Transactions on Nuclear Science* 63.3 (June 2016), pp. 1768–1776. ISSN: 0018-9499. DOI: 10.1109/TNS.2016.2550503.

[3] Craig Woody et al. "A Prototype Combination TPC Cherenkov Detector with GEM Readout for Tracking and Particle Identification and its Potential Use at an Electron Ion Collider". In: 2015. arXiv: 1512.05309 [physics.ins-det]. URL: https://inspirehep.net/record/1409973/files/arXiv:1512.05309.pdf.

[4] B. Azmoun et al. "Initial studies of a short drift GEM tracking detector". In: *2014 IEEE Nuclear Science Symposium and Medical Imaging Conference (NSS/MIC)*. Nov. 2014, pp. 1–2. DOI: 10.1109/NSSMIC.2014.7431059.

[5] M. L. Purschke et al. "Test beam study of a short drift GEM tracking detector". In: *2013 IEEE Nuclear Science Symposium and Medical Imaging Conference (2013 NSS/MIC)*. Oct. 2013, pp. 1–4. DOI: 10.1109/NSSMIC.2013.6829463.

Florida Tech publications:

[1] Marcus Hohlmann et al. "Low-mass GEM detector with radial zigzag readout strips for forward tracking at the EIC". In: *2017 IEEE Nuclear Science Symposium and Medical Imaging Conference (NSS/MIC 2017) Atlanta, Georgia, USA, October 21-28, 2017*. 2017. arXiv: 1711.05333 [physics.ins-det]. URL: http://inspirehep.net/record/1636290/files/arXiv:1711.05333.pdf.

[2] Aiwu Zhang et al. "A GEM readout with radial zigzag strips and linear charge-sharing response". In: *Nucl. Instrum. Meth.* A887 (2018), pp. 184–192. arXiv: 1708.07931 [physics.ins-det].

[3] Aiwu Zhang and Marcus Hohlmann. "Accuracy of the geometric-mean method for determining spatial resolutions of tracking detectors in the presence of multiple Coulomb scattering". In: *JINST* 11.06 (2016), P06012. DOI: 10.1088/1748-0221/11/06/P06012. arXiv: 1604.06130 [physics.data-an].

[4] Aiwu Zhang et al. "R&D on GEM detectors for forward tracking at a future Electron-Ion Collider". In: *Proceedings, 2015 IEEE Nuclear Science Symposium and Medical Imaging Conference (NSS/MIC 2015): San Diego, California, United States*. 2016, p. 7581965. DOI: 10.1109/NSSMIC.2015.7581965. arXiv: 1511.07913 [physics.ins-det]. URL: http://inspirehep.net/record/1406551/files/arXiv:1511.07913.pdf.

[5] Aiwu Zhang et al. "Performance of a Large-area GEM Detector Read Out with Wide Radial Zigzag Strips". In: *Nucl. Instrum. Meth.* A811 (2016), pp. 30–41. DOI: 10.1016/j.nima.2015.11.157. arXiv: 1508.07046 [physics.ins-det].

INFN publications:

[1] J. Agarwala et al. "The MPGD-based photon detectors for the upgrade of COMPASS RICH-1 and beyond". In: *Nuclear Instruments and Methods in Physics Research Section A: Accelerators, Spectrometers, Detectors and Associated Equipment* (2018). ISSN: 0168-9002. DOI: https://doi.org/10.1016/j.nima.2018.10.092. URL: http://www.sciencedirect.com/science/article/pii/S0168900218314062.

[2] J. Agarwala et al. "Study of MicroPattern Gaseous detectors with novel nanodiamond based photocathodes for single photon detection in EIC RICH". In: *Nuclear Instruments and Methods in Physics Research Section A: Accelerators, Spectrometers, Detectors and Associated Equipment* (2019). ISSN: 0168-9002. DOI: https://doi.org/10.1016/j.nima.2019.03.022. URL: http://www.sciencedirect.com/science/article/pii/S0168900219303213.

SBU publications:

[1] M. Blatnik et al. "Performance of a Quintuple-GEM Based RICH Detector Prototype". In: *IEEE Trans. Nucl. Sci.* 62.6 (2015), pp. 3256–3264. DOI: 10.1109/TNS.2015.2487999. arXiv: 1501.03530 [physics.ins-det].

TU publications:

[1] M. Posik and B. Surrow. "Construction of a Triple-GEM Detector Using Commercially Manufactured Large GEM Foils". In: 2018. arXiv: 1806.01892 [physics.ins-det].

[2] M. Posik and B. Surrow. "Construction of Triple-GEM Detectors Using Commercially Manufactured Large GEM Foils". In: *Proceedings, 2016 IEEE Nuclear Science Symposium and Medical Imaging Conference: NSS/MIC 2016: Strasbourg, France*. 2016, p. 8069743. DOI: 10.1109/NSSMIC.2016.8069743. arXiv: 1612.03776 [physics.ins-det].

[3] M. Posik and B. Surrow. "Optical and electrical performance of commercially manufactured large GEM foils". In: *Nucl. Instrum. Meth.* A802 (2015), pp. 10–15. DOI: 10.1016/j.nima.2015.08.048. arXiv: 1506.03652 [physics.ins-det].

[4] M. Posik and B. Surrow. "R&D of commercially manufactured large GEM foils". In: *Proceedings, 2015 IEEE Nuclear Science Symposium and Medical Imaging Conference (NSS/MIC 2015): San Diego, California, United States*. 2016, p. 7581802. DOI: 10.1109/NSSMIC.2015.7581802. arXiv: 1511.08693 [physics.ins-det].

[5] M. Posik and B. Surrow. "Research and Development of Commercially Manufactured Large GEM Foils". In: *Proceedings, 21st Symposium on Room-Temperature Semiconductor X-ray and Gamma-ray Detectors (RTSD 2014): Seattle, WA, USA, November 8-15, 2014*. 2016, p. 7431060. DOI: 10.1109/NSSMIC.2014.7431060. arXiv: 1411.7243 [physics.ins-det].

UVa publications:

[1] Kondo Gnanvo et al. "Large Size GEM for Super Bigbite Spectrometer (SBS) Polarimeter for Hall A 12 GeV program at JLab". In: *Nucl. Instrum. Meth.* A782 (2015), pp. 77–86. DOI: 10.1016/j.nima.2015.02.017. arXiv: 1409.5393 [physics.ins-det].

[2] Kondo Gnanvo et al. "Performance in test beam of a large-area and light-weight GEM detector with 2D stereo-angle (UV) strip readout". In: *Nucl. Instrum. Meth.* A808 (2016), pp. 83–92. DOI: 10.1016/j.nima.2015.11.071. arXiv: 1509.03875 [physics.ins-det].

Yale publications:

[1] S. Aiola et al. "Combination of two Gas Electron Multipliers and a Micromegas as gain elements for a time projection chamber". In: *Nucl. Instrum. Meth.* A834 (2016), pp. 149–157. DOI: 10.1016/j.nima.2016.08.007. arXiv: 1603.08473 [physics.ins-det].